

Studying the role of Ran-GTP in cytokinesis in *C. elegans* embryos

Imge Özügergin

A
Thesis
In the Department
Of
Biology

Presented in Partial Fulfillment of the Requirements
For the Degree of
Master of Science (Biology) at
Concordia University
Montreal, Quebec, Canada

December 2018

©Imge Özügergin, 2018

CONCORDIA UNIVERSITY
School of Graduate Studies

This is to certify that the thesis prepared

By: Imge Özügergin
Entitled: Studying the role of Ran-GTP in in early *C. elegans*
embryo cytokinesis

and submitted in partial fulfillment of the requirements for the degree of

Master of Science (Biology)

complies with the regulations of the University and meets the accepted standards with respect to originality and quality.

Signed by the final Examining Committee:

_____	Chair
Dr. Michael Sacher	
_____	External Examiner
Dr. Aashiq Kachroo	
_____	Examiner
Dr. Michael Sacher	
_____	Examiner
Dr. Malcolm Whiteway	
_____	Supervisor
Dr. Alisa Piekny	

Approved by _____
Dr. Robert Weladji, Graduate Program Director

_____ 2018 _____
Dean of Faculty

ABSTRACT

Studying the role of Ran-GTP in cytokinesis in *C. elegans* embryos

Imge Özügergin

Cytokinesis is a well-conserved process where one cell divides into two daughters, and must be tightly regulated to prevent aneuploidy and fate changes. The mitotic spindle regulates the assembly and ingression of an actomyosin ring that pinches in the cortex. Though less understood, microtubule-independent mechanisms also regulate cytokinesis and their requirement may vary depending on cell type. Our lab discovered that a novel chromatin pathway signals through Ran-GTP to regulate cytokinesis in human cells, and my thesis explored the biological relevance of this pathway in *Caenorhabditis elegans* embryos. Our model is that importin-alpha or beta forms an inverse gradient to Ran-GTP and facilitates the recruitment and/or activation of contractile regulators. To test this model, I explored the requirement of the Ran pathway in regulating cytokinesis of P₀ (one-celled zygote), AB (anterior daughter) and P₁ (posterior daughter fated to be germline) cells. I found that each cell has unique ingression kinetics, and reducing Ran-GTP by partial RNAi of RCC-1 (Ran-GEF) increased their rate of ingression. Through co-depletion experiments, I found that the Ran pathway regulates ANI-1 (anillin) in P₀ and AB cells, but not in P₁ cells. Anillin is a scaffold that coordinates cytokinesis and is directly regulated by importin in human cells. I also found that regulators of contractility, such as ECT-2 (RhoA GEF) and LET-502 (Rho binding kinase) are in the Ran pathway in P₀, AB and P₁ cells. Thus, the Ran pathway regulates cytokinesis in all cell types, but the molecular effectors vary depending on cell type.

Acknowledgements

Above all, I would like to thank my supervisor, Dr. Alisa Piekny, for taking a chance on me and putting me on this project. Without you, I would not be here. I feel privileged to be under your tutelage, and there are no words to properly thank you for your selfless time, care and guidance.

I would also like to thank my committee members Dr, Malcolm Whiteway, Dr. Michael Sacher and Dr. Aashiq Kachroo for bearing through all the graphs in this thesis, and for their time and support throughout this project.

In addition, I would like to thank *The Centre for Microscopy and Cellular Imaging* (CMCI), and Dr. Chris Law especially for his help, valuable input and contributions. It has been a huge help to have someone with your knowledge and skill to run ideas by.

Lastly, I'd like to thank the other Piekny lab members. Karina, thanks for showing me the ropes before I knew an L1 from an L4. Brittany, it's been a while, but your encouragement has not been forgotten. Victoria, many thanks for being a genuinely cheerful helping hand. Nhat, Kevin, Noha, Mathieu – you all make work a better place to be. Your support and friendship, on good days but more importantly the bad days, has been invaluable to me and has kept me going.

Dedications

This thesis is dedicated to my family (who is officially and unequivocally the best). To my mom, the cheerleader, thank you for being eternally and ceaselessly interested in me and my work. To my dad, the ultimate problem-solver, thank you for reminding me “Serenity Now!”, and, let’s be honest, for the laptop. To my sister, I still think you should have chosen a less depressing field, but I am immensely proud of you. Our commiseration sessions have gotten me through. A special thank you to my grandparents, who showed great selflessness in supporting me moving away, yet again. And lastly, to Caniko, I would have run for the hills were it not for your support. As a token of appreciation, you do not have to read past this page.

Contribution of Authors

Figure 7. Karina Mastronardi and I both contributed to the time-lapse images. Dr. Chris Law plotted the heat maps.

Figure 8: Karina Mastronardi and I both contributed to the time-lapse images. Dr. Chris Law plotted the heat maps.

Figure 9: Dr. Chris Law plotted the heat maps.

Figure 10: Dr. Chris Law plotted the heat maps.

Figure 11: Karina Mastronardi contributed the time-lapse images.

Figure 12: Dr. Chris Law plotted the heat maps.

Figure 13: Dr. Chris Law plotted the heat maps.

Figure 14: Dr. Chris Law plotted the heat maps.

Figure 15: Dr. Chris Law plotted the heat maps.

Figure 16: Dr. Chris Law plotted the heat maps.

Figure 17: Dr. Chris Law plotted the heat maps.

Figure 18: Dr. Chris Law plotted the heat maps.

Figure 19: Dr. Chris Law plotted the heat maps.

Figure 20: Model drawn by Daniel Beaudet.

Table of Contents

Chapter 1: Introduction.....	1
1.1 Cytokinesis.....	1
1.1.1 Microtubule-dependent pathways of regulation	6
1.1.1.1 Central spindle pathway.....	8
1.1.1.2 Astral pathways	9
1.1.2 Microtubule-independent pathways of regulation	10
1.1.2.1 The Ran pathway	12
1.2 <i>C. elegans</i>	16
1.2.1 <i>C. elegans</i> as a model organism.....	16
1.2.2 Role of asymmetric division in establishment of polarity and cell fate.....	16
1.2.3 <i>C. elegans</i> contractile ring: its inherent asymmetry and model of kinetics	19
1.3 Summary.....	21
Chapter 2: Methods	22
2.1 Strains and alleles	22
2.2 RNA interference.....	23
2.3 Microscopy.....	24
2.4 Data analysis	24
2.4.1 Image analysis.....	24
2.4.2 Quantitative data analysis	25

Chapter 3: Results	30
3.1 Ran-GTP influences cortical activity during anaphase in early <i>C. elegans</i> embryos..	30
3.1.1 P ₀ , AB and P ₁ cells have different ingressin kinetics in control embryos ..	30
3.1.2 Ingression kinetics are altered in P ₀ , AB and P ₁ cells in <i>ran-3</i> and <i>ima-3</i> embryos	33
3.1.3 ANI-1 could be a target of the Ran pathway in P ₀ and AB cells	41
3.1.4 ECT-2 could be in the Ran pathway in P ₀ , AB and P ₁ cells	49
3.1.5 LET-502 has different threshold requirements in P ₁ cells, and is Ran-dependent in P ₀ , AB and P ₁ cells	56
3.2 Ingression kinetics is cell-fate dependent	59
3.3 Ran-GTP influences the correlation between ingressin and cell size in early <i>C. elegans</i> embryos.....	63
Chapter 4: Discussion	69
Chapter 5: References	77

List of Figures

Figure 1: Graphical summary of cytokinesis	3
Figure 2: Localization of anillin and structure of anillin homologues.....	5
Figure 3: Microtubule-dependent and -independent regulation of cytokinesis.....	7
Figure 4: Cartoon schematic of the ‘free’ importin gradient in a cell	14
Figure 5: Division of the early <i>C. elegans</i> embryo.....	17
Figure 6: Determining phase duration with tangents.....	27
Figure 7: Characterization of control P ₀ divisions.....	31
Figure 8: Characterization of control AB and P ₁ divisions.....	34
Figure 9: <i>ran-3</i> causes P ₀ , AB and P ₁ cells to initiate and ingress sooner.....	37
Figure 10: <i>ima-3</i> causes hypercontractility in divisions	39
Figure 11: A mild decrease in Ran-GTP does not alter the spindle or polarity	42
Figure 12: Ingression in <i>ani-1</i> embryos is delayed.....	44
Figure 13: ANI-1 could be in the Ran pathway in P ₀ and AB cells	46
Figure 14: Ingression in <i>ect-2</i> embryos is delayed	51
Figure 15: ECT-2 could be in the Ran pathway in all cells	53
Figure 16: Ingression in <i>let-502</i> embryos is delayed.....	57
Figure 17: LET-502 may be in the Ran pathway in all cells.....	60
Figure 18: Switching cell fate changes ingression kinetics.....	64
Figure 19: Decreasing Ran-GTP increases the correlation between ingression and cell size.....	67
Figure 20: Model for the Ran regulation of cytokinesis	76

Chapter 1: Introduction

This project uses the soil nematode *Caenorhabditis elegans* as a model organism to study the Ran regulation of cytokinesis *in vivo*. Recent studies in our lab uncovered a novel mode of cytokinesis regulation in cultured human cells, whereby chromatin provides a cue in the form of active Ran that modulates the activity of cortical proteins. Our goal is to determine if this pathway is conserved in metazoans using *C. elegans* as a model, and study the biological relevance for this pathway *in vivo*. The invariant cell lineage of *C. elegans* is very well described, and the highly stereotypical, reproducible divisions allow the easy detection of deviations from wild-type. In addition to being amenable to RNAi, transgenics and live imaging, 60-80% of *C. elegans* genes have human homologues, including key regulators of cytokinesis and the Ran pathway, which are the focus of this thesis (Bamba et al., 2002; Askjaer et al., 2002; Kaletta and Hengartner, 2006; Lundquist, 2006). The introductory chapter of this thesis will first provide a general review of cytokinesis in mammalian cells and *C. elegans*, followed by an overview of early *C. elegans* embryonic development. The chapter will then conclude with a brief overview of our findings.

1.1 Cytokinesis

Cytokinesis, the final step of mitosis, is the physical separation of a cell into two daughter cells. It is a highly conserved process that must be tightly regulated both in time and space to avoid aneuploidy and changes in cell fate (Green et al., 2012; Glotzer, 2017). In early anaphase, actomyosin filaments assemble at a broad region of the cortex and then transition into a tight contractile ring, which is the main structure that drives cytokinesis in metazoans (D'avino et al., 2015; Beaudet et al., 2017; Glotzer, 2017). The ring is assembled just below the plasma

membrane in a plane perpendicular to the spindle and forms the division plane (Oliferenko et al., 2009; Fededa and Gerlich, 2012). As the ring constricts, it pulls in the attached cortex and forms an ingressing furrow, followed by its transition to a midbody ring and abscission (Fededa and Gerlich, 2012). A graphic summary of cytokinesis is shown in Figure 1.

The division plane must be aligned with the mitotic spindle to ensure the equal distribution of genomic content, and correct partitioning of cytoplasmic material into the daughter cells (D'avino et al., 2015; Petry, 2016; Glotzer, 2017). The prevailing dogma in the field is that the anaphase spindle determines the division plane of cytokinesis by directing the assembly and ingression of the contractile ring (Bement et al., 2005; Piekny et al., 2005; Green et al., 2012), however signals from other cellular components have also been shown to affect the localization of contractile proteins (e.g., von Dassow et al., 2009; Sedzinski et al., 2011; Kiyomitsu and Cheeseman, 2013; Rodrigues et al., 2015).

Although the mechanism of contractile ring assembly is not fully understood, the role of key players is well-described. Actin and myosin are the main components of the contractile ring (D'avino et al., 2015; Glotzer, 2017). Active RhoA mediates contractile ring assembly through its effectors, including formin and Rho kinase (ROCK or RhoK; *C. elegans* LET-502) (D'avino et al., 2015; Glotzer, 2017). Formin (*C. elegans* CYK-1) and profilin stimulate actin polymerization to form unbranched F-actin (Severson et al., 2002; Piekny et al., 2005). Rho kinase (ROCK; *C. elegans* LET-502) phosphorylates the regulatory light chain of nonmuscle myosin for filament assembly and to regulate its activity for ingression (Piekny and Mains, 2002). Other proteins associate with and regulate the contractile ring. One of these proteins is anillin, a highly conserved scaffold protein that serves as a link between the actomyosin cortex, plasma membrane and microtubules (MTs) to position the ring (Piekny and Glotzer, 2008; Piekny and

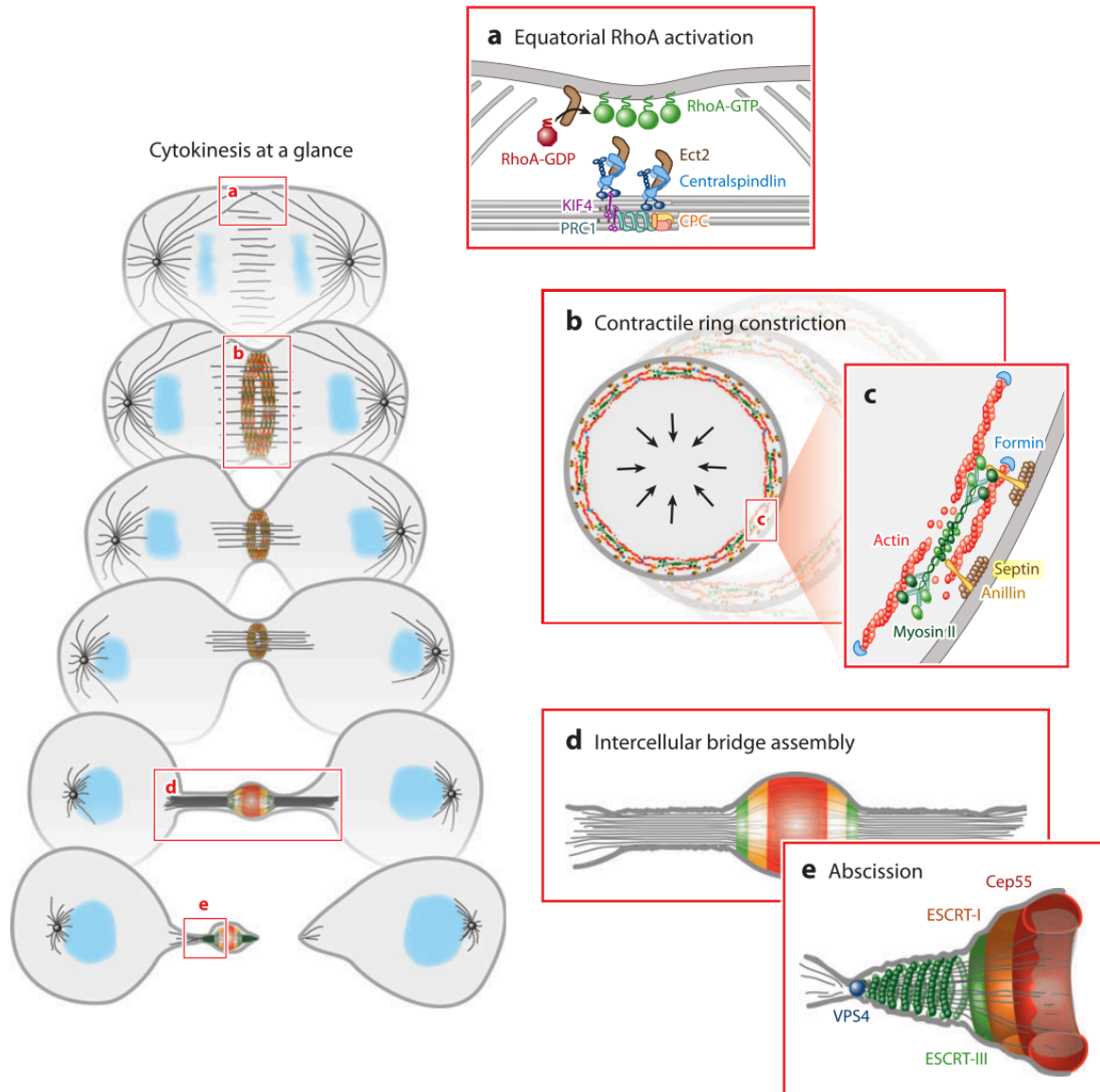


Figure 1. Graphical summary of cytokinesis. A) An active zone of RhoA is generated at the equatorial zone of the cell. This occurs through a combination of positive signaling from the central spindle (via Ect2), and negative signaling from the astral microtubules (MTs). B) Active RhoA coordinates the assembly of the actomyosin ring. C) The contractile ring is made up of filamentous actin (F-actin; nucleated by formin) and myosin and is anchored to the membrane by anillin, which also recruits the membrane-associated filament, septin. D) In abscission, the final stage of cytokinesis, the contractile ring forms the midbody, which organizes an intercellular bridge. E) An ESCRT-III mediated process generates two daughter cells by membrane scission occurring on either flanking side of the midbody. Figure taken from Green et al., 2012.

Maddox, 2010; Beaudet et al., 2017). Anillin directly binds and is recruited by active RhoA. It also has binding domains for F-actin, myosin, septins, phospholipids and MTs (Piekny and Maddox, 2010; Green et al., 2012). While anillin is essential for cytokinesis in *Xenopus* embryos, *C. elegans* neuroblasts, *Drosophila* cells and cultured mammalian cells, it is not clear if it is required for cytokinesis in the early *C. elegans* embryo (Maddox et al., 2007; Straight et al., 2005; Wernike et al., 2014). Part of this discrepancy is due to limitations with the model system – it is impossible to have complete knockdown of the *C. elegans* homologue ANI-1 in the early embryo due to its requirement in the germline, and the threshold may be different in the early embryo due to redundancy with other pathways that ensure cytokinesis is robust. *C. elegans* has two other anillin homologues, ANI-2 and ANI-3, which will not be further discussed since ANI-2 does not function in the early embryo and ANI-3 has no known function (**Figure 2**; Maddox et al., 2005).

The mechanisms mediating contractile ring constriction vary depending on the cell. The first model is based on force generation through myosin motor activity: contractility is achieved through a sliding filament mechanism similar to muscle, where motor heads walk along actin filaments. The regulatory light chain of non-muscle myosin is phosphorylated by Rho kinase (ROCK) to promote their assembly into bipolar filaments. Through ATP hydrolysis, the motor heads at either end of the bipolar myosin filament associate with F-actin and attempt to walk towards their plus ends, causing the filaments to generate force and ring constriction. The second model is based on changes in cortical properties through crosslinking F-actin: many different crosslinkers, such as anillin, septin and myosin have unique ways of crosslinking neighboring actin filaments to generate different types of cortical tension in the equatorial plane, and the

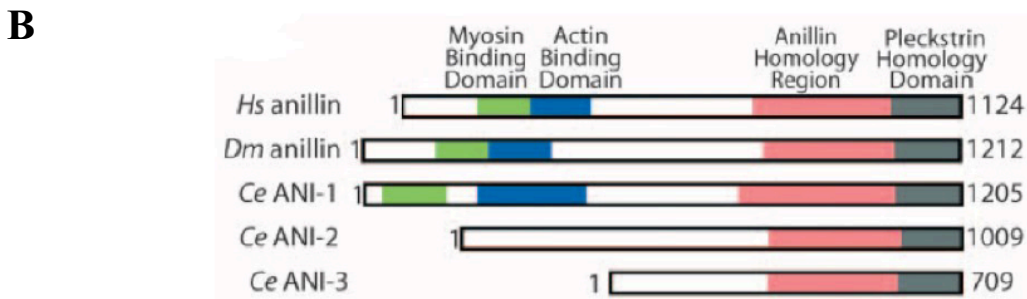
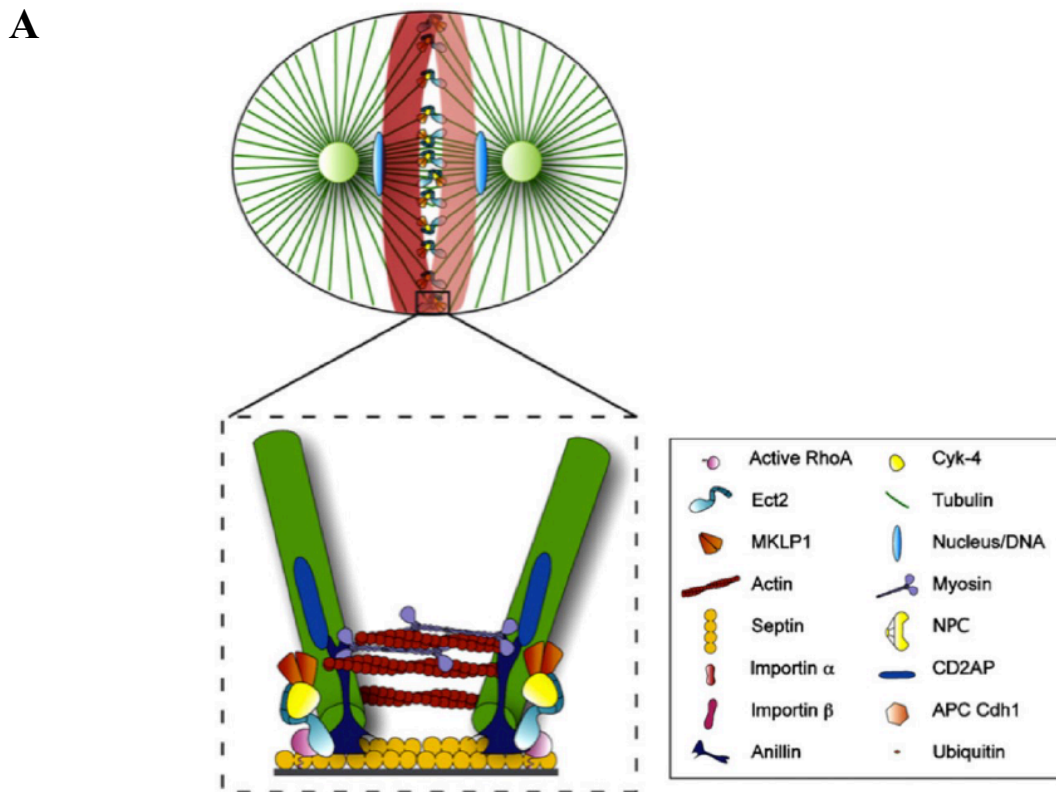


Figure 2. Localization of anillin and structure of anillin homologues. A) A cartoon schematic of a cell in anaphase, with the inset showing anillin acting as a scaffold for its binding partners at the contractile ring (depicted by the red ring in the cell). B) Structure of human, *Drosophila melanogaster* and *C. elegans* anillin. Binding domains are highlighted: N-terminal myosin-binding (green) and actin-binding (blue) domains, C-terminal anillin homology regions (red), and pleckstrin homology (PH) domains. The AHD of human anillin and ANI-1 contains a C-terminal NLS. Figures taken from Piekny and Maddox, 2010 (A), and Maddox et al., 2005 (B).

depolymerization of actin filaments drives ingression of the ring (Mendes et al., 2013; Descovich et al., 2017; Heer and Martin, 2017).

Multiple MT-dependent and -independent pathways work together to regulate cytokinesis and have varying levels of importance depending on cell architecture, fate, and spindle morphology (**Figure 3**; Dechant and Glotzer, 2003; Murthy and Wadsworth, 2008; Basant et al., 2015; Price and Rose, 2017).

1.1.1 Microtubule (MT)-dependent pathways regulating cytokinesis

The anaphase spindle is one of the main regulators of cytokinesis. It consists of astral MTs, which emanate from the centrosomes toward the cortex, and the central spindle, which are antiparallel bundled MTs that arise between segregating chromatids in anaphase (Fededa and Gerlich, 2012). Both sets of MTs position the division plane, and the current model is that the central spindle promotes contractility, whereas astral MTs inhibit contractility at the cell poles (Fededa and Gerlich, 2012; van Oostende Triplet et al., 2014; D'avino et al., 2015). Promoting contractility at the cell equator while inhibiting it at the cell poles creates a narrow zone in the equator to mediate ingression (Zanin et al., 2013; van Oostende Triplet et al., 2014). The requirement for astral and/or central spindle pathways varies among cell types and organisms, and likely depends on spindle morphology, cell size or shape. For example, early *C. elegans* embryos have spindles with large asters, which dominantly regulate contractile ring assembly (D'avino et al., 2015).

The model for how cytokinesis is regulated by MTs in the *C. elegans* embryo can be split into early anaphase and late anaphase/early telophase (Lewellyn et al., 2010). In early anaphase, aster-mediated inhibition refines active myosin to a broad equatorial region (Tse et al., 2011).

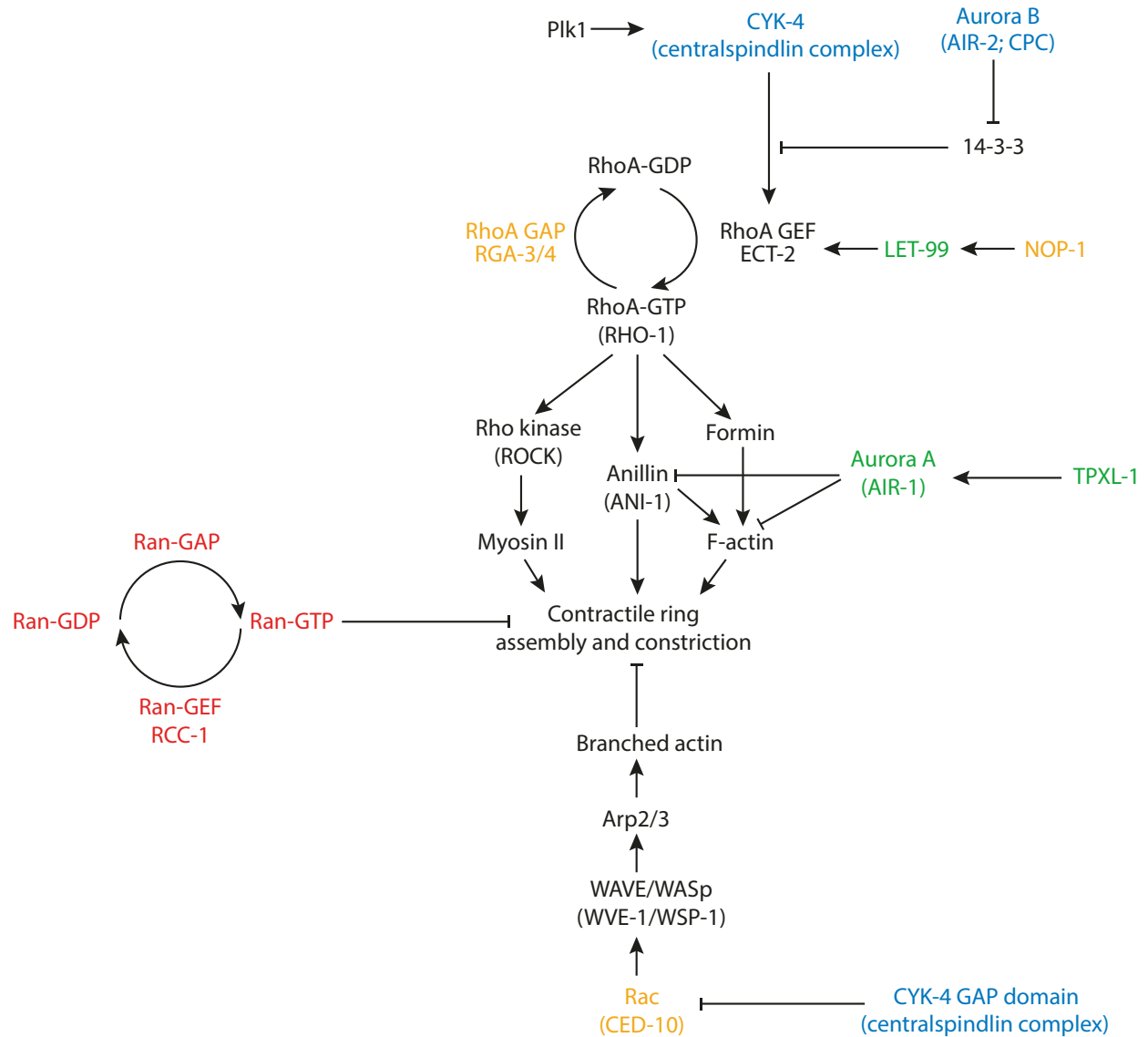


Figure 3. MT-dependent and -independent regulation of cytokinesis. Key pathways that regulate cytokinesis are shown. They can be divided into MT-dependent (central spindle; blue, and astral; green) pathways, and MT-independent (Ran pathway; red, cortical; orange) pathways. Mitotic spindle MTs stimulate ring assembly via the central spindle pathway (CYK-4, AIR-2) or inhibit assembly via the astral pathways (TPXL-1). MT-independent pathways include the chromatin-associated Ran-GTP pathway, where Ran-GTP and importin (not shown) gradients function as a molecular ruler to ensure optimal ring assembly or placement. Abbreviations: CPC (chromosomal passenger complex).

Then, in late anaphase/early telophase, the central spindle promotes the coalescence and ingression of the contractile ring (Lewellyn et al., 2010).

1.1.1.1 Central spindle pathway

The central spindle generates active RhoA in the equatorial cortex. The centralspindlin complex, a heterotetramer composed of MKLP1/ZEN-4 and Cyk-4/CYK-4 bundles microtubules and recruits Ect2/ECT-2, the RhoGEF to the equatorial plane. Cdk1-mediated phosphorylation of Ect2 causes it to form an autoinhibited conformation that prevents it from binding to Cyk-4 or being recruited to the plasma membrane until Cdk1 activity drops in anaphase (Yüce et al., 2005; Hara et al., 2006; Green et al., 2012). In addition, Polo-like kinase 1 (Plk1) phosphorylates Cyk-4, permitting it to form a complex with Ect2 (Petronczki et al., 2007; Wolfe et al., 2009; Glotzer, 2017). This temporally couples RhoA activation with mitotic exit. Other proteins also help regulate Cyk-4/Ect2 complexes at the cortex. For example, the inhibition of a protein called 14-3-3 permits the plasma membrane recruitment of Cyk4 via its membrane-binding C1 domain, where it helps activate RhoA by binding to Ect2 (Yüce et al., 2005; Petronczki et al., 2007; Lekomtsev et al., 2012; Basant et al., 2015; Kotynkova et al., 2016). The clustering of centralspindlin is regulated by the antagonistic interplay between Aurora B kinase and 14-3-3 (Douglas et al., 2010; Basant et al., 2015). 14-3-3 is found uniformly in the cytoplasm and on the cortex (Morton et al., 2002; Rose and Gönczy, 2014). When bound to 14-3-3, centralspindlin is cytosolic, but when another complex called the CPC localizes to the central spindle and cortex during anaphase, it inhibits 14-3-3 activity. This results in the recruitment of centralspindlin to the central spindle and overlying cortex. The localization of centralspindlin to the plasma membrane is crucial because this is where active RhoA needs to be generated for contractile ring

assembly and ingression. The central spindle is quite small and centrally positioned far from the cortex in the early *C. elegans* embryo, and the cortical localization of centralspindlin is essential to control active RhoA for cytokinesis (Lekomtsev et al., 2012; Basant et al., 2015; Kotynkova et al., 2016).

1.1.1.2 Astral pathways

Astral MTs have been shown to inhibit polar contractility, since promoting their depolymerization leads to ectopic activation of RhoA and an increase in the breadth of contractile proteins (Murthy and Wadsworth, 2008; van Oostende Triplet et al., 2014). Although it is not clear how astral MTs do this, several mechanisms have been proposed. One model for the aster-mediated regulation of cytokinesis is the local sequestering of anillin by MTs, which inhibits anillin localization at the cortex to create cortical domains with different contractile properties (Tse et al., 2011). This supports the observation that ingression is promoted in regions with the lowest MT density (Dechant and Glotzer, 2003). Studies have demonstrated that anillin promotes the cortical recruitment and stabilization of myosin, therefore the binding of anillin by astral MTs creates a difference in cortical anillin between the polar regions vs. equatorial zone of the embryo (Tse et al., 2011).

Other astral pathway components in *C. elegans* include LET-99, which is a cortical protein important for spindle positioning (Bringmann et al., 2007; Price and Rose, 2017). LET-99 is hypothesized to promote division by binding to or acting as a scaffold for RhoA, thereby promoting ring assembly and ingression (Price and Rose, 2017). In anaphase, LET-99 localizes as a band around the posterior cortex, which shifts to align with the ingressing furrow, and is regulated by the mitotic spindle (Price and Rose, 2017).

Another mechanism for the polar clearance of contractile proteins via astral MTs may occur via Aurora A kinase (Mangal et al., 2018). TPXL-1 (*C. elegans* homologue of TPX2) regulates the activity and localization of AIR-1 (*C. elegans* Aurora A kinase) at the minus ends of astral MTs (Mangal et al., 2018). The activation of AIR-1 is linked to the clearance of anillin and F-actin from the nearby polar cortex (Mangal et al., 2018). The proposed model is that during anaphase, TPXL-1 binds to centrosomal MTs where it recruits and activates AIR-1, which could relocate and/or create a gradient of kinase activity that can influence the nearby cortex. For example, AIR-1 could phosphorylate proteins at the cortex, causing a change in their function that suppresses contractility at the cell poles (Mangal et al., 2018). However, there is no biochemical evidence to support this model and it is not known if this pathway is conserved in other metazoans.

1.1.2 MT-independent pathways regulating cytokinesis

A variety of MT-independent pathways have also been found to regulate cytokinesis. These pathways may play redundant roles in symmetrically dividing cells, but may be essential in polarized cells. Some of these pathways rely more strictly on the cortex, centrosomes, kinetochores, and/or chromosomes (Dechant and Glotzer, 2003; Deng et al., 2007; Petronczki et al., 2007; Silverman-Gavrila et al., 2008; Cabernard et al., 2010; Kiyomitsu and Cheeseman, 2013; Zanin et al., 2013; Rodrigues et al., 2015; Beaudet et al., 2017).

Several cortical mechanisms enrich actomyosin filaments in the equatorial plane for cytokinesis. The M phase GAP (MPGAP or RGA-3/4 in *C. elegans*) localizes to the cortex and globally downregulates RhoA, and this inhibition is overcome by Ect2 in the equatorial plane (Schmutz et al., 2007; Zanin et al., 2013). This leads to different types of F-actin, which are long

and unbranched equatorially vs. short and branched at the poles. The regulation of Rac (*C. elegans* CED-10), a member of the Rho family of GTPases, provides another type of MT-independent regulation of the cortex (Canman et al., 2008). Active Rac gives rise to branched actin filaments through the WAVE/WASp complex and regulation of Arp2/3 (*C. elegans* WVE-1/WSP-1). In the equatorial plane, Rac is inactivated by the GAP-activity of Cyk-4, which prevents these filaments from being formed. The presence of branched actin filaments hinders ring constriction, possibly by acting as a physical barrier against constriction, or by competing for contractile ring components (Canman et al., 2008; Saenz-Narciso et al., 2016). However, it is not clear if a reduction in Rac activity is required in the equatorial plane, or if it needs to be active at the cell poles.

In early *C. elegans* embryos, ECT-2, which regulates RhoA activity, is regulated by both CYK-4 and NOP-1 (NO Pseudocleavage) (Tse et al., 2012). NOP-1 is a novel, maternal protein with no known homologues and localizes to the cytoplasm and ingressing furrow in the early embryo. It is not essential for cytokinesis but is required for contractility during pseudocleavage and causes strong cytokinesis defects when depleted in combination with *ani-1* (Tse et al., 2012). The cortical recruitment of myosin and ANI-1, as well as the organization of F-actin is dependent on NOP-1 activity (Tse et al., 2012). Although the molecular mechanism of NOP-1 has not been determined, it is postulated that it directly regulates ECT-2 (Tse et al., 2012).

Kinetochores also have been shown to provide signals for cytokinesis (Rodrigues et al., 2015). The regulatory subunit Sds22 of PP1 phosphatase recruits the complex to kinetochores where it dephosphorylates and inactivates ezrin/radixin/moesin (ERM) proteins (Rodrigues et al., 2015). ERM proteins are cytoskeletal regulators with FERM domains that crosslink F-actin to the membrane (Roubinet et al., 2011). During early anaphase, as the chromosomes start to

segregate toward the poles, PP1 dephosphorylation of ERM at the cell poles softens the cortex to enable anaphase cell elongation (Rodrigues et al., 2015). However, this pathway is only functional for a very short period of time during early anaphase and is not essential for cytokinesis.

1.1.2.1 The Ran pathway

Another MT-independent mechanism regulating cytokinesis involves a Ran-GTP gradient formed around chromatin (Kiyomitsu and Cheeseman, 2013; Beaudet et al., 2017). In interphase cells, the Ran-GTP gradient controls nucleocytoplasmic transport (Moore and Blobel, 1993; Xu and Massagué, 2004). In the cytosol, importin-alpha and/or beta bind to cargo containing nuclear localization signals (NLS) and transports the cargo into the nucleus (Xu and Massagué, 2004). Once inside the nucleus, Ran-GTP binds to importins causing them to release the cargo (Görlich et al., 1996). The RanGEF RCC-1 is tethered to chromatin, and generates high Ran-GTP in the nucleus, while the RanGAP is in the cytosol and stimulates hydrolysis to Ran-GDP (Xu and Massagué, 2004). After nuclear envelope breakdown, the Ran-GTP gradient persists until early telophase, when the envelope begins to re-assemble (Kalab et al., 2002; Kalab et al., 2006; Clarke and Zhang, 2008; Kalab and Heald, 2008). During metaphase, high Ran-GTP near chromatin promotes the release of spindle assembly factors (SAFs) from importins (Kalab et al., 2002; Kalab et al., 2006; Clarke and Zhang, 2008; Kalab and Heald, 2008). The SAFs then form active complexes to nucleate and organize MTs (Kalab et al., 2002; Kalab et al., 2006; Clarke and Zhang, 2008; Kalab and Heald, 2008). In this way, Ran-GTP promotes spindle assembly in the vicinity of chromosomes. However, recent studies suggest that SAFs could be differently regulated depending on how they bind to importins.

Our lab found that Ran-GTP also regulates the cortex for cytokinesis (Beaudet et al., 2017). A gradient of importins ‘free’ from Ran-GTP form with high levels near the cortex and lower levels in the vicinity of chromatin (**Figure 4**; Clarke and Zhang, 2008). We found that anillin has an NLS that binds to importin-beta, which regulates the cortical localization of anillin (Beaudet et al., 2017). Increasing the levels of Ran-GTP, or mutating the NLS in anillin cause a decrease in anillin in the equatorial furrow and cytokinesis phenotypes (Beaudet et al., 2017). We propose that importin-beta stabilizes an open conformation of anillin that makes it more accessible to the cortex. However, we also found that high over-expression of importin-beta also decreases anillin’s cortical localization, suggesting that there is an ideal concentration of importin-beta that facilitates vs. hinders anillin function (Beaudet et al., 2017). This supports a model where the importin gradient functions as a molecular ruler to control placement of the contractile ring to ensure that it forms between segregating chromosomes.

Our findings reconcile two opposing theories as to how Ran-GTP regulates the cortex in cytokinesis (Kiyomitsu and Cheeseman, 2013; Silverman-Gavrila et al., 2008). An earlier study showed that importins could regulate anillin function during cellularization in *Drosophila* embryos (Silverman-Gavrila et. al, 2008). This process is when membranes ingress around syncytial nuclei. They found that over-expression of importin-alpha outcompeted binding of anillin to septins, causing a decrease in the cortical localization of anillin (Silverman-Gavrila et. al, 2008). They proposed a model where in the vicinity of nuclei, high Ran-GTP promotes the release of importins from anillin, so it can bind to septins for its cortical recruitment (Silverman-Gavrila et. al, 2008). However, there were many issues with this model. First, anillin was not recruited close to nuclei, and second the entire study was based on over-expression vs. loss-of-

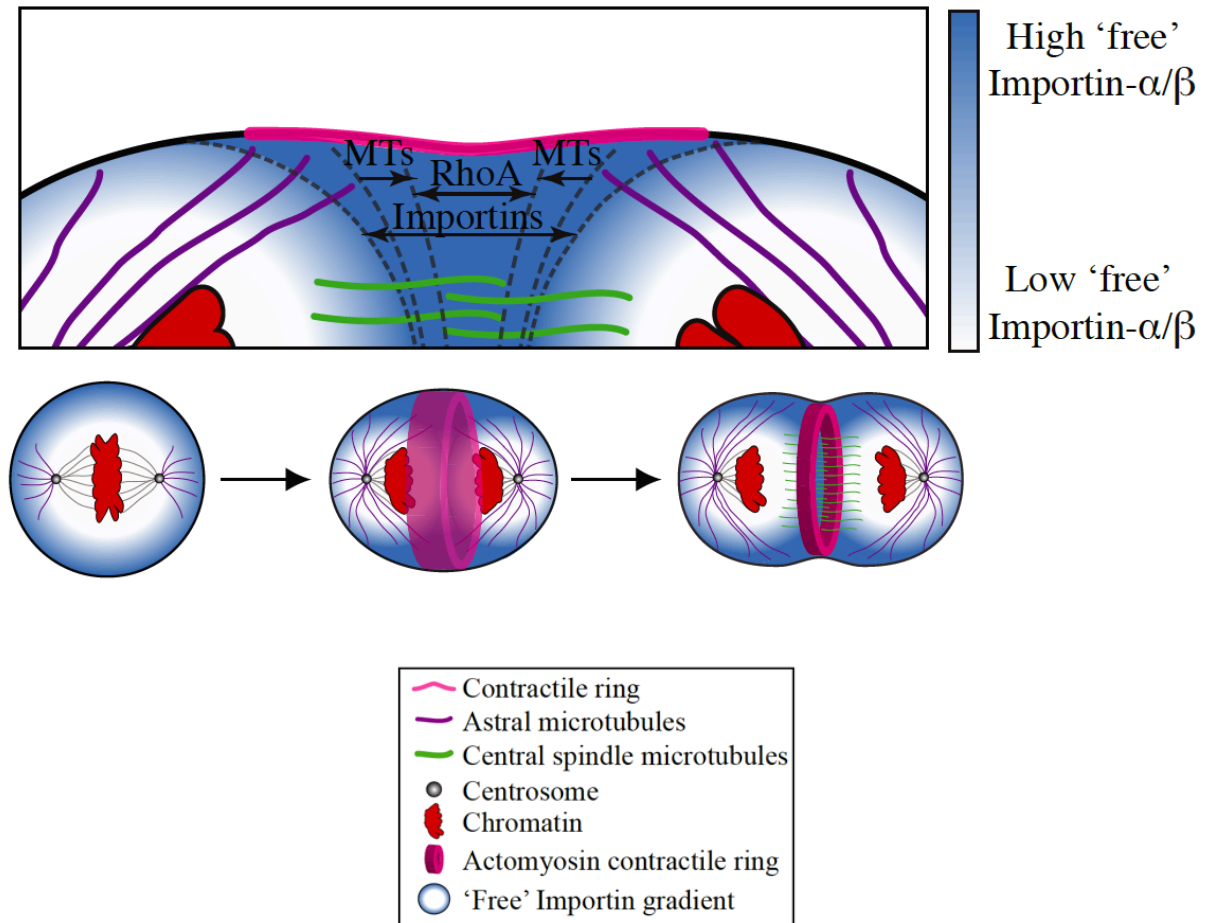


Figure 4. Cartoon schematic of the importin gradient in a cell. During anaphase, a gradient of importins 'free' from Ran-GTP forms with higher levels (dark blue) near the cortex and lower levels (white) in the vicinity of chromatin (red). Importin-alpha or beta near the cortex could bind to and influence the localization of contractile ring components (pink). This pathway works in concert with mitotic spindle pathways (green and purple MTs) that control active RhoA in the equatorial plane. Figure adapted from Beaudet et al., 2017.

function studies. In another study in mammalian cells, Ran-GTP was shown to inhibit the cortical localization of contractile proteins, such as anillin (Kiyomitsu and Cheeseman, 2013).

In cells lacking MTs, contractile proteins failed to accumulate at the cortex close to chromatin and if Ran-GTP was reduced, they recovered (Kiyomitsu and Cheeseman, 2013). This study showed that there was a correlation with chromatin position and elongation of the cortex during anaphase (Kiyomitsu and Cheeseman, 2013). Thus, they proposed a model where chromatin-enriched Ran-GTP inhibits the recruitment of cortical proteins when the mitotic spindle shifts too close to part of the cortex to permit recovery of the division plane (Kiyomitsu and Cheeseman, 2013). However, this study did not explore the molecular mechanism by which the Ran pathway regulates the cortex.

The advantage of a model whereby the importin gradient acts as a molecular ruler to regulate the cortex is that it provides plasticity to cells. If chromatin position changes, the cortex can rapidly respond. If the spindle is perturbed, this can provide a back-up system to ensure that chromosomes are properly inherited by the daughter cells. It can also ensure a robust division plane in cells with altered size, ploidy, or geometry. We also postulate that the Ran pathway regulates multiple cortical regulators vs. only anillin. For example, Ect2 contains a conserved NLS in the middle of the protein, and is located nearby the phosphorylation site for Cdk1 regulation of Ect2 autoinhibition (Hara et al., 2006). An exciting hypothesis is that importin binding could stabilize the open conformation of Ect2 to control RhoA activity.

Importantly, the biological relevance of the Ran pathway in regulating cytokinesis needs to be tested *in vivo*. For example, is it essential in smaller cells or polarized cells where chromatin is positioned closer to the cortex vs. larger cells? Does the requirement vary depending on cell fate, based on the expression of different pathways? Also, it is crucial to

establish a genetic model system where molecular components of the Ran pathway can be identified. To address some of these questions my thesis involved testing the role of the Ran pathway in cytokinesis in *C. elegans* embryos.

1.2 *C. elegans*

1.2.1 *C. elegans* as a model organism

C. elegans is a well-established genetic model amenable to transgenics, and its transparency lends itself to cell division studies and fluorescence microscopy. The invariant cell lineage was determined by John Sulston, and the highly stereotypical divisions allow for the detection of those that deviate from wild-type. In addition, genes of interest can be knocked down by RNAi using simple protocols involving the feeding of bacteria expressing double-stranded RNA (dsRNA) (Brenner, 1974; Riddle et al., 1997, Corsi et al., 2015). *C. elegans* homologues for 60-80% of human genes have been identified, including components of the Ran pathway – the focus of this thesis (Bamba et al., 2002; Askjaer et al., 2002; Kaletta and Hengartner, 2006; Lundquist, 2006).

1.2.2 Role of asymmetric division in establishment of polarity and cell fate

Proper establishment of cell fate and polarity are crucial aspects of early embryonic development (Rose and Gönczy, 2014). Asymmetric division is an important mechanism by which cell fates are correctly established in the embryo (Hawkins and Garriga, 1998; Rose and Gönczy, 2014). Six founder cells give rise to the different tissues; the AB, MS, E, C, D and P₄ cells. These cells are generated through five asymmetric divisions, as detailed in Figure 5. This research project focuses on the first three divisions (P₀, AB and P₁).

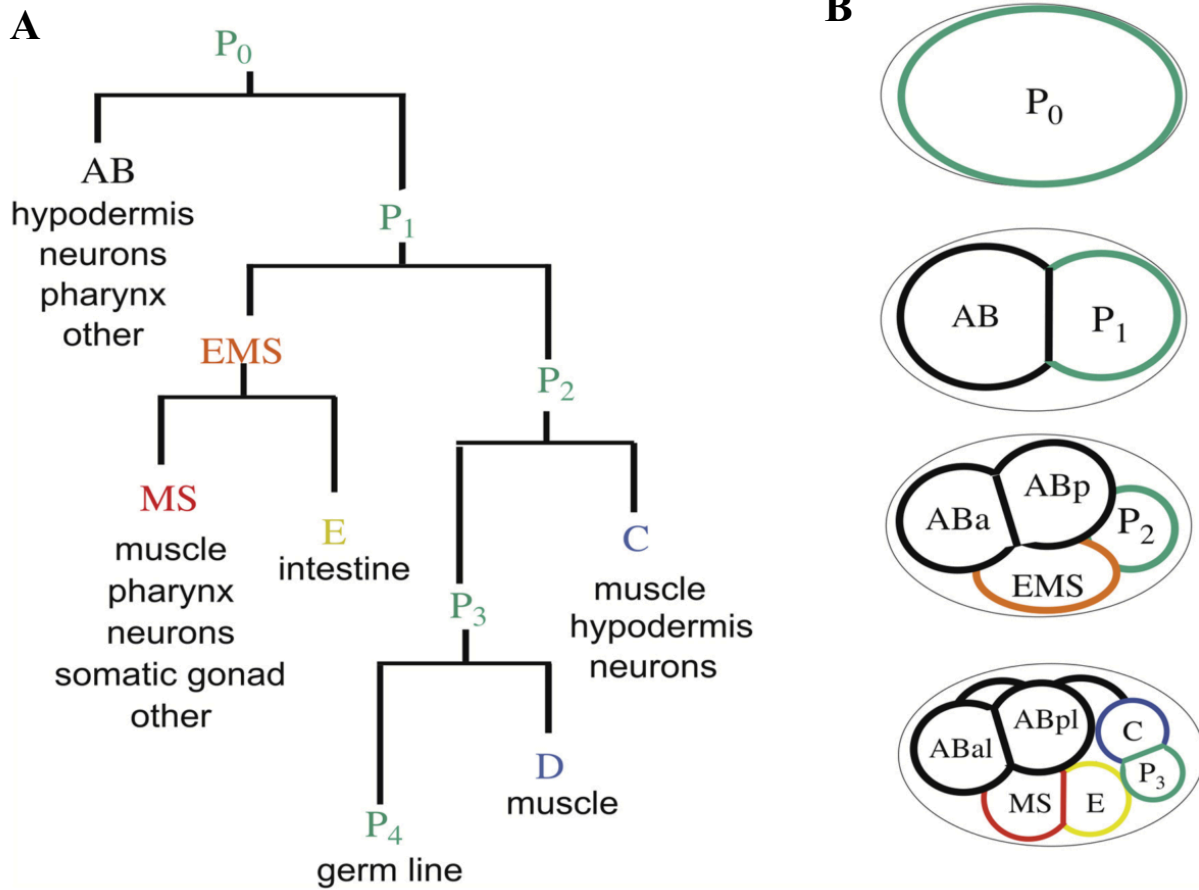


Figure 5. Division of the early *C. elegans* embryo. A) Diagram showing the invariant cell lineage of the early embryo. Horizontal lines represent sister cells arising from one division, and the length of the vertical line represents the duration of the cell cycle. B) Diagram shows the symmetric (black) and asymmetric (color) division of the early embryo that generate the founder cells. The germ-line precursor P cells are in green. As is convention, anterior is to the left of the image, posterior to the left, dorsal up and ventral down. ABa: AB anterior daughter, ABp: AB posterior daughter; ABal: ABa left daughter; ABpl: AB posterior left daughter. Figure taken from Rose and Gönczy, 2014.

The first division (P_0) divides the zygote into a larger anterior blastomere called the AB cell, and a smaller posterior blastomere called the P_1 cell (Rose and Gönczy, 2014). This first asymmetric division requires symmetry breaking and polarization of the zygote. The posterior of the zygote is determined by the location of sperm entry, which may bring in excess CYK-4 (Wallenfang and Seydoux, 2000; Jenkins et al., 2006; Zonies et al., 2010). CYK-4 locally inactivates RhoA at the posterior to initiate anterior-posterior (AP) polarity (Jenkins et al., 2006). Hence, the initial uniformity of the cortical actomyosin network is broken and mutually inhibitory contractile domains are established: a retracting, contractile anterior domain and an expanding, non-contractile posterior domain (Rose and Gönczy, 2014). PAR (for *partitioning defective*) proteins play a role in symmetry breaking and are required to establish polarity in the zygote (Kemphues et al., 1988; Watts et al., 1996; Morton et al., 2002; Goldstein and Macara, 2007; Rose and Gönczy, 2014). Their fundamental role is carried out through their mutually exclusive, asymmetric cortical localization: the PAR-3/PAR-6/PKC-3 complex remains anteriorly-localized, and PAR-2/PAR-1 is enriched on the posterior cortex (Riddle et al., 1997; Rose and Gönczy, 2014). Establishment of the AP axis also contributes to the asymmetry of division by asymmetric positioning of the mitotic spindle: though formed in the center of the cell, the spindle is displaced towards the posterior of the cell through unequal pulling forces regulated by cortical PAR proteins (Grill et al., 2001; Labbe et al., 2004). In addition to the role of cortical PAR proteins in asymmetric divisions, their AP polarity also enables the formation of cytoplasmic asymmetries/gradients of cell fate regulators, helping to further specify the fate of founder cell descendants (Schubert et al., 2000; Cuenca et al., 2003).

The AB cell divides symmetrically, and its descendants give rise to tissues such as the nervous system, hypodermis and pharynx. The P_1 cell divides asymmetrically likely via similar

mechanisms that regulate AP polarity in the P₀ cell, to produce a P₂ daughter that is fated to become the germline via further rounds of asymmetric divisions. The other P₁ daughter is the EMS cell, which in turn gives rise to the MS and E blastomeres (Gilbert, 2000; Rose and Gönczy, 2014).

Whereas the AB cell divides equatorially and perpendicular to the AP axis, division of the P₁ cell is slightly delayed and occurs after a 90° rotation of the centrosomes in late prophase, causing the spindle to orient longitudinally to the AP axis (Goldstein et al., 1993; Riddle et al., 1997; Rose and Gönczy, 2014). This heterochronicity is thought to be based on AP polarity cues that are determined by PAR proteins, as *par* mutants undergo synchronous divisions (Kemphues et al., 1988; Watts et al., 1996; Goldstein and Macara, 2007). For example, the PAR proteins influence the asymmetric distribution of regulators of cell cycle progression, such as polo-like kinase PLK-1 and cyclin-dependent kinase phosphatase CDC-25, which are enriched in the AB cell (Budirahardja and Gönczy, 2008; Rivers et al., 2008). In addition, higher amounts of DNA replication factors are inherited by the larger AB cell, making them rate limiting in the smaller P₁ cell (Brauchle et al., 2003; Rose and Gönczy, 2014). Collectively, these molecular mechanisms delay the P₁ cell cycle in comparison to the AB cell (Budirahardja and Gönczy, 2008; Rose and Gönczy, 2014).

1.2.3 *C. elegans* contractile ring: its inherent asymmetry and model of kinetics

The contractile ring ingresses asymmetrically in the early embryo. Not to be confused with anterior-posterior polarity – asymmetric ingression refers to the ‘off-centre’ axis of the ring as it constricts. This asymmetry could arise stochastically and provide mechanical advantages for ingression, making cytokinesis more robust (Maddox et al., 2007). The underlying cause for

asymmetric furrowing may be due to the unequal distribution of anillin and septins around the contractile ring (Maddox et al., 2007). It has been proposed that anillin recruits septins and F-actin, which in turn recruits additional anillin to that side of the contractile ring to further enhance the asymmetry of components to one side of the ring (Maddox et al., 2007).

The current model for ring constriction in *C. elegans* takes into consideration several observations: first, the duration of cytokinesis is uniform across cells of different sizes where the large P₀ cell has a faster rate of closure compared to the relatively smaller AB and P₁ cells. This makes the duration of cytokinesis independent of cell size, which could have an impact developmentally and help coordinate the cell cycle. Second, an increase in constriction rate is observed as the ring perimeter decreases, but the concentration of actin and myosin per unit length of the contractile ring remains constant (Carvalho et al., 2009). The proposed model for *C. elegans* ring constriction assumes that the ring consists of individual “contractile units”. These contractile units are of fixed size and function, and are progressively disassembled as the ring constricts. Since the rings of larger cells incorporate proportionally more units, their rate of constriction is proportionally faster than smaller rings of fewer units. The kinetics of constriction occur in two phases: first, there is a constant rate of constriction that decreases linearly with ring perimeter, which is followed by a second phase in which there is a strong negative linear relationship between ring perimeter and the average constriction rate (Carvalho et al., 2009). It is important to note that the measurement of constriction rates that were the basis of these phases were based on data collected every 20 seconds, whereas ingression kinetics described in this thesis are based on five second intervals. This has allowed us to refine the phase definitions of cytokinesis, and hence elucidate the role of Ran in the early phases of cytokinesis.

1.3 Summary

This thesis elucidated the role of Ran-GTP in cytokinesis in early *C. elegans* embryos. By studying cytokinesis in *C. elegans* P₀, AB and P₁ cells with high temporal and spatial resolution, I was able to define three phases after anaphase onset reflecting the different kinetics of cytokinesis: ring assembly (no change), furrow initiation (shallow ingression) and ring constriction. P₀ and P₁ cells have all three phases, however, they are less distinct and more uniform in AB cells. Partially decreasing Ran-GTP by weak RCC-1 RNAi or decreasing importin-alpha by IMA-3 RNAi, increased ingression kinetics in P₀, AB and P₁ cells. Interestingly, P₁ cells also showed a strong delay in prophase, which is not explored in this thesis. The ingression kinetics in P₀ and P₁ cells was suppressed by co-depletion of contractile regulators such as ECT-2 or LET-502, however ANI-1 suppressed kinetics in P₀ and AB cells, but not in P₁ cells. Thus, the Ran pathway regulates cytokinesis through different molecular effectors depending on the cell type. We propose that similar to human cells, Ran-GTP can influence the cortex by regulating the gradient of importins binding to contractile regulators (**Figure 4**). While decreasing Ran-GTP may free more importins for binding to cargo, lowering importin alpha may free importin beta for cargo binding.

Chapter 2: Materials and Methods

2.1 Strains and alleles

C. elegans strains were maintained according to standard protocol (Brenner, 1974) on NGM (Nematode Growth Medium) plates seeded with *E. coli* OP50, kept at 20°C. NGM plates were made by adding 3g NaCl, 17g Agar, 2.5g BactoPeptone to 1 L of distilled water. After autoclaving and cooling down to 55°C, 1mM CaCl₂, 1 mM MgSO₄, 5 µg/ml cholesterol solution, and 25 mM potassium phosphate buffer was added. The following strains were received from the *Caenorhabditis* Genetics Center (CGC): N2 (wild type), OD95 (*unc-119(ed3) III; ItIs37 IV; ItIs38*) - *ItIs37 [(pAA64 Ppie-1::mCherry::HIS-58 + unc-119(+)) ItIs38 [pie-1p::GFP::PH(PLC1delta1) + unc-119(+)]*, TY3558 *unc-119(ed3) ruIs32 III; ojIs1 - ruIs32 [pie-1p::GFP::H2B + unc-119(+)] ojIs1 [Ppie-1::GFP::tbb-2 + unc-119(+)]*. The following strains were generously obtained from Dr. Labbé (IRIC, Université de Montréal): UM445 *ItIs38 [pie-1p::GFP::PH(PLC1delta1) + unc-119(+)] zuls244[Pnmy-2::PGL-1::mRFP-1; unc-119(+)]*, UM463 *cpIs42[Pmex-5::mNeonGreen::PLCδ-PH::tbb-2 3'UTR; unc-119(+)] II; ItIs37[pAA64; Ppie-1::mCherry::HIS-58; unc-119(+)] IV*. In addition, the following strain were made in-house for this study: *ItIs37 [(pAA64 Ppie-1::mCherry::HIS-58 + unc-119(+)) ItIs38 [pie-1p::GFP::PH(PLC1delta1) + unc-119(+)] ojIs1 [Ppie-1::GFP::tbb-2 + unc-119(+)]*, and *cpIs42[Pmex-5::mNeonGreen::PLCδ-PH::tbb-2 3'UTR; unc-119(+)] II itIs37 [pie-1p::mCherry::H2B::pie-1 3'UTR + unc-119(+)] IV*.

2.2 RNA interference

RNA interference (RNAi) was carried out using feeding vectors for induction of dsRNA expression in *E. coli*, as described in Kamath et al., 2001. The following strains were generously provided by Dr. Roy (McGill University): *ran-3* (C26D10.1), *ima-3* (F32E10.4), *ect-2* (T19E10.1). The following strains were generously provided by Dr. Glotzer (University of Chicago): *ani-1* (Y49E10.19), *let-502* (C10H11.9). The following strains were generously provided by Dr. Labbé (IRIC, Université de Montréal): *par-1* (H39E23.1), *par-3* (F54E7.3), *par-6* (T26E3.3).

Bacteria transformed with the various plasmids were grown in overnight cultures, then centrifuged and resuspended in the following volumes of LB media (5g yeast extract, 10g NaCl, 10g tryptone in 1 L of distilled water): 100 μ L for *ran-3*, *par-1*, *par-3*, *par-6*, and *let-502*; 300 μ L for *ima-3*; 300 or 500 μ L for *ani-1*; and concentrations ranging from 400 to 1400 μ L for *ect-2*. Resuspension volumes were optimized based on the severity of embryonic phenotypes. Since all phenotypes in this study are based on a partial knockdown of the protein, RNAi concentrations were optimized accordingly. For example, cytokinesis was analyzed only in embryos with proper DNA segregation and full ingression.

The resuspended bacterial cultures were plated on NGM plates with IPTG (final concentration of 1mM) and ampicillin (final concentration of 100 μ g/mL) and left overnight for the liquid to dry, and to ensure induction of the dsRNA. Approximately 10-12 L4 hermaphrodites were placed onto each dsRNA plate and kept for 24 hours, except for *ima-3* RNAi, where worms were kept for 30 hours. Embryos were dissected out of the gravid hermaphrodites and imaged as discussed in the following section.

2.3 Microscopy

M9 was added into the well of a depression slide, and gravid hermaphrodites were placed into the liquid. They were dissected at two points corresponding to the spermatheca in order to obtain early embryos. To prepare slides for imaging, an air-permeable silicone pad with a square cut out was stuck onto a slide to hold the agarose pad in place. Agarose pads were prepared by dissolving 0.08g agarose in 4mL distilled water. After the solution was heated for 30 seconds, a drop was placed in the cut-out of the silicon pad, and another glass slide was placed on top until the solution dried. Embryos were then mouth pipetted onto the agarose pad (along with liquid to ensure that embryos were covered), and a coverslip was placed onto the slide. Phenotypes were then assessed using live imaging. This was done on an inverted Nikon Eclipse Ti microscope fitted with the Livescan Sweptfield scanner (Nikon), Piezo Z stage (Prior), an Andor IXON 897 EMCCD camera, and 488 and 561 lasers. Using NIS Elements (Nikon) acquisition software, images were collected using the 100x/1.45 NA objective. Images of 0.7 μm Z-stacks for a total range of 4 μm were collected at 5 second intervals. Images were exported as ND2 files.

2.4 Data Analysis

2.4.1 Image analysis

Time-lapse images were analysed in FIJI (NIH, MD, USA) using a macro developed by Dr. Chris Law. Images were staged to anaphase onset based on DNA (mCherry-tagged and imaged via the 561 laser), which was subsequently removed to analyze the membrane (mNeonGreen or GFP-tagged imaged via the 488 laser). A line was drawn manually over the ingression furrow at every time point starting from anaphase onset until furrow closure; 5 pixels on each side of the line were aligned parallel with each other, and placed in order by time,

producing the kymographs used throughout this thesis. The width of the advancing ingression furrow was measured manually at each timepoint using the straight line tool.

2.4.2 Quantitative data analysis

Measurements from FIJI were exported to Google Sheets or Microsoft Excel (Version 16.16.2) for data analysis. The diameter of the cell at the time of anaphase onset was used to normalize ingression. This distance was used to convert inter-membrane distances to a percentile, with 100% as the maximum distance between the two sides of the cortex before furrowing, and decreasing values reflect ingression - closure of the ring as the sides come into contact. To account for biological variability, a minimum of 10 cells was measured for each dataset.

Excel was used to calculate the means and SEM (standard error) and plot them in a graph of inter-membrane distance (% ingression, where 100% is before furrowing) against time (in seconds). To characterize ingression and determine changes in velocity (distance/time), data was plotted using GraphPad Prism 7. All data-points were used when possible, or until ~40% closure due to technical challenges in imaging at this stage, but also because variability tended to increase in the latter stages of ingression in the various RNAi conditions. First, a sigmoidal line of best fit was plotted using the control data for the different cells, then the second derivative of the best fit line was plotted. The x (time) values of the minimum and maximum values of this second derivative curve represent the time points at which there is a change of slope in the original data. The y (% ingression) value at the last time point of Phase 1, 2 and 3 was noted for each control cell. These values were used as a cut-off to define phase transitions in the RNAi treated embryos. These values were then verified in Excel, and the rate of each phase of ingression was determined by drawing tangents to the curve for each phase. To calculate

tangents, data for each treatment were first separated into three phases, and the data points of each individual phase were then plotted as a scatter graph. For example, in Control P₀ cells, the first phase transition occurs at 96% normalized inter-membrane distance, so the tangent for Phase 1 of *ran-3* P₀ was drawn by plotting the subset of y- values that lie between timepoint 0, and the last timepoint before the inter-membrane distances drop below 96%. A linear trendline of best fit was then drawn through this subset of data to determine the slope of ingression (tangent) at that phase. Due to changes in the quality of imaging data at the end of ingression, coupled with increased variability due to RNAi, there tended to be high noise at the end of the curves. To improve the fit of tangents, data was cut off at 40% closure.

A change in the slope of the tangent to the curve reflects a change in velocity, hence defining the change from one phase to the next. The tangents were used to determine the timepoints for each phase (**Figure 6**). If the tangent was parallel to the data between two time points, the latter was included in the phase, if not (i.e. the data sloped away from the tangent), it would indicate a phase transition and the beginning of the subsequent phase. If the first two tangents overlapped or were parallel to each other (for example in the case of curves missing the plateau of the first phase), the end of phase 2 was the last time point in which the curve was still parallel to the tangent.

Two sets of heat maps were generated by Dr. Chris Law using MatLab (MathWorks) to visualize the data. Data was plotted by ingression rate using a color scale, with changes in colors indicating different relative rates - the 'Jet' colormap was used for its wide dynamic range. The heat maps show the ingression rates for the main phases. The duration of the phase was determined by the timepoints found with the tangent method, and the distance travelled by the cortex was determined using the y values at those timepoints. Ingression rate was then calculated

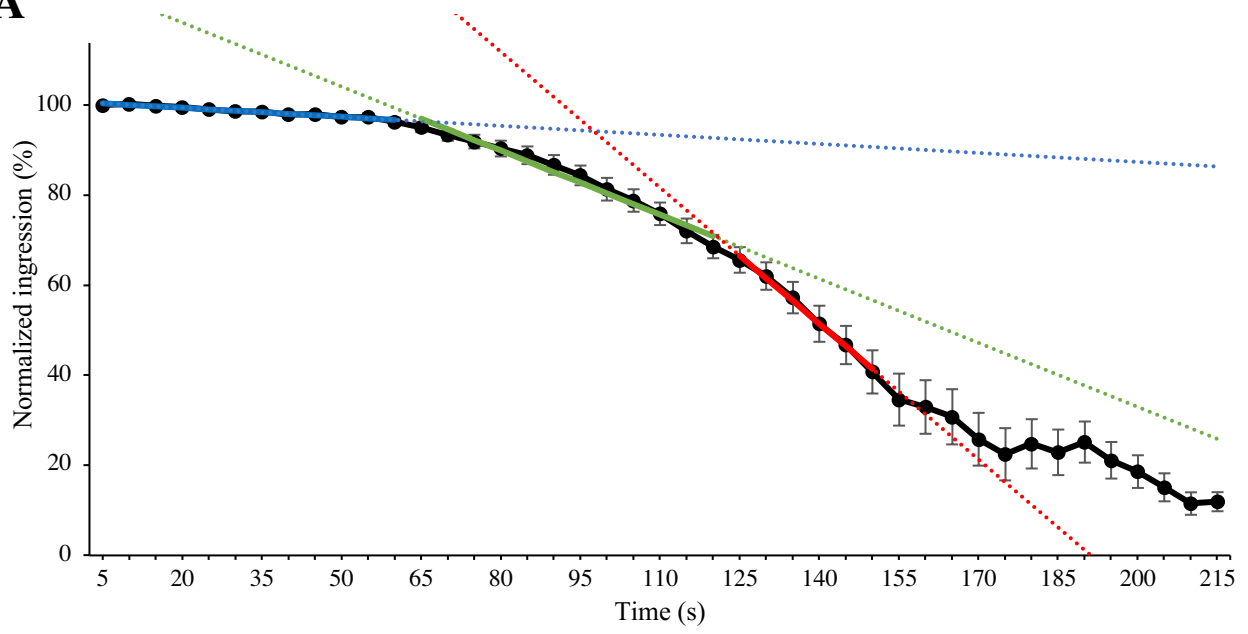
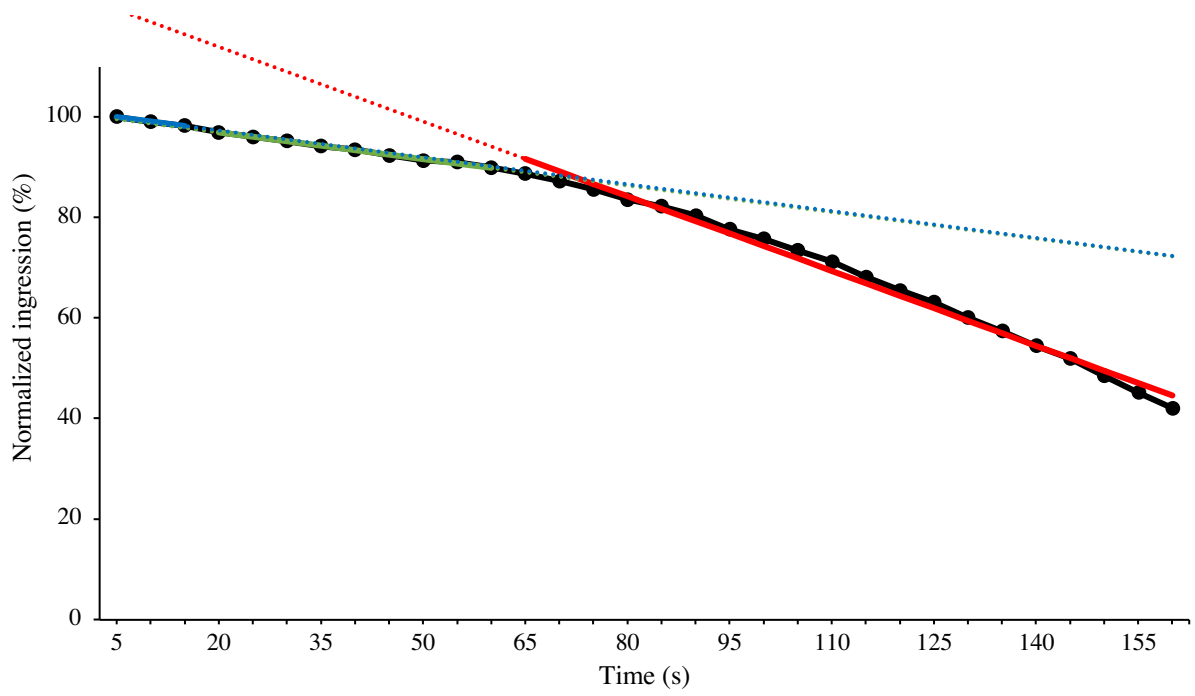
A**B**

Figure 6. Determining phase duration with tangents. A) A graph shows tangents to the three phases of ingress for an *ani-1* P₁ cell. The tangent to the first phase is in blue, the tangent to the second phase in green, and the tangent to the third phase is in red. Data is cut off at 40% closure. B) A graph shows tangents to the three phases of ingress for *ect-2* AB cells. The tangent to the first phase is in blue, the tangent to the second phase in green, and the tangent to the third phase is in red. Data is cut off at 40% closure.

as follows, with a = first time point of the phase, and b = last time point of the phase, and reported in units of percent/s:

$$ingression\ rate = \frac{\% \ ingression(timepoint_a - timepoint_b)}{time(timepoint_a - timepoint_b)}$$

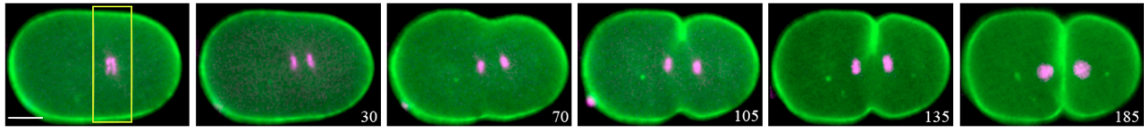
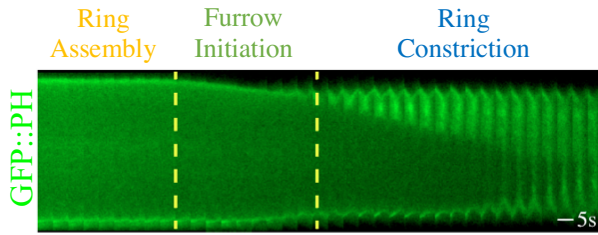
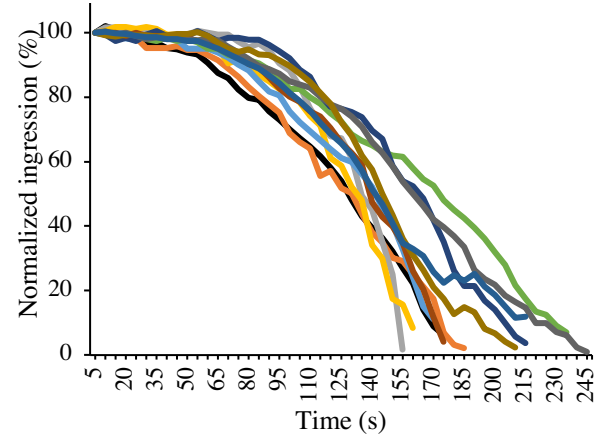
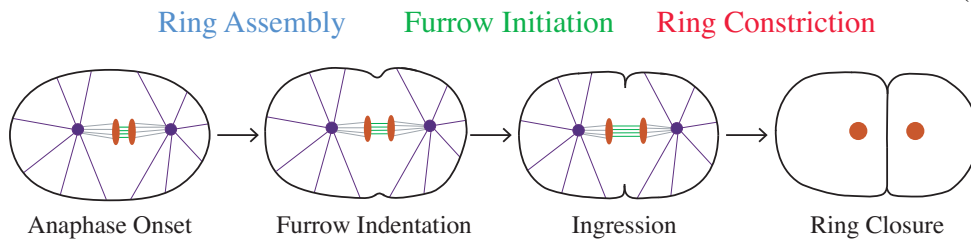
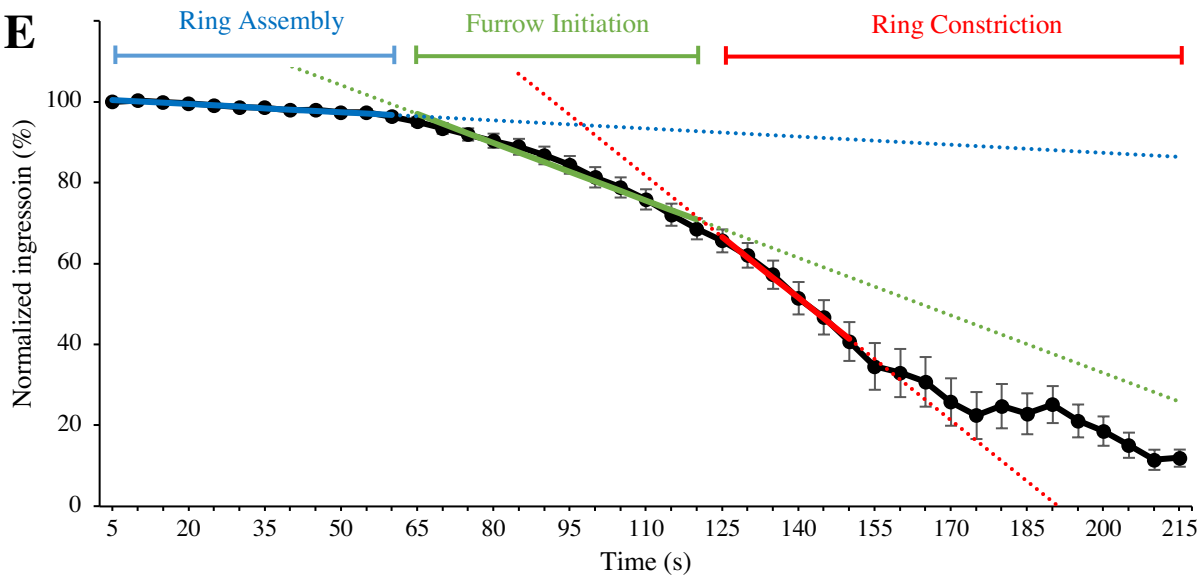
In addition, graphs of normalized % ingression for all cells (P₀, AB and P₁) for control or *ran-3* were grouped together and plotted with a color scale for cell size by Dr. Chris Law using MatLab. The ‘Cool’ colormap was used to indicate initial cell size (diameter at t=0), and scaled to accentuate the variation in cell diameter. The scale was derived from the diameter of cells within the same treatment type.

Chapter 3: Results

3.1 Ran-GTP influences cortical activity during anaphase in early *C. elegans* embryos

3.1.1 P₀, AB and P₁ cells have different ingression kinetics in control embryos

The overall goal of this project was to determine if and how the Ran pathway regulates cytokinesis in early *C. elegans* embryos. Before doing this, we needed to characterize the kinetics of cytokinesis in control embryos. Strains with a marker for the cortex (PH tagged with GFP or mNeonGreen, which localizes to the membrane) and a marker for DNA (H2B or HIS-58 tagged with mCherry, which localizes to chromatin) were used to visualize membrane ingression at 5 second intervals from anaphase onset until furrow closure. Time-lapse images of dividing P₀ cells from control embryos (**Figure 7A**) were used to generate kymographs (**Figure 7B**) that were measured to plot the % change in normalized distance (ingression) over time (**Figure 7C**). To account for biological variability, we obtained an n of at least 10 for each cell (**Figure 7C**). We noticed that cells did not ingress linearly, but rather had an initial plateau phase with no ingression, followed by indentation and subsequently more rapid ingression. These phases have been described previously in the literature as ‘ring assembly’, ‘furrow initiation’ and ‘ring constriction’ (**Figure 7D**; Osorio et al., 2018). I defined these phases in an unbiased way by plotting tangents for subsets of data determined via plotting sigmoidal lines of best fit and second derivatives for these lines as described in the methods section (also **Figure 7E**). I found that the ring assembly phase had a slow velocity of 0.07 percent/s, the furrow initiation phase was 0.5 percent/s and constriction phase was 1 percent/s (**Figure 7F**). To better show changes in the

AmCherry::HIS-58;
GFP::PH**B****C****D****E**

F

	Ring assembly phase	Furrow initiation phase	Ring constriction phase
Control P ₀	0.07	0.5	1

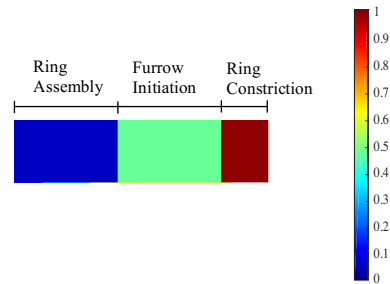
G

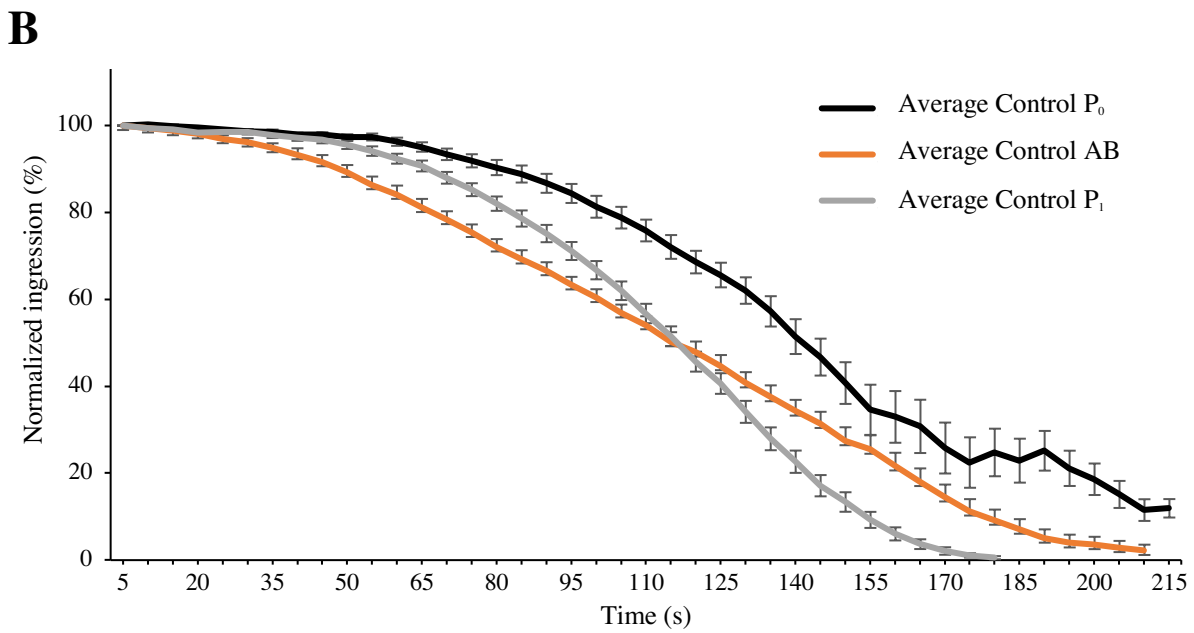
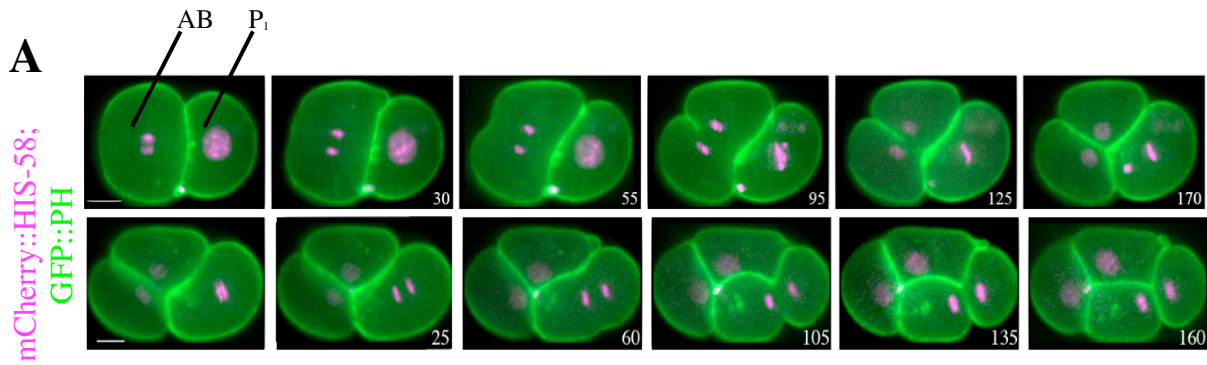
Figure 7. Characterization of control P₀ divisions. A) Time-lapse images show a P₀-cell division in a *C. elegans* embryo expressing mCherry::HIS-58 (magenta) and GFP::PH (green). The times shown are after anaphase onset in seconds. The scale bar is 10 μm. B) A kymograph was generated from a box drawn around the division plane (see box in A), and shows changes in the membrane every 5 seconds from anaphase onset until closure. Yellow dashed lines indicate the time at which the cell transitions from one phase to the next (i.e. Figure 7D). C) A graph shows the % ingression of the membrane (ring closure) over time (in seconds), where each line represents a different P₀ cell. D) Cartoon schematics show the three phases of ingression; ring assembly phase (blue), furrow initiation (green) and ring constriction (red). DNA is in red, central spindle microtubules are in green, and the astral microtubules and centrosomes are in purple. E) A graph shows the average % ingression of P₀-cell ring closure over time in seconds (n = 10). Tangents are drawn to show the transition for each phase (blue for ring assembly, green for furrow initiation, red for ring constriction). Error bars show SEM. F) Table shows rates of ingression (percent/s), represented in G. G) A color heat map shows the different rates for each phase of ingression. The corresponding color for each rate of ingression (percent/s) is shown on the scale (right). Rates of ingression were plotted from anaphase onset until 40% furrow closure.

cortex during earlier stages of cytokinesis (*e.g.* until 40% closure), we generated a heat map to show the relative rate of ingression (in percent/s) and duration of each phase (**Figure 7G**). In these heat maps, the cool colors show no/little ingression or slow ingression rate and warmer colors show more ingression or faster ingression rate.

Using the same methods for control P₀ cells, we also characterized ingression in control AB and P₁ cells (**Figure 8**). Kymographs generated from time-lapse imaging of embryos at five-second intervals from anaphase onset until furrow closure (*e.g.* **Figure 8A**) were measured to plot the average % ingression over time (**Figure 8B**). Ingression rates were measured (**Figure 8C**) and heat maps of the relative changes in phase rates were plotted as described above (**Figure 8D**). We observed that the ingression kinetics of AB and P₁ cells are different from each other. While the P₁ cells had ingression kinetics that resembled P₀ cells for the plateau/ring assembly phase (0.1 percent/s), this phase was very short in AB cells (**Figure 8B, C, D**). P₁ and AB cells had a shorter furrow initiation phase in comparison to P₀ cells (0.4 percent/s and 0.3 percent/s, respectively; **Figure 8B, C, D**). P₁ cells had a similar ingression rate for the ring constriction phase, but longer in duration vs. P₀ cells (0.9 percent/s; **Figure 8B, C, D**). Strikingly, AB cells had a long, slower constriction phase compared to the other cells (0.7 percent/s; **Figure 8B, C, D**). Our detailed characterization of P₀, AB and P₁ cell divisions uncovered interesting differences in ingression kinetics during cytokinesis, suggesting that their regulation may require different mechanisms or combinations thereof.

3.1.2 Ingression kinetics are altered in P₀, AB and P₁ cells in *ran-3* and *ima-3* embryos

Our next step was to perturb the Ran pathway and compare ingression kinetics in P₀, AB and P₁ cells with control embryos. Based on our hypothesis and mammalian model of Ran-



C

	Ring assembly phase	Furrow initiation phase	Ring constriction phase
Control P_0	0.07	0.5	1
Control AB	0.1	0.3	0.6
Control P_1	0.1	0.4	0.9

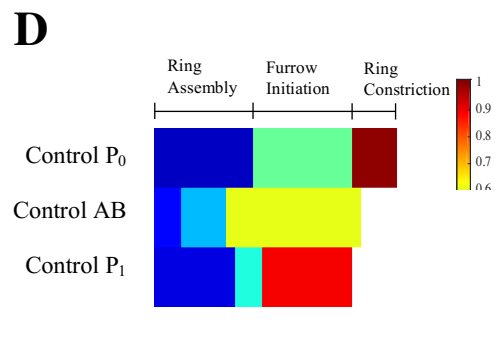
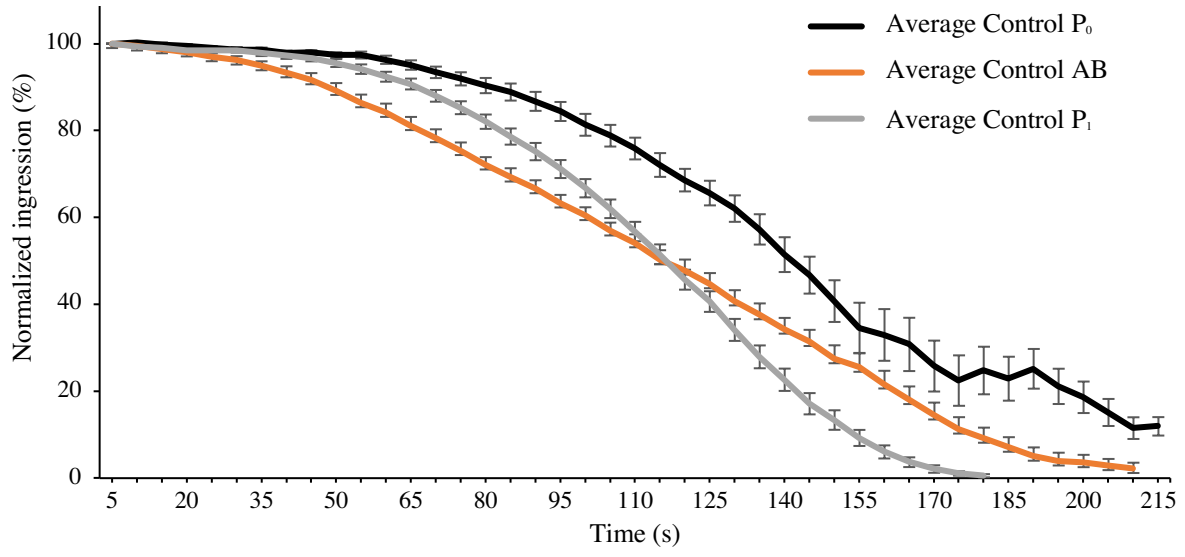
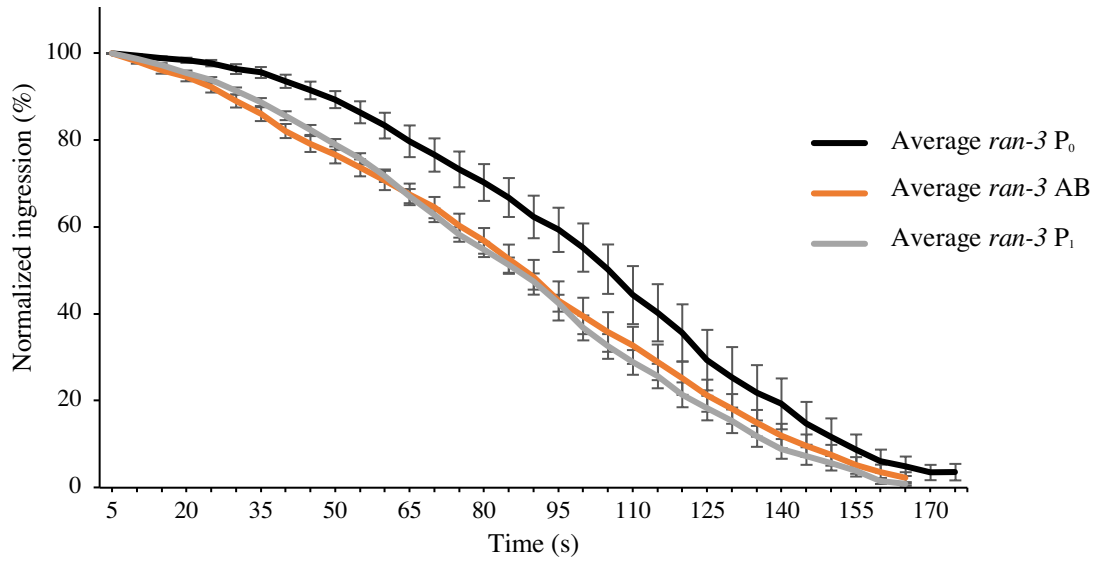


Figure 8. Characterization of control AB and P₁ divisions. A) Time-lapse images showing AB (top, cell indicated by line) and P₁ (bottom, cell indicated by line) divisions in a *C. elegans* embryo expressing mCherry::HIS-58 (magenta) and GFP::PH (green). The times shown are after anaphase onset in seconds. The scale bar is 10 μm. B) A graph shows the average % ingression rates of control P₀ (black curve; n = 10), AB (orange curve; n = 16) and P₁-cell (grey curve; n = 35) ring closure over time in seconds. Error bars show SEM. C) Table shows rates of ingression (percent/s), represented in D. D) Color heat map shows the different rates for each phase of ingression in P₀ (top), AB (middle) and P₁ (bottom) cells. The corresponding color for each rate of ingression (percent/s) is shown on the scale (right). Rates of ingression were plotted from anaphase onset until 40% furrow closure.

modulation of cytokinesis, we expected to see more rapid ring assembly and/or initiation due to increased contractility via a decrease in active Ran. To test this, we knocked down *ran-3* (RCC-1 - the GEF for Ran) via partial RNAi and analyzed kinetics as described for control cells. Mild depletion of *ran-3* caused faster ingression kinetics in P₀, AB and P₁ cells compared to control cells (**Figure 9A, B**). In particular, furrowing initiated sooner, and cytokinesis completed in a shorter overall time compared to control cells (**Figure 9A, B**). Ingression rates were calculated (**Figure 9C**) and shown as heat maps (**Figure 9D**). As shown in the heat maps in Figure 9D, the plateau ring assembly phases were shorter, or absent compared to cells in control embryos, and the subsequent furrow initiation phases were faster. Thus, in support of our hypothesis, reducing Ran-GTP stimulates an increase in cortical contractility during mitotic exit.

To determine if RCC-1's role in cytokinesis occurs via regulating Ran vs. having an independent function in cytokinesis, we compared ingression kinetics after perturbing another component of the Ran pathway – IMA-3 (importin-alpha; **Figure 10**). Our hypothesis is that importin-alpha or beta binding to contractile proteins, such as anillin, potentiates an open, accessible conformation to positively regulate their activity. Since importin-alpha forms a complex with importin-beta, lowering alpha should 'free' more importin-beta for binding to contractile regulators. The ingression kinetics of *ima-3* RNAi embryos phenocopied *ran-3*, such that ingression initiated sooner, and completed in a shorter overall time in P₀, AB and P₁ cells compared to cells in control embryos (**Figure 10A, B**). Ingression rates were measured as described previously and used to generate heat maps (**Figure 10C, D**). The heat maps in Figure 10D show that similar to *ran-3*, all cells in *ima-3* RNAi embryos had a shorter ring assembly plateau phase, followed by a shorter and/or faster furrow initiation phase. Thus, in support of our hypothesis, reducing importin-alpha increases furrow ingression kinetics of cytokinesis, possibly

A**B**

C

	Ring assembly phase	Furrow initiation phase	Ring constriction phase
Control P ₀	0.07	0.5	1
Control AB	0.1	0.3	0.6
Control P ₁	0.1	0.4	0.9
<i>ran-3</i> P ₀	0.1	0.6	0.9
<i>ran-3</i> AB		0.4	0.7
<i>ran-3</i> P ₁	0.3	0.6	0.8

D

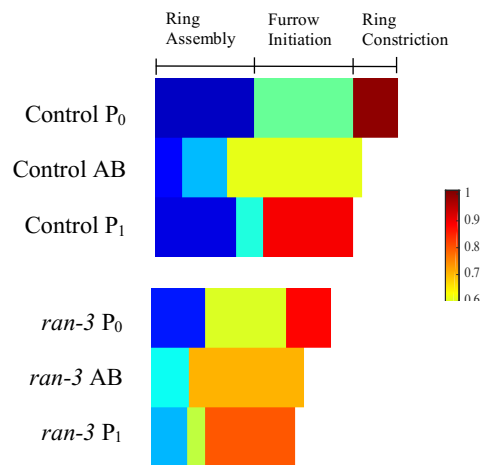
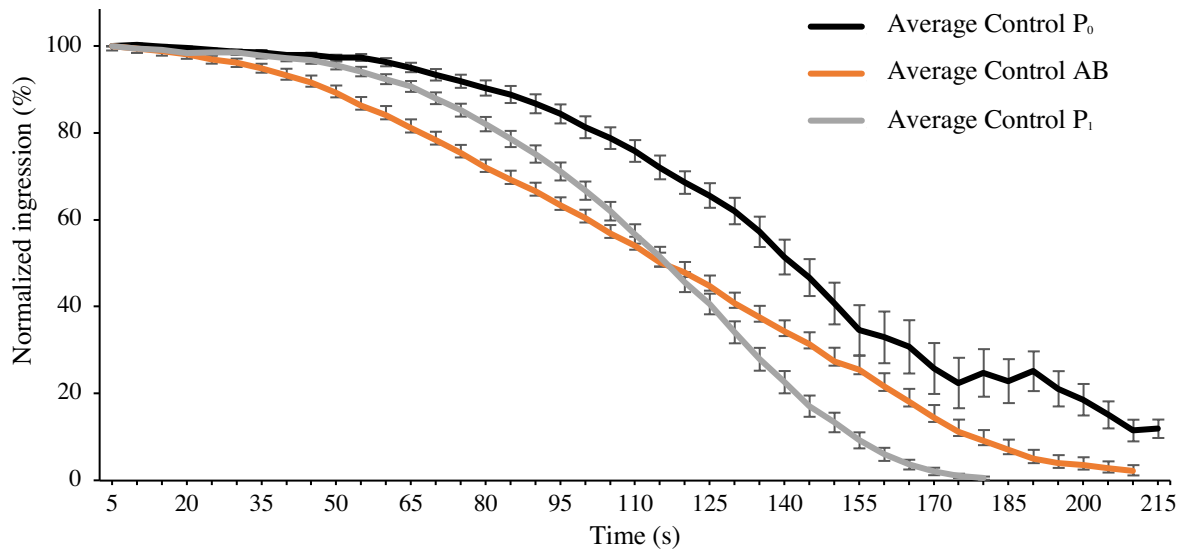
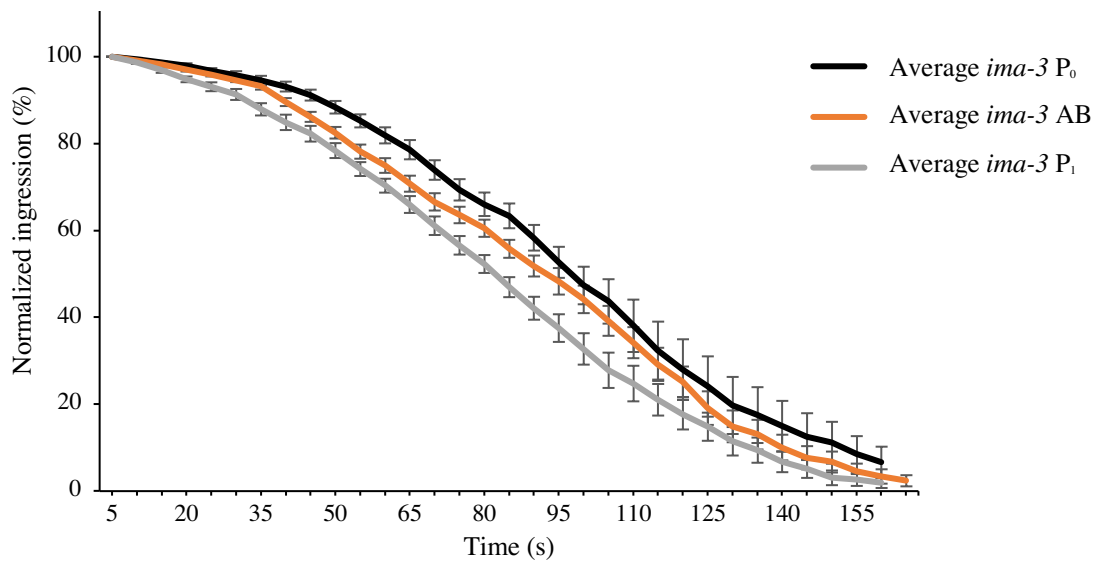


Figure 9. *ran-3* causes P₀, AB and P₁ cells to initiate and ingress sooner. A) A graph shows the average % ingress rates of control P₀ (black curve; n = 10), AB (orange curve; n = 16) and P₁-cell (grey curve; n = 35) ring closure over time in seconds. Error bars show SEM. B) A graph shows the average % ingress rates of *ran-3* P₀ (black curve; n = 10), AB (orange curve; n = 11) and P₁-cell (grey curve; n = 21) ring closure over time in seconds. Error bars show SEM. C) Table shows rates of ingress (percent/s), represented in D. D) Color heat maps show the different rates for each phase of ingress for control (top) and *ran-3* (bottom) embryos. The corresponding color for each rate of ingress (percent/s) is shown on the scale (right). Rates of ingress were plotted from anaphase onset until 40% furrow closure.

A**B**

C

	Ring assembly phase	Furrow initiation phase	Ring constriction phase
Control P ₀	0.07	0.5	1
Control AB	0.1	0.3	0.6
Control P ₁	0.1	0.4	0.9
<i>ima-3</i> P ₀	0.2	0.6	1
<i>ima-3</i> AB	0.2	0.4	0.8
<i>ima-3</i> P ₁	0.3	0.3	0.8

D

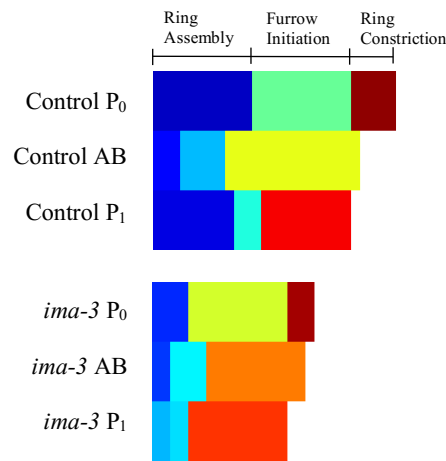


Figure 10. *ima-3* causes hypercontractility in divisions. A) A graph shows the average % ingress rates of control P₀ (black curve; n = 10), AB (orange curve; n = 16) and P₁-cell (grey curve; n = 35) ring closure over time in seconds. Error bars show SEM. B) A graph shows the average % ingress rates of *ima-3* P₀ (black curve; n = 10), AB (orange curve; n = 12) and P₁-cell (grey curve; n = 15) ring closure over time in seconds. Error bars show SEM. C) Table shows rates of ingress (percent/s), represented in D. D) Color heat maps show the different rates for each phase of ingress for control (top) and *ima-3* (bottom) embryos. The corresponding color for each rate of ingress (percent/s) is shown on the scale (right). Rates of ingress were plotted from anaphase onset until 40% furrow closure.

via freeing importin-beta for binding to contractile regulators.

One caveat to our studies is that perturbing components of the Ran pathway could affect the mitotic spindle, which also regulates cytokinesis, or could disrupt polarity and indirectly lead to changes in cytokinesis due to altered cell fate. Spindle assembly factors are released from importin-binding in the vicinity of Ran-GTP, which potentiates their activity for nucleating microtubules and regulating assembly of the mitotic spindle. Thus, decreasing Ran-GTP could prevent their release and disrupt mitotic spindle formation. We do not think that this occurs in our experiments because we titrate down the levels of RNAi to ensure that sister chromatid segregation occurs successfully, and cytokinesis completes to give rise to daughter cells. However, to be sure, we imaged embryos expressing mCherry::HIS-58 (to visualize chromatin), GFP::PH (to visualize membrane) and GFP::TBB-2 (to visualize tubulin) and compared morphology of the mitotic spindles between control and *ran-3*-treated embryos (**Figure 11A**). As expected, there was no noticeable difference in cells in control and RNAi embryos. To determine if there were any changes in cell fate caused by altered polarity after *ran-3* RNAi, we imaged embryos co-expressing GFP::PH and PGL-1::RFP (marker for P granules) in control or *ran-3* RNAi embryos at the 2-cell and 4-cell stage (**Figure 11B**). P granules segregate exclusively to the germ line (Rose and Gönczy, 2014), which still occurred in *ran-3* RNAi embryos, suggesting that polarity is not affected by depletion of *ran-3*.

3.1.3 ANI-1 could be a target of the Ran pathway in P₀ and AB cells

Our data shows that the Ran pathway increases furrow ingression kinetics in P₀, AB and P₁ cells. We found that rings assemble faster and ingression completes sooner after decreasing Ran-GTP or importin-alpha in comparison to control cells, supporting our hypothesis that ‘free’

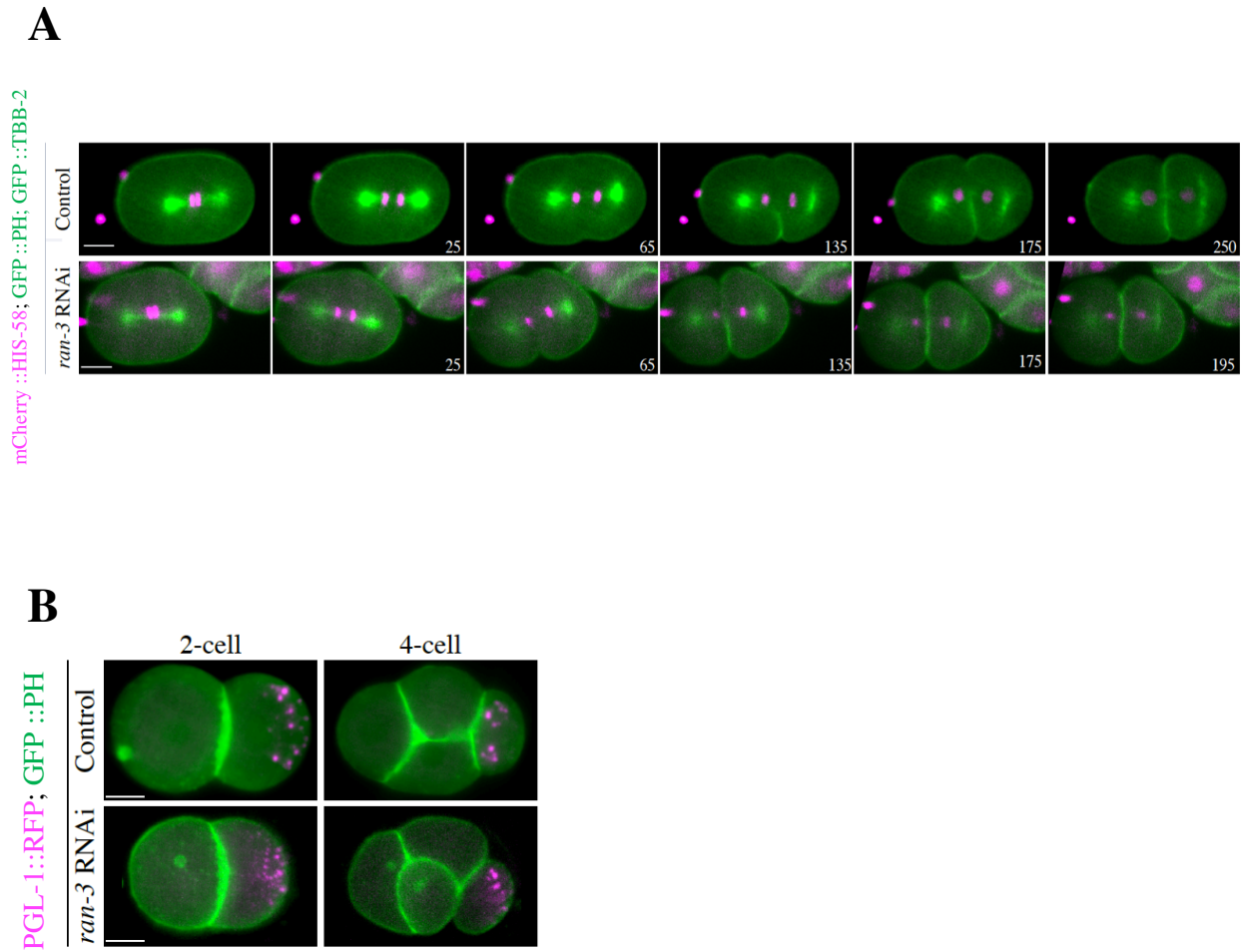
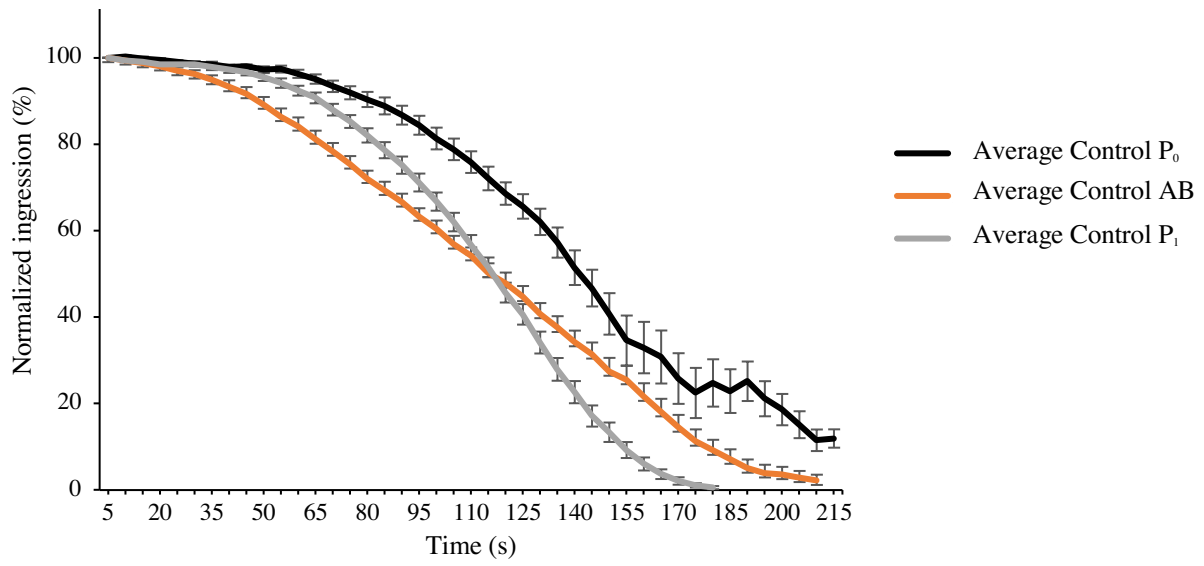
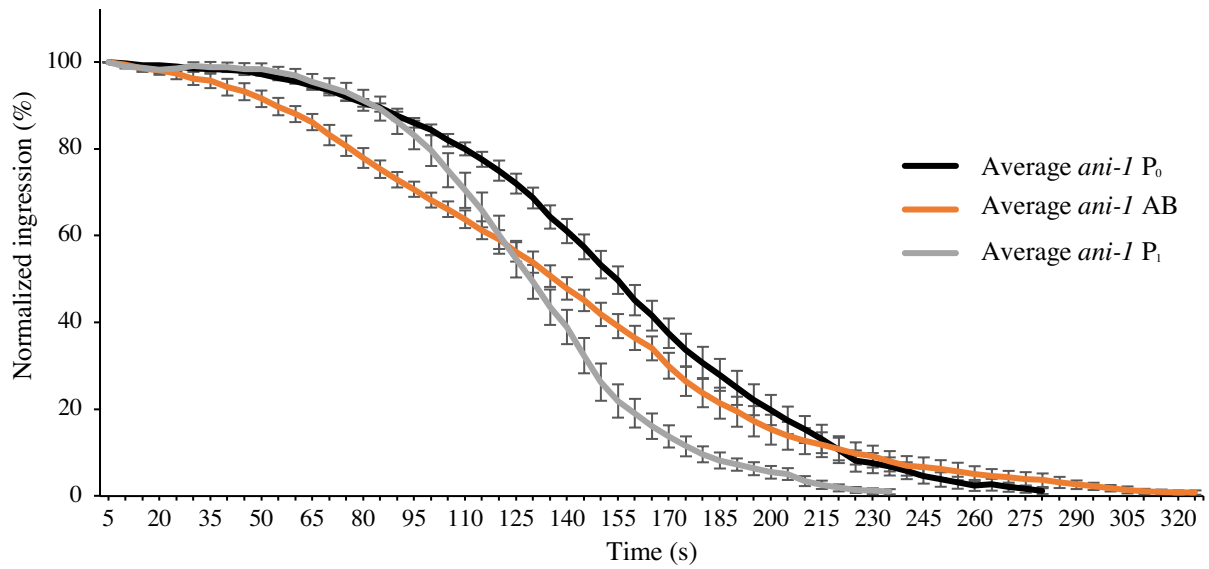


Figure 11. A mild decrease in Ran-GTP does not alter the spindle or polarity. A) Time-lapse images show a control (top) and *ran-3* (bottom) P₀-cell division in a *C. elegans* embryo expressing mCherry::HIS-58 (to visualize chromatin; magenta), GFP::PH (to visualize the membrane; green), and GFP::TBB-2 (to visualize microtubules; green). The times shown are after anaphase onset in seconds. The scale bar is 10 μ m. B) To show that *ran-3* depletion does not alter anterior-posterior polarity, embryos co-expressing PGL-1::RFP (P granules; magenta) and GFP::PH (green) are shown for control or *ran-3* RNAi at the 2-cell and 4-cell stage. The scale bar is 10 μ m. Time-lapse images taken by Karina Mastronardi.

importins potentiate the activity of cortical proteins for cytokinesis. In human cells, our lab found that importin-beta binds to and facilitates anillin's recruitment to the cortex, and regulates its function for cytokinesis (Beaudet et al., 2017). We tested if ANI-1 is in the Ran pathway in P₀, AB and P₁ cells in *C. elegans* embryos. We depleted ANI-1 using RNAi and characterized ingression as previously described (**Figure 12**). Compared to control embryos, *ani-1* RNAi caused overall delays in the ingression of P₀, AB and P₁ cells (**Figure 12B**). As shown in the heat maps in Figure 12D, *ani-1* P₀ cells had a slightly shorter ring assembly phase of comparable ingression rate, but this was followed by longer furrow initiation and ring constriction phases that were slower than in control embryos. AB cells had a longer ring assembly phase of comparable ingression rate in *ani-1* RNAi embryos, followed by a shorter, but slower furrow initiation phase, and a longer and slower ring constriction phase in comparison to control embryos. P₁ cells had a longer and slower ring assembly plateau phase, followed by a longer and slower furrow initiation phase, and a faster constriction phase compared to control embryos. The overall net increase in duration of cytokinesis was expected for P₀, AB and P₁ cells based on *ani-1*'s function as a regulator of cytokinesis, but we were surprised to see that each cell showed a unique response to *ani-1* perturbation, reflecting different requirements in different cell types.

Next, we determined if ANI-1 is in the Ran pathway in P₀, AB and P₁ cells. To do this, we co-depleted *ani-1* and *ran-3*, and measured ingression kinetics to see if they were similar to *ani-1*, which would be predicted if ANI-1 was a target of Ran regulation. To better compare the different experimental treatments, P₀, AB and P₁ cells were graphed separately (**Figure 13, A, B, C**). As shown in the graphs, P₀ and AB cells in embryos co-depleted for *ani-1* and *ran-3* displayed ingression kinetics similar to control or *ani-1* RNAi embryos (**Figure 13A, B**), whereas P₁ cell ingression was similar to *ran-3* RNAi embryos (**Figure 13C**). A more detailed

A**B**

C

	Ring assembly phase	Furrow initiation phase	Ring constriction phase
Control P ₀	0.07	0.5	1
Control AB	0.1	0.3	0.6
Control P ₁	0.1	0.4	0.9
<i>ani-1</i> P ₀	0.06	0.3	0.8
<i>ani-1</i> AB	0.1	0.3	0.5
<i>ani-1</i> P ₁	0.06	0.3	1

D

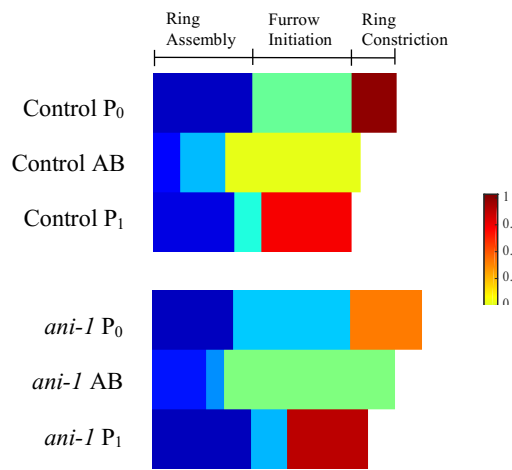
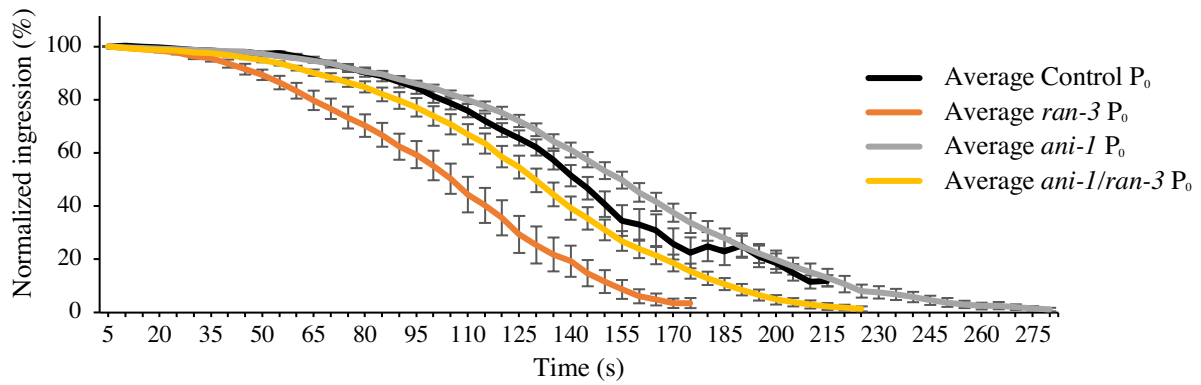
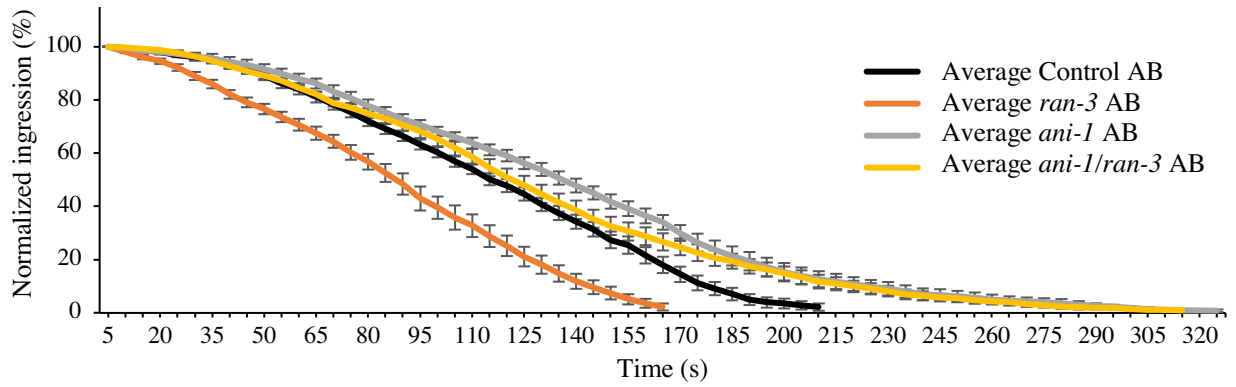
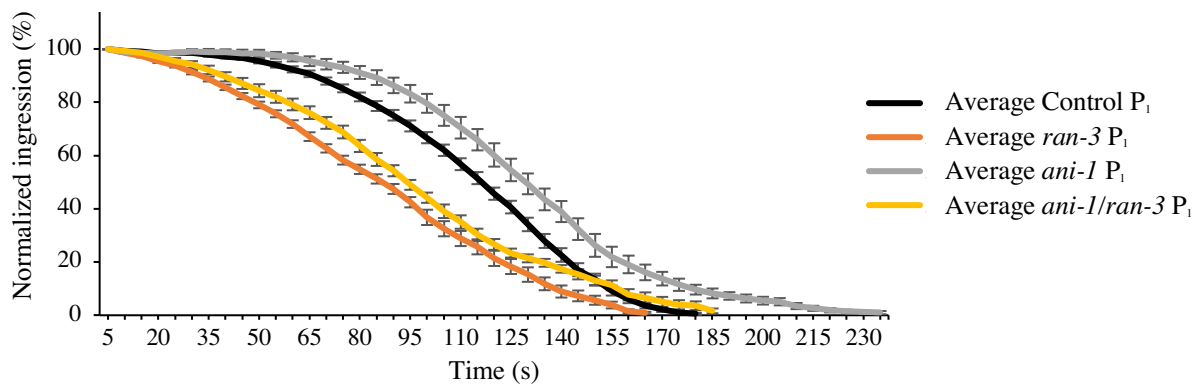


Figure 12. Ingression in *ani-1* embryos is delayed. A) A graph shows the average % ingression rates of control P₀ (black curve; n = 10), AB (orange curve; n = 16) and P₁-cell (grey curve; n = 35) ring closure over time in seconds. Error bars show SEM. B) A graph shows the average % ingression rates of *ani-1* P₀ (black curve; n = 10), AB (orange curve; n = 10) and P₁-cell (grey curve; n = 14) ring closure over time in seconds. Error bars show SEM. C) Table shows rates of ingression (percent/s), represented in D. D) Color heat maps show the different rates for each phase of ingression for control (top) and *ani-1* (bottom) embryos. The corresponding color for each rate of ingression (percent/s) is shown on the scale (right). Rates of ingression were plotted from anaphase onset until 40% furrow closure.

A**B****C**

D

	Ring assembly phase	Furrow initiation phase	Ring constriction phase
Control P ₀	0.07	0.5	1
<i>ran-3</i> P ₀	0.1	0.6	0.9
<i>ani-1</i> P ₀	0.06	0.3	0.8
<i>ani-1/ran-3</i> P ₀	0.1	0.4	0.8
Control AB	0.1	0.3	0.6
<i>ran-3</i> AB		0.4	0.7
<i>ani-1</i> AB	0.1	0.3	0.5
<i>ani-1/ran-3</i> AB	0.08	0.4	0.6
Control P ₁	0.1	0.4	0.9
<i>ran-3</i> P ₁	0.3	0.6	0.8
<i>ani-1</i> P ₁	0.06	0.3	1
<i>ani-1/ran-3</i> P ₁	0.2	0.5	0.9

E

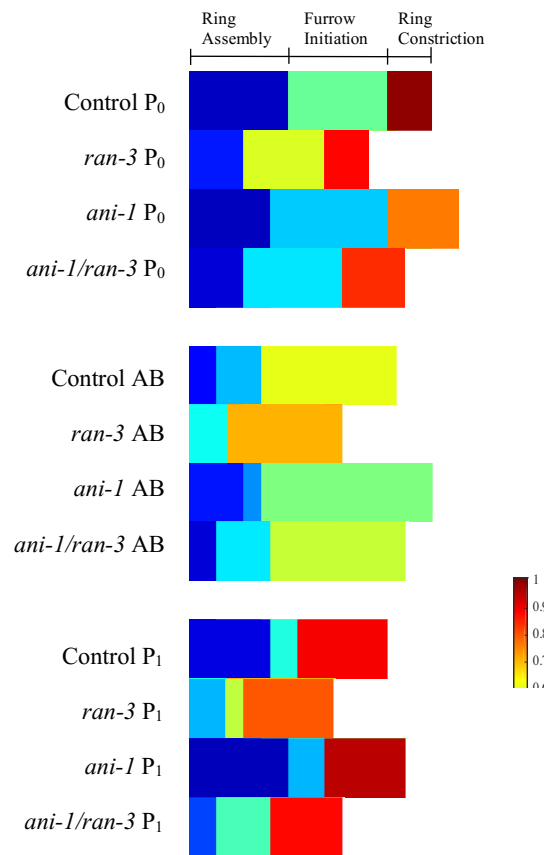


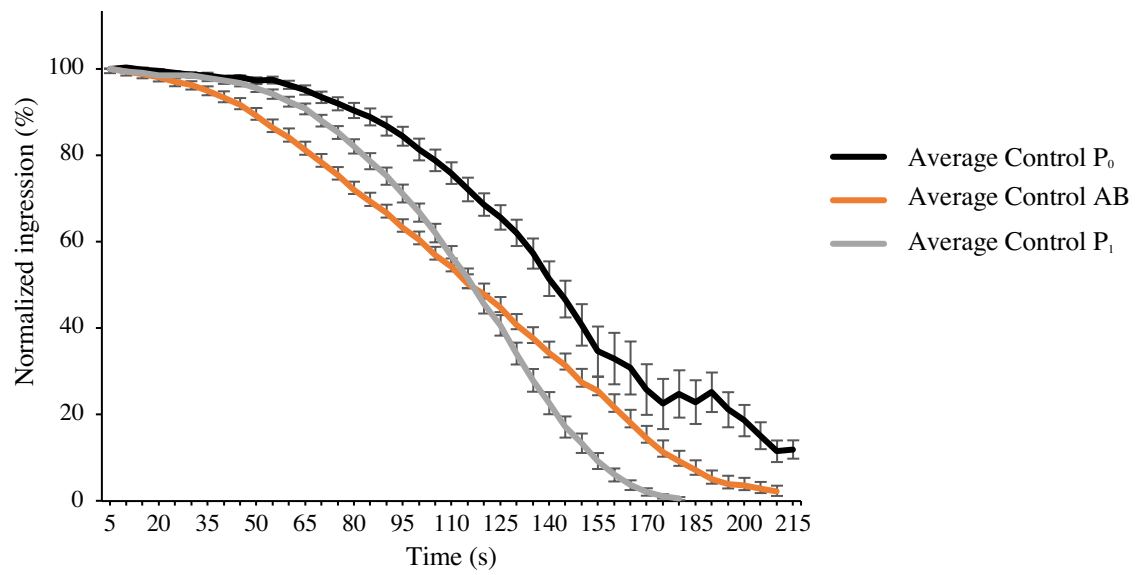
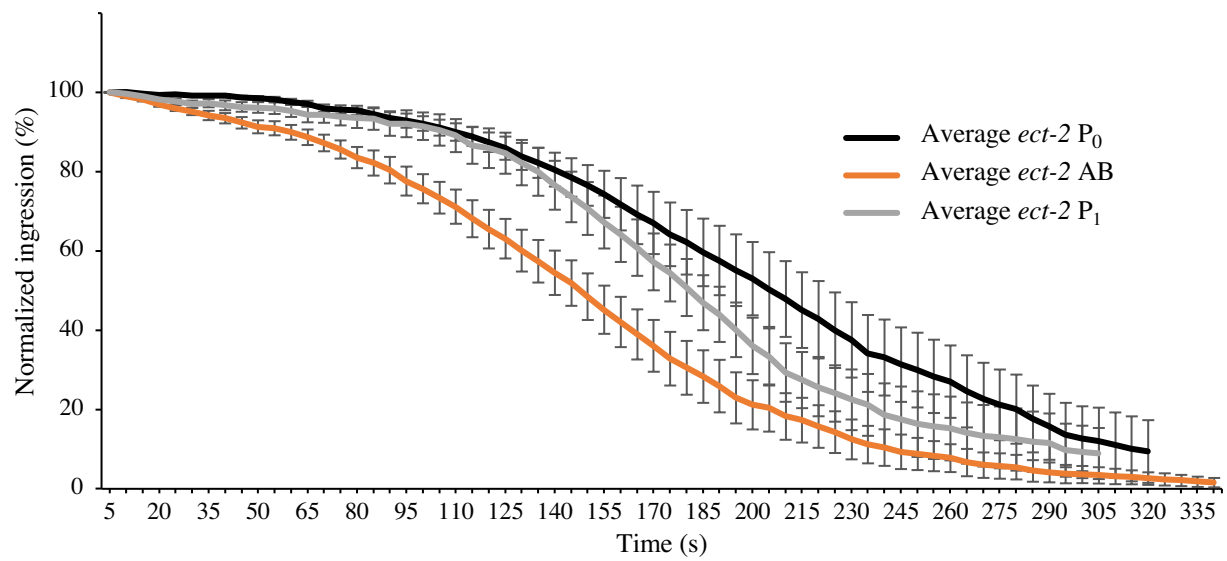
Figure 13. ANI-1 could be in the Ran pathway in P₀ and AB cells. A) A graph shows the average % ingression over time (in seconds) of P₀-cell division under Control (black curve; n = 10), *ran-3* RNAi (orange curve; n = 10), *ani-1* RNAi (grey curve; n = 10) and *ani-1/ran-3* RNAi (yellow curve, n = 12) treatment conditions. Error bars show SEM. B) A graph shows the average % ingression over time (in seconds) of AB-cell divisions under Control (black curve; n = 16), *ran-3* RNAi (orange curve; n = 11), *ani-1* RNAi (grey curve; n = 10) and *ani-1/ran-3* RNAi (yellow curve, n = 12) treatment conditions. Error bars show SEM. C) A graph shows the average % ingression over time (in seconds) of P₁-cell divisions under Control (black curve; n = 35), *ran-3* RNAi (orange curve; n = 21), *ani-1* RNAi (grey curve; n = 14) and *ani-1/ran-3* RNAi (yellow curve, n = 11) treatment conditions. Error bars show SEM. D) Table shows rates of ingression (percent/s), represented in E. E) Color heat maps show the different rates for each phase of ingression for P₀, AB, P₁ under indicated treatment conditions. The corresponding color for each rate of ingression (percent/s) is shown on the scale (right). Rates of ingression were plotted from anaphase onset until 40% furrow closure.

analysis of their ingression rates is shown in the heat maps in Figures 13E. P₀ cells in embryos co-depleted for *ani-1* and *ran-3* had a ring assembly plateau phase that was slower vs. *ran-3* RNAi. The rest of the kinetics were similar to control or *ani-1* cells, such as a longer, slower furrow initiation phase, and a longer constriction phase (**Figure 13E**). AB cells in embryos co-depleted for *ani-1* and *ran-3* had ingression kinetics similar to control embryos for all three phases (**Figure 13E**). P₁ cells in embryos co-depleted for *ani-1* and *ran-3* had a very short ring assembly plateau phase, similar to *ran-3* RNAi, which was followed by a long, but fast ring initiation phase (unique vs. other RNAi conditions) and short constriction phase (**Figure 13E**). Since the kinetics for the ring assembly and/or initiation phases in P₀ and AB cells in co-depleted *ani-1* and *ran-3* embryos were similar to control or *ani-1* RNAi embryos, we propose that ANI-1 could be a target of the Ran pathway in these cells. However, ANI-1 does not appear to be a target of the Ran pathway in P₁ cells, since their kinetics in co-depleted embryos were more similar to *ran-3*. Thus, a different regulator of cytokinesis is regulated by Ran-GTP in P₁ cells.

3.1.4 ECT-2 could be in the Ran pathway in P₀, AB and P₁ cells

ECT-2 is another key regulator of cytokinesis, which functions as a RhoA GEF that activates RhoA for contractile ring assembly and ingression. ECT-2 has not been studied biochemically. However, its homologue, Ect2, has been studied more extensively (Yüce et al., 2005; Hara et al., 2006; Niiya et al., 2006). Ect2 has a well-conserved NLS in the middle of the protein that regulates nucleocytoplasmic transport, and has a well-conserved Cdk1 phosphorylation site close to the NLS that regulates changes in its conformation (Tatsumoto et al., 1999; Hara et al., 2006). Prior studies showed that dephosphorylation of the Cdk1 site is required for the activation of Ect2 during mitotic exit (Hara et al., 2006). An exciting hypothesis

is that importin-binding to the NLS of Ect2 potentiates an open conformation to increase its activity for cytokinesis. Previous studies showed that *ect-2* RNAi prevents or delays furrowing as expected for a regulator of cytokinesis (Motegi et al., 2006). We predict that if ECT-2 is in the Ran pathway, then its co-depletion with *ran-3* should show phenotypes closer to *ect-2* RNAi or control. Using mild *ect-2* RNAi, we first characterized ingression kinetics in P₀, AB and P₁ cells compared to control embryos (**Figure 14A, B**). As shown in Figure 14C and D it was difficult to distinguish the transition in phases, which took longer and/or were slower for P₀, AB and P₁ cells in *ect-2* RNAi embryos compared to control embryos. Thus, furrowing was severely delayed after mild *ect-2* RNAi, as expected for a crucial regulator of contractile ring assembly and constriction. Next, we co-depleted *ect-2* and *ran-3* and measured ingression kinetics to determine if the cells ingressed similar to those in *ect-2* RNAi or control embryos. As with *ani-1*, we graphed P₀, AB and P₁ cells separately to better compare their phenotypes in the different treatment conditions (**Figure 15A, B, C**). All cells in embryos co-depleted for *ect-2* and *ran-3* had ingression kinetics that resembled cells in either control or weak *ect-2* RNAi embryos, and cytokinesis took longer to complete, similar to *ect-2* RNAi embryos. As shown in the heat maps in Figure 15E, the ring assembly and furrow initiation phases were longer and/or slower in P₀, AB and P₁ cells in co-depleted *ect-2* and *ran-3* RNAi embryos compared to *ran-3* RNAi embryos. Our data suggests that ECT-2 could be in the Ran pathway in P₀, AB and P₁ cells. However, due to the crucial role that ECT-2 plays in ring assembly and constriction, our experimental approach does not provide direct evidence for ECT-2 as a target of the Ran pathway. On the other hand, it does support that Ran regulates cortical contractility.

A**B**

C

	Ring assembly phase	Furrow initiation phase	Ring constriction phase
Control P ₀	0.07	0.5	1
Control AB	0.1	0.3	0.6
Control P ₁	0.1	0.4	0.9
<hr/>			
<i>ect-2</i> P ₀	0.04	0.2	0.5
<i>ect-2</i> AB		0.2	0.5
<i>ect-2</i> P ₁	0.09	0.1	0.6

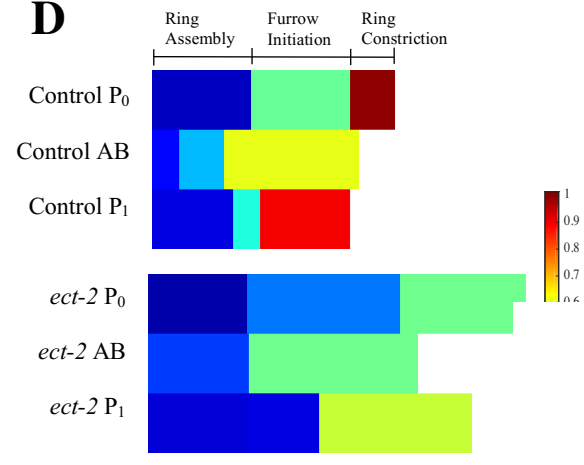
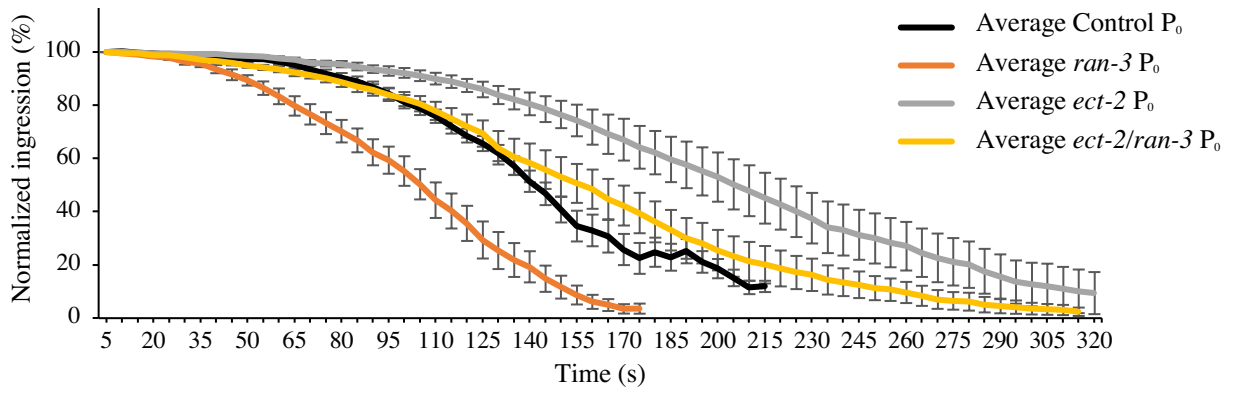
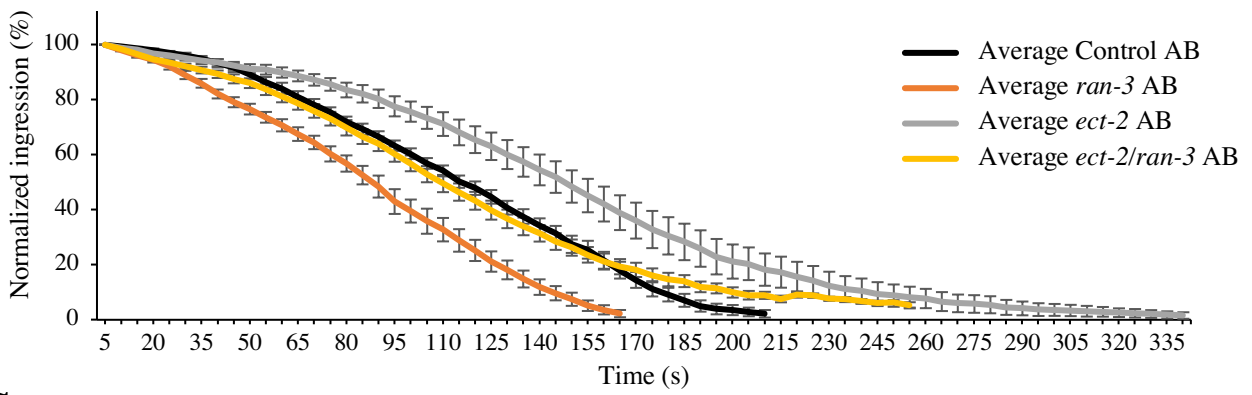
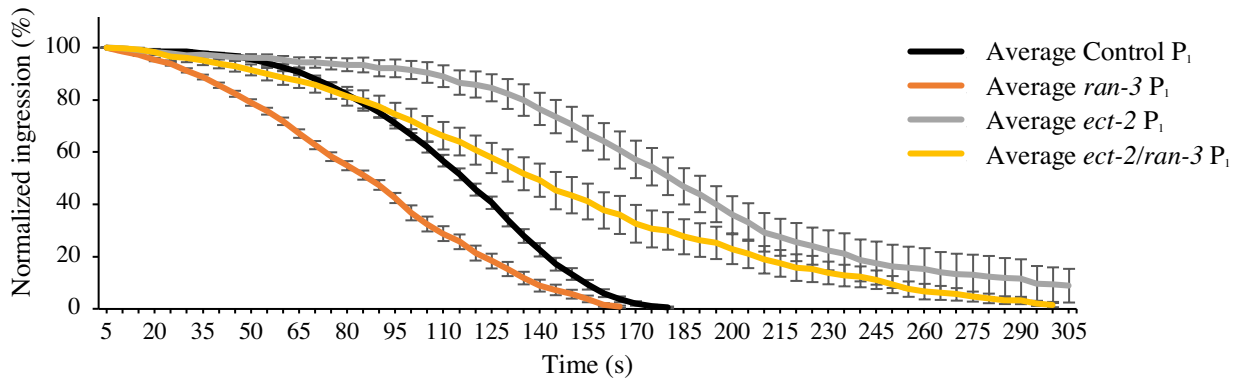
D

Figure 14. Ingression in *ect-2* embryos is delayed. A) A graph shows the average % ingression rates of control P₀ (black curve; n = 10), AB (orange curve; n = 16) and P₁-cell (grey curve; n = 35) ring closure over time in seconds. Error bars show SEM. B) A graph shows the average % ingression rates of *ect-2* P₀ (black curve; n = 10), AB (orange curve; n = 11) and P₁-cell (grey curve; n = 12) ring closure over time in seconds. Error bars show SEM. C) Table shows rates of ingression (percent/s), represented in D. D) Color heat maps show the different rates for each phase of ingression for control (top) and *ect-2* (bottom) embryos. The corresponding color for each rate of ingression (percent/s) is shown on the scale (right). Rates of ingression were plotted from anaphase onset until 40% furrow closure.

A**B****C**

D

	Ring assembly phase	Furrow initiation phase	Ring constriction phase
Control P ₀	0.07	0.5	1
<i>ran-3</i> P ₀	0.1	0.6	0.9
<i>ect-2</i> P ₀	0.04	0.2	0.5
<i>ect-2/ran-3</i> P ₀	0.09	0.3	0.6
Control AB	0.1	0.3	0.6
<i>ran-3</i> AB		0.4	0.7
<i>ect-2</i> AB		0.2	0.5
<i>ect-2/ran-3</i> AB		0.3	0.6
Control P ₁	0.1	0.4	0.9
<i>ran-3</i> P ₁	0.3	0.6	0.8
<i>ect-2</i> P ₁	0.09	0.1	0.6
<i>ect-2/ran-3</i> P ₁	0.2	0.3	0.5

E

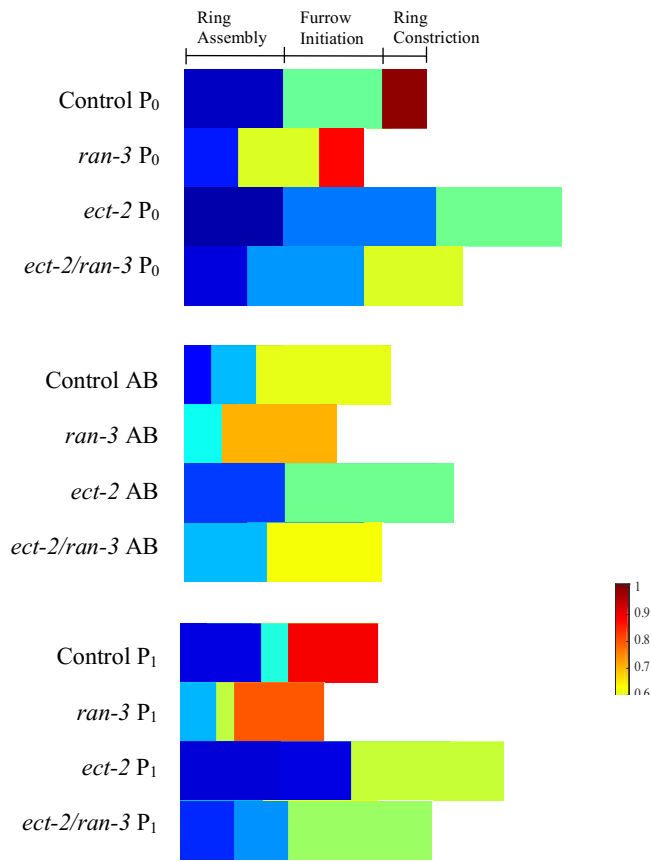
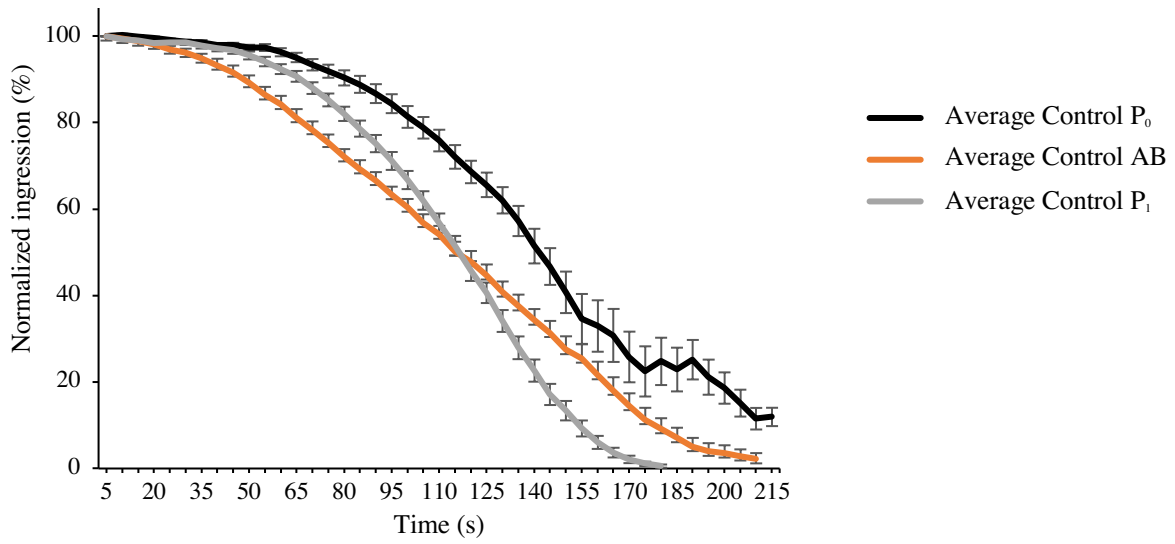
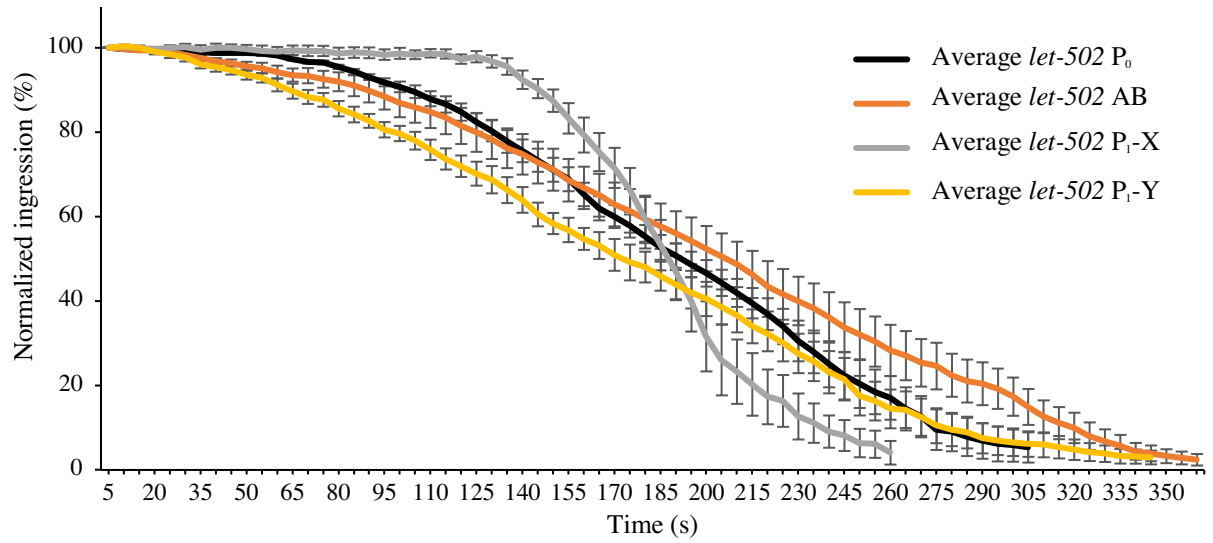


Figure 15. ECT-2 could be in the Ran pathway in all cells. A) A graph shows the average % ingression over time (in seconds) of P₀-cell division under Control (black curve; n = 10), *ran-3* RNAi (orange curve; n = 10), *ect-2* RNAi (grey curve; n = 10) and *ect-2/ran-3* RNAi (yellow curve, n = 14) treatment conditions. Error bars show SEM. B) A graph shows the average % ingression over time (in seconds) of AB-cell divisions under Control (black curve; n = 16), *ran-3* RNAi (orange curve; n = 11), *ect-2* RNAi (grey curve; n = 11) and *ect-2/ran-3* RNAi (yellow curve, n = 10) treatment conditions. Error bars show SEM. C) A graph shows the average % ingression over time (in seconds) of P₁-cell divisions under Control (black curve; n = 35), *ran-3* RNAi (orange curve; n = 21), *ect-2* RNAi (grey curve; n = 12) and *ect-2/ran-3* RNAi (yellow curve, n = 11) treatment conditions. Error bars show SEM. D) Table shows rates of ingression (percent/s), represented in E. E) Color heat maps show the different rates for each phase of ingression for P₀, AB, P₁ under indicated treatment conditions. The corresponding color for each rate of ingression (percent/s) is shown on the scale (right). Rates of ingression were plotted from anaphase onset until 40% furrow closure.

3.1.5 LET-502 has different threshold requirements in P₁ cells, and is Ran-dependent in P₀, AB and P₁ cells

To further show that Ran regulates cortical contractility, we studied phenotypes caused by co-depleting *ran-3* with *let-502*. The homologue of LET-502, Rho-binding kinase, regulates cortical contractility by phosphorylating myosin light chain, which is required to form bipolar filaments and mediate force generation on F-actin via crosslinking and/or cross-bridge cycling (Piekny and Mains, 2002; Piekny et al., 2005). LET-502 has been shown to regulate furrow ingression, but does not have an NLS and would not be regulated directly by the Ran pathway (Piekny and Mains, 2002). As expected, P₀, AB and P₁ cells in *let-502* RNAi embryos had slower ingression kinetics and an overall increase in the length of cytokinesis compared to control embryos (**Figure 16A, B**). However, we observed some very interesting differences in ingression kinetics in the different cells. First, we observed that AB cells were particularly sensitive to depletion of *let-502* and ingression was delayed/slower in comparison to the other cell types (**Figure 16A, B**). Second, we found that P₁ cells had a bimodal distribution of ingression that we classified as P₁-X or P₁-Y (**Figure 16A, B**). To our knowledge, such a distribution has not been previously reported. P₁-X cells had a severely delayed plateau, followed by rapid ingression that was comparable to control, while P₁-Y cells had kinetics that resembled AB cells. As shown in the heat maps in Figure 16D, all phases were longer and slower after *let-502* RNAi in P₀ and AB cells compared to control embryos. However, in *let-502* RNAi embryos, P₁-X cells had an extended ring assembly phase followed by a short furrow initiation phase and a constriction phase that more closely resembled control embryos. In addition, P₁-Y cells had ingression kinetics for the three phases that resembled AB cells. Thus, furrowing was delayed after *let-502* RNAi as expected for a regulator of contractile ring assembly and constriction.

A**B**

C

	Ring assembly phase	Furrow initiation phase	Ring constriction phase
Control P ₀	0.07	0.5	1
Control AB	0.1	0.3	0.6
Control P ₁	0.1	0.4	0.9
<i>let-502</i> P ₀	0.05	0.3	0.5
<i>let-502</i> AB	0.06	0.1	0.4
<i>let-502</i> P ₁ -X	0.02	0.4	1
<i>let-502</i> P ₁ -Y	0.1	0.3	0.4

D

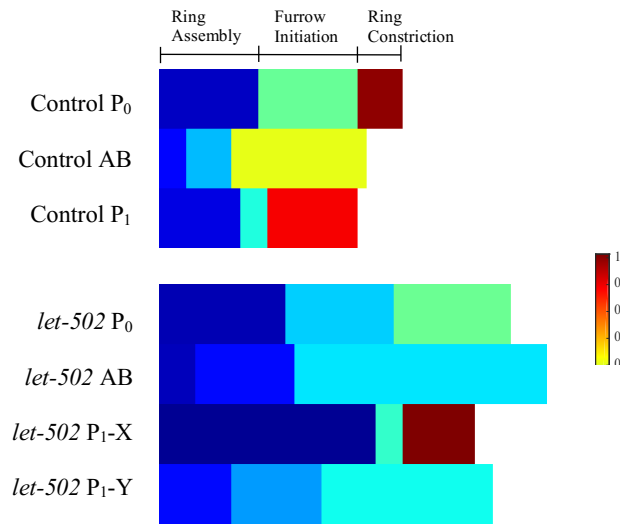


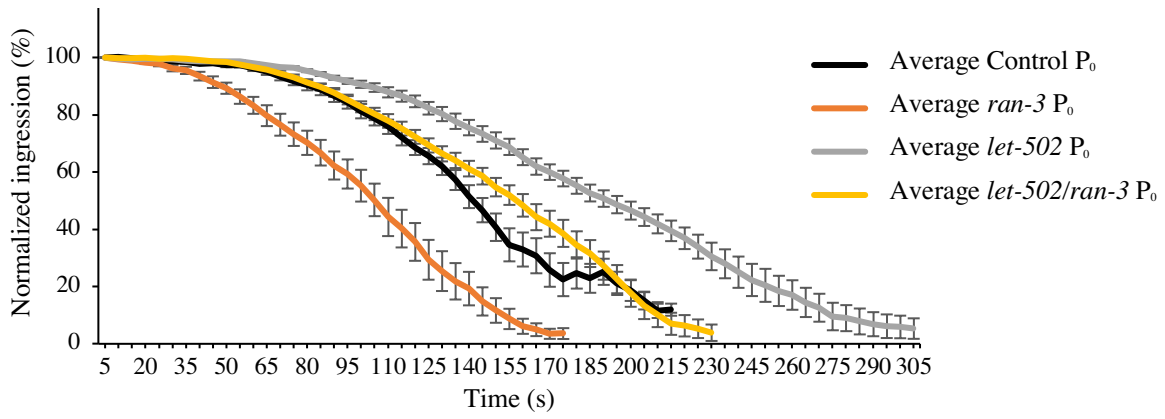
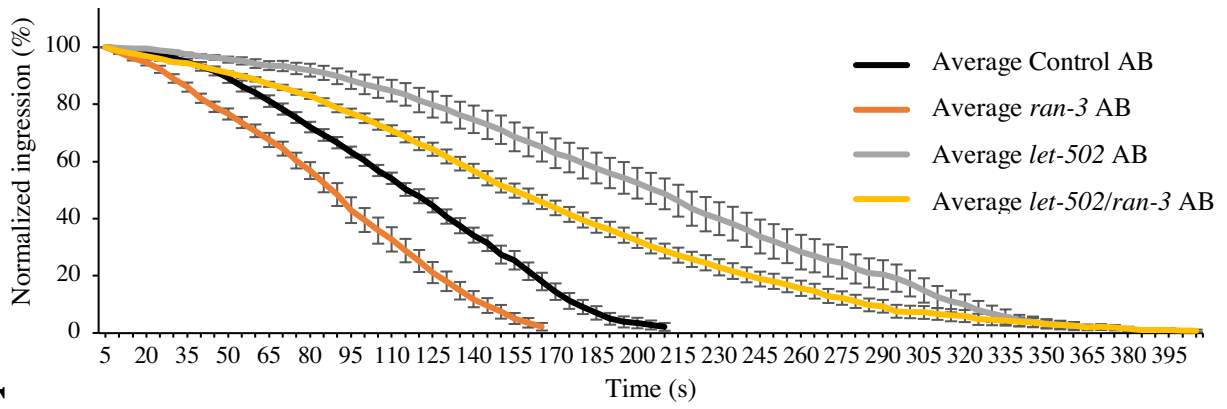
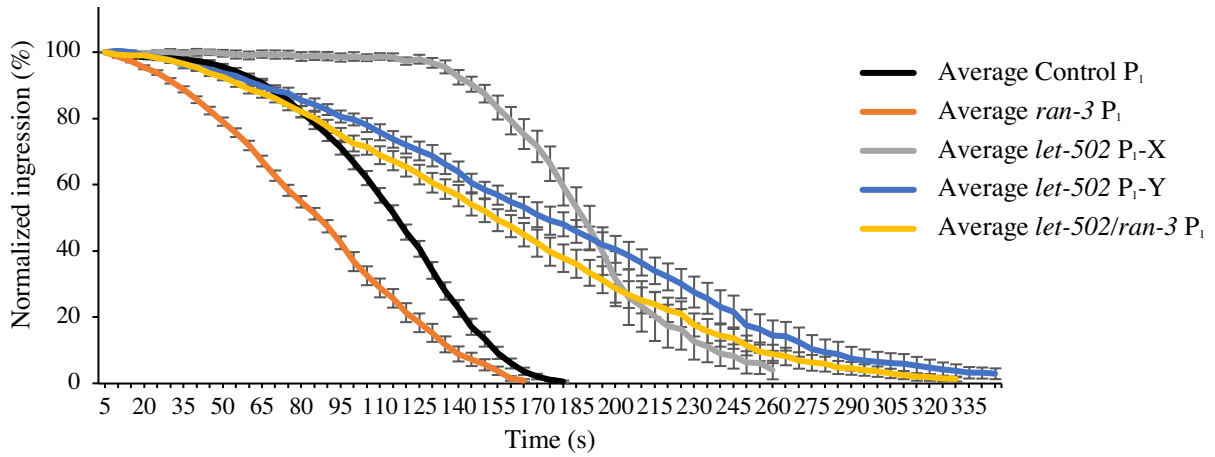
Figure 16. Ingression in *let-502* embryos is delayed. A) A graph shows the average % ingress rates of control P₀ (black curve; n = 10), AB (orange curve; n = 16) and P₁-cell (grey curve; n = 35) ring closure over time in seconds. Error bars show SEM. B) A graph shows the average % ingress rates of *let-502* P₀ (black curve; n = 10), AB (orange curve; n = 10) and P₁-cell ring closure over time in seconds. P₁ divisions have been separated into two groups based on kinetics, group X (grey curve; n = 9) and group Y (yellow curve; n = 6). Error bars show SEM. C) Table shows rates of ingress (percent/s), represented in D. D) Color heat maps show the different rates for each phase of ingress for control (top) and *let-502* (bottom) embryos. The corresponding color for each rate of ingress (percent/s) is shown on the scale (right). Rates of ingress were plotted from anaphase onset until 40% furrow closure.

However, there may be unique requirements and different thresholds for *let-502* depending on the cell type.

Next, we determined how co-depletion of *let-502* and *ran-3* affects ingress kinetics in P₀, AB and P₁ cells. We predicted that if the Ran pathway regulates contractility, depletion of *let-502* should suppress the faster kinetics caused by *ran-3* RNAi. P₀ cells in embryos co-depleted of *let-502* and *ran-3* ingressed similar to cells in control embryos (**Figure 17A**), while AB cells took longer to ingress and complete cytokinesis similar to *let-502* RNAi embryos (**Figure 17B**). P₁ cells in co-depleted embryos no longer separated into two groups – all cells displayed similar ingress kinetics, which resembled AB cells (**Figure 17C**). As shown in the heat maps in Figure 17E, the ring assembly and furrow initiation phases were longer and/or slower in P₀ and AB cells in co-depleted embryos compared to control or *ran-3* RNAi embryos. P₁ cells in co-depleted embryos had interesting kinetics – with a shorter ring assembly phase, but a longer, slower furrow initiation phase and slower constriction phase compared to control or *ran-3* RNAi embryos, highly reminiscent of AB cells in *let-502* RNAi embryos. Thus, our data supports that the faster kinetics observed after perturbation of the Ran pathway is via regulating cortical contractility. We also found unique requirements for *let-502* in AB vs. P₁ cells, which could reflect different mechanistic regulation of cytokinesis in different cell types. Our data also hints toward a polarity phenotype in *let-502* RNAi embryos, where P₁ cells may no longer retain their identity.

3.2 Ingression kinetics is cell-fate dependent

Our data supports that P₀, AB and P₁ have different ingress kinetics, and we wondered if changing the fate of AB and P₁ cells would also change these kinetics. In early *C. elegans*

A**B****C**

D

	Ring assembly phase	Furrow initiation phase	Ring constriction phase
Control P ₀	0.07	0.5	1
<i>ran-3</i> P ₀	0.1	0.6	0.9
<i>let-502</i> P ₀	0.05	0.3	0.5
<i>let-502/ran-3</i> P ₀	0.05	0.4	0.6
Control AB	0.1	0.3	0.6
<i>ran-3</i> AB		0.4	0.7
<i>let-502</i> AB	0.06	0.1	0.4
<i>let-502/ran-3</i> AB	0.3	0.2	0.4
Control P ₁	0.1	0.4	0.9
<i>ran-3</i> P ₁	0.3	0.6	0.8
<i>let-502</i> P ₁ -X	0.02	0.4	1
<i>let-502</i> P ₁ -Y	0.1	0.3	0.4
<i>let-502/ran-3</i> P ₁	0.1	0.3	0.4

E

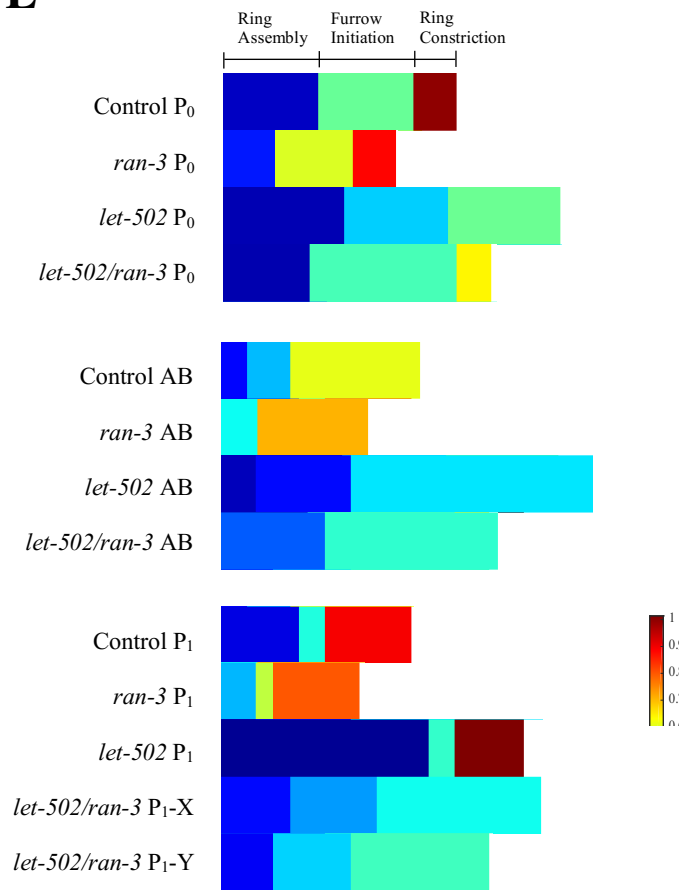
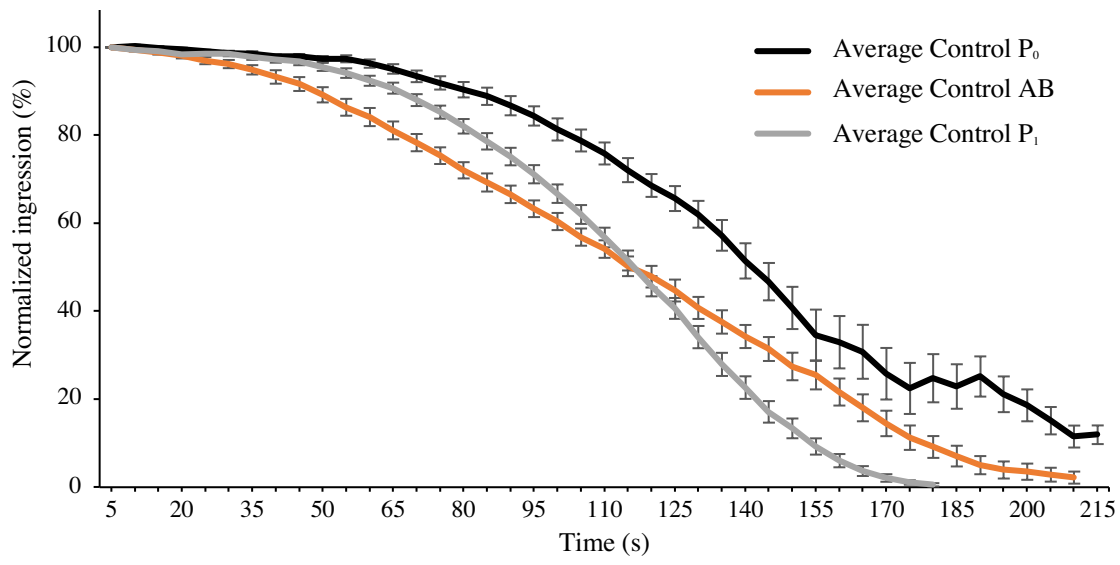
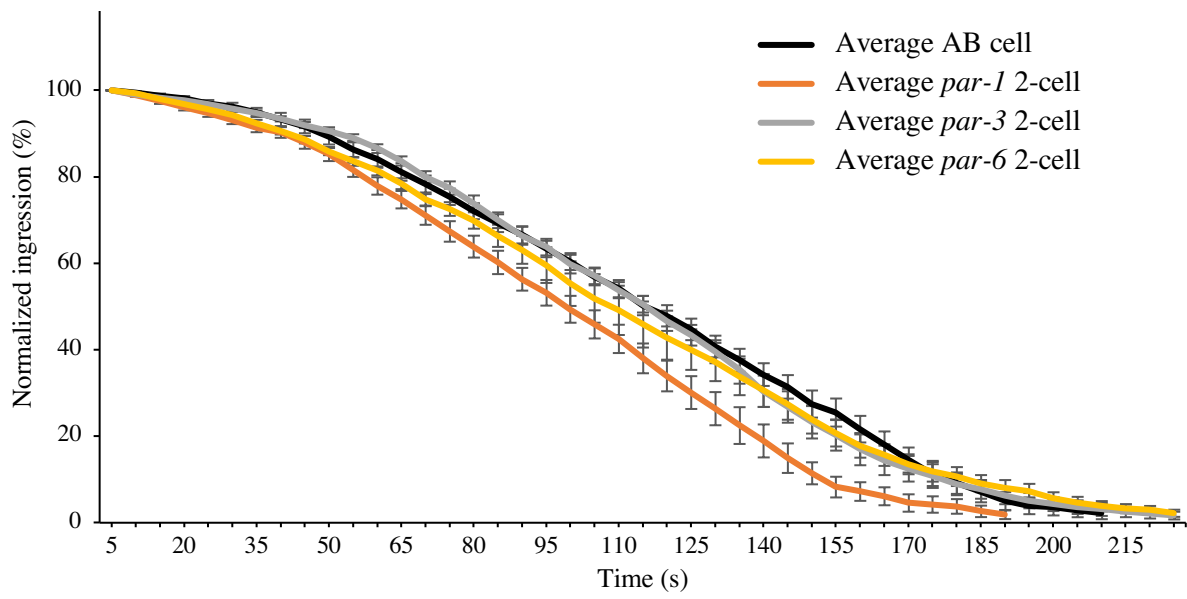


Figure 17. LET-502 may be in the Ran pathway in all cells. A) A graph shows the average % ingression over time (in seconds) of P₀-cell division under Control (black curve; n = 10), *ran-3* RNAi (orange curve; n = 10), *let-502* RNAi (grey curve; n = 10) and *let-502/ran-3* RNAi (yellow curve, n = 11) treatment conditions. Error bars show SEM. B) A graph shows the average % ingression over time (in seconds) of AB-cell divisions under Control (black curve; n = 16), *ran-3* RNAi (orange curve; n = 11), *let-502* RNAi (grey curve; n = 10) and *let-502/ran-3* RNAi (yellow curve, n = 11) treatment conditions. Error bars show SEM. C) A graph shows the average % ingression over time (in seconds) of P₁-cell divisions under Control (black curve; n = 35), *ran-3* RNAi (orange curve; n = 21), *let-502* RNAi (Group X (grey curve), n = 9; and Group Y (blue curve), n = 6) and *let-502/ran-3* RNAi (yellow curve, n = 12) treatment conditions. Error bars show SEM. D) Table shows rates of ingression (percent/s), represented in E. E) Color heat maps show the different rates for each phase of ingression for P₀, AB, P₁ under indicated treatment conditions. The corresponding color for each rate of ingression (percent/s) are shown on the scale (right). Rates of ingression were plotted from anaphase onset until 40% furrow closure.

embryos, the first division occurs asymmetrically to produce a larger, anterior AB daughter, and a smaller, posterior P₁ daughter, which is fated to become the germline (Rose and Gönczy, 2014). This anterior/posterior asymmetry is controlled by the PAR proteins, where PAR-3, PAR-6 and PKC-3 form a complex at the anterior, and mutually exclude PAR-1 and PAR-2, which form a complex at the posterior (Rose and Gönczy, 2014). Cortical contractility is enriched in the anterior as it is controlled by and feeds back to reinforce the anterior PAR complex (Cowan and Hyman, 2007). To determine how changing polarity affects ingression kinetics, we performed RNAi to *par-3*, *par-6* or *par-1*. We predicted that depletion of any of the PARs would cause ingression kinetics to be uniform between cells, and resemble a hybrid of AB/P₁ cells, but *par-1* depletion should have caused faster ingression kinetics, because these cells would have ectopic cortical contractility. We focused our analysis on the daughters of P₀ in the *par*-depleted embryos to compare their ingression kinetics to AB and P₁ cells in control embryos. As shown in Figure 18, cells had similar kinetics for each RNAi condition, and there was no difference between cells in *par-3* or *par-6* RNAi embryos, which resembled AB cells in control embryos. Cytokinesis was faster in *par-1* RNAi embryos, although this difference was not as large as expected (**Figure 18B**). As shown in the heat maps in Figure 18D, only two distinct phases were observed for cells in *par* RNAi embryos, and their duration and rate of ingression were more similar to AB cells.

3.3 Ran-GTP influences the correlation between ingression and cell size in early *C. elegans* embryos

Previous studies described a correlation between the rate of ingression and cell size – large cells with more contractile units (larger rings with more actomyosin) ingress faster vs.

A**B**

C

	Ring assembly phase	Furrow initiation phase	Ring constriction phase
Control AB	0.1	0.3	0.6
<i>par-1</i> 2-cell	0.2	0.3	0.7
<i>par-3</i> 2-cell	0.2	0.3	0.6
<i>par-6</i> 2-cell	0.1	0.3	0.6

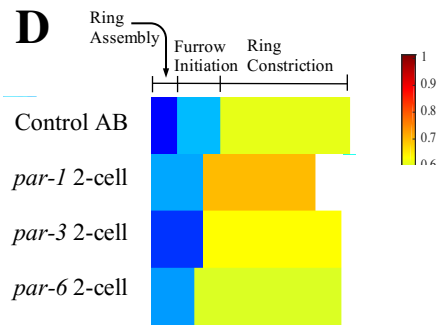


Figure 18. Switching cell fate changes ingress kinetics. A) A graph shows the average % ingress rates of control P₀ (black curve; n = 10), AB (orange curve; n = 16) and P₁-cell (grey curve; n = 35) ring closure over time in seconds. Error bars show SEM. B) A graph shows the average % ingress rates of control AB cells (black curve; n=16) and 2-cell embryos treated with *par-1* (orange curve; n = 10), *par-3* (grey curve; n = 12) and *par-6* (yellow curve; n = 10) RNAi. Error bars show SEM. C) Table shows rates of ingress (percent/s), represented in D. D) Color heat maps show the different rates for each phase of ingress for control and RNAi treated embryos. The corresponding color for each rate of ingress (percent/s) are shown on the scale (right). Rates of ingress were plotted from anaphase onset until 40% furrow closure.

small cells with fewer contractile units (Carvalho et al., 2009). This mechanism equalizes the rates between cells to ensure that their timing is coordinated in the early embryo regardless of size. However, prior studies only measured rates of ring constriction and ignored kinetics in earlier stages of cytokinesis. This is partly because their temporal resolution was lower in comparison to our study (20 second intervals vs. 5 second intervals). In addition, they grouped AB and P₁ cells together, even though these cells have different sizes (~30%), which may have skewed their outcome. Knowing the impact of cell size on furrowing/ingression kinetics is important for our study, since we hypothesize that the Ran pathway has a larger influence on cytokinesis in smaller cells when chromatin is closer to the cortex. First, to determine if there is a difference in ingression kinetics based on cell size from anaphase onset, we plotted the ingression of all control cells (P₀, AB and P₁) and colour coded them according to their size (*e.g.* red is large, blue is medium, and green is small; **Figure 19**). We observed a large distribution in the completion of cytokinesis (>125 seconds between cells) with the bulk of green cells completing cytokinesis sooner vs. red cells, which does not agree with the previous study (Carvalho et al., 2009; **Figure 19**). Further, we observed that some of the green cells had a longer ring assembly phase, but faster ingression and this difference in early vs. late phase kinetics makes it difficult to study their correlation with cell size (**Figure 19**). Next, we plotted multiple P₀, AB and P₁ cells from *ran-3* RNAi embryos in the same way (**Figure 19**). This time we saw a tighter distribution where cytokinesis of all cells completed <100 seconds of each other, and most completed within 50-75 seconds, and only the larger cells had a more obvious assembly phase (**Figure 19**). Thus, the larger cells tended to take longer overall to complete vs. the smaller cells as before, but their rates were more comparable. For example, it takes longer to assemble a contractile ring in a larger cell, but once it is assembled, it can constrict as quickly, or

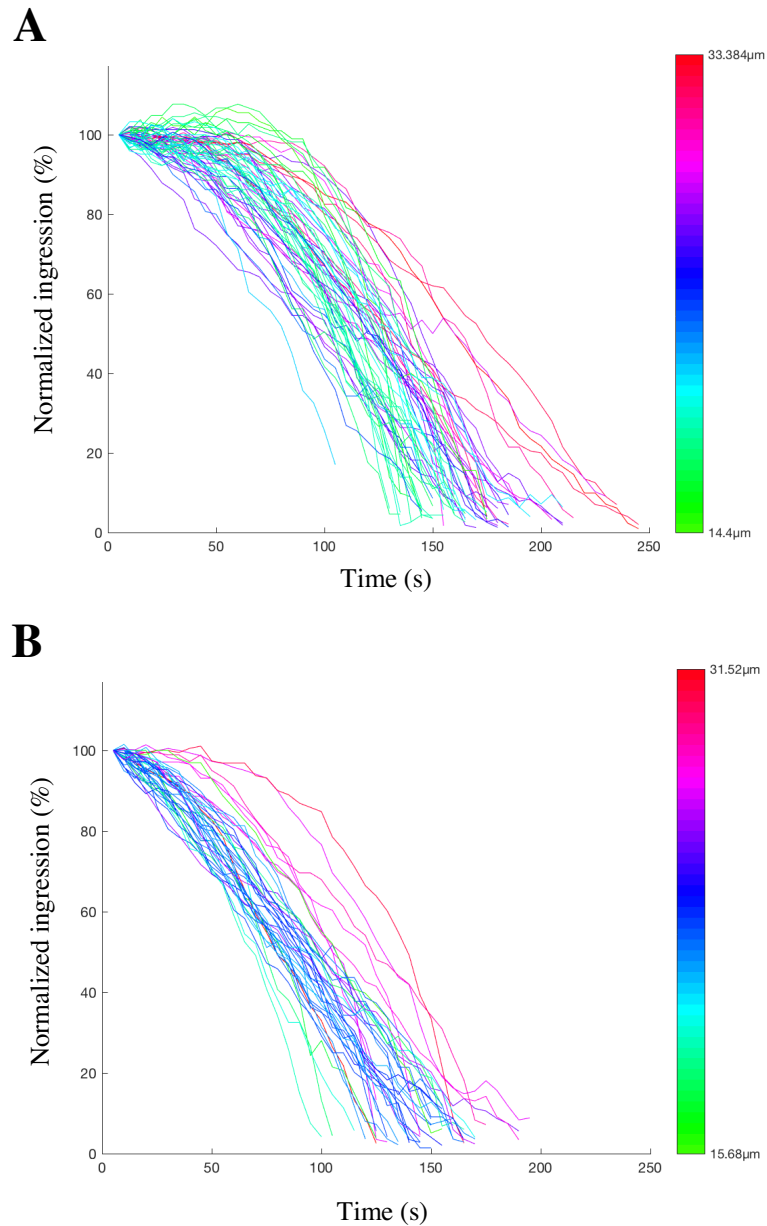


Figure 19. Decreasing Ran-GTP increases the correlation between ingress and cell size.

A) Graph shows the rates of ring closure for Control embryos ($n = 61$), color-coded according to the size of the cell. Color scale (right) is in microns, with the smallest cell (green) being a Control P_0 , and the largest cell (red) being a Control P_1 . B) Graph shows the rates of ring closure for *ran-3* RNAi embryos ($n = 42$), color-coded according to the size of the cell. Color scale (right) is in microns, with the smallest cell (green) being a *ran-3* P_0 , and the largest cell (red) being a *ran-3* P_1 .

more rapidly in comparison to smaller cells. Therefore, our data suggests that the Ran pathway mostly affects the early phases of cytokinesis – ring assembly and/or furrow initiation in smaller vs. larger cells.

Chapter 4: Discussion

In this thesis, we studied the conservation and biological relevance of the Ran pathway in regulating cytokinesis in early *C. elegans* embryos. Cytokinesis requires tight spatial and temporal control to prevent changes in ploidy or cell fate (Green et al., 2012). Microtubule-dependent and –independent pathways work together to ensure that the division plane is properly positioned (Dechant and Glotzer, 2003; Murthy and Wadsworth, 2008; Basant et al., 2015; Price and Rose, 2017). However, many of these pathways have not been well-studied, in particular their requirement in different organisms and cell types. Our lab recently discovered a role for the Ran pathway in regulating human cell cytokinesis, and we wanted to determine if the pathway also regulates cytokinesis in *C. elegans* embryos. Using an *in vivo* model system permits us to study the biological relevance of this pathway, and how its requirement varies depending on cell type. For example, in the early *C. elegans* embryo, the first asymmetric division creates two daughter cells (AB and P₁) with different fates. First, through extensive characterization of cytokinesis in the P₀ (fertilized zygote), AB and P₁ cells, we found that cytokinesis can be divided into three phases based on changes in velocity of the ingressing membrane, and each cell has unique ingression kinetics. The first phase is the plateau in our graphs of ingression, with very slow velocity (<0.1 percent/s) and is called the ring assembly phase, during which actomyosin filaments accumulate in the equatorial plane (Osorio et al., 2018). The ring assembly phase was prominent in P₀ and P₁ cells, and was noticeably shorter in the AB cells (**Figure 8B, C**). The second phase has an intermediate ingression rate (~0.3-0.5 percent/s) and is called furrow initiation phase, where actomyosin filaments align in the equatorial plane and the membrane starts to visibly indent (Osorio et al., 2018). This phase varied in duration between P₀,

AB and P₁ cells. The third is the fastest (>0.6 percent/s) and is called the constriction phase due to shortening of the actomyosin ring, which brings the membrane together (Osorio et al., 2018). This phase is also variable in duration between the P₀, AB and P₁ cells. Next, we found that decreasing the level of Ran-GTP in the cells by partially knocking down the Ran-GEF (*ran-3*; RCC-1) through RNAi caused a change in ingression kinetics in P₀, AB and P₁ cells – where ingression appeared more linear (**Figure 9**). Most notably, the ring assembly phase was proportionally shorter in duration, or gone altogether. We observed a similar effect after partially knocking down *ima-3*/importin-alpha (**Figure 10**). Therefore, the change in ingression kinetics is not RAN-3/RCC-1-specific, but rather involves other components of the pathway. In our model, importin-beta binds to cargo, such as ANI-1/anillin or other contractile regulators, and potentiates their recruitment to the cortex and/or activity by stabilizing an open conformation (e.g. Beaudet et al., 2017). Thus, since importin-beta forms a complex with importin-alpha that in turns binds to Ran-GTP to release importin from cargo, reducing Ran-GTP or importin-alpha should free up additional importin-beta for cargo binding.

To test our model, we needed to show that contractile ring components are regulated by the Ran pathway. The faster ingression kinetics observed in *ran-3* or *ima-3*-depleted cells suggests that the actomyosin filaments assemble more rapidly, and may be more contractile. First we studied anillin, since our lab previously showed in mammalian cells that anillin directly binds to importin and is regulated by Ran-GTP for its function in cytokinesis (Beaudet et al., 2017). While *ani-1* RNAi caused overall delays in ingression in all three cells, the ring assembly phase was particularly extended in P₁ cells (**Figure 12**). Following co-depletion with *ran-3*, the length and/or ingression rate of the different phases in P₀ and AB cells more closely resembled control cells, but P₁ *ani-1*; *ran-3* cells showed phenotypes more similar to *ran-3* (**Figure 13**). Thus,

while ANI-1 could be a target in P₀ and AB cells, it may not be in P₁ cells, revealing differences in how the Ran pathway affects cytokinesis in cells with different fates. Studies currently being done by our lab have found that ANI-1 is highly enriched at the cortex in AB, but not P₁ cells (data not shown). Since the Ran pathway regulates mammalian anillin via importin binding near the cortex, these lower levels of cortical ANI-1 may not require regulation via this pathway.

To study the impact of Ran on contractility, we studied the effects of partially knocking down ECT-2, the GEF that generates active RhoA to form F-actin and active myosin for cytokinesis. As expected, weak *ect-2* RNAi delayed and/or slowed all phases of ingression in P₀, AB and P₁ cells (**Figure 14**). Co-depletion of *ect-2* and *ran-3* caused phenotypes of all cells to more closely resemble control cells (**Figure 15**). These results indicate that ECT-2 could be in the Ran pathway in P₀, AB and P₁ cells. This effect could be direct or indirect. As a major regulator of cytokinesis, one possibility is that the protein being regulated directly by the Ran pathway increases cortical contractility in *ran-3* embryos, and reducing a global regulator of active RhoA reduces this ectopic contractility to restore balance to the cells (Glotzer, 2005). However, another exciting possibility is that ECT-2 is a direct target of the Ran pathway. Mammalian Ect2 has an NLS in the middle of the protein, which lies near a Cdk1 phosphorylation site that promotes autoinhibition of Ect2. A prevailing model in the field is that removal of this phosphorylation at anaphase onset permits Ect2 to bind to Cyk4, timing its activation and the generation of active RhoA with mitotic exit (Yuce et al., 2005; Hara et al., 2006; Niiya et al., 2006; Wolfe et al., 2009). But one of the caveats to this model is whether dephosphorylation would be sufficient to drastically alter Ect2's conformation. An exciting hypothesis is that importin binding to the nearby NLS could aide this step, to help open Ect2 for

mitotic exit. Since the NLS is conserved in *C. elegans* importin binding could mediate ECT-2 activation.

To extend our studies of the impact of Ran on contractility, we also studied another regulator of cytokinesis, the Rho kinase LET-502, which activates myosin (Piekny and Mains, 2002). As expected, *let-502* RNAi extended and/or decreased the rate of all phases of ingression in P₀ and AB cells (**Figure 16**). The AB cells seemed to be particularly affected by the reduction of LET-502, with some P₁ cells furrowing well before AB. In addition, reducing LET-502 had a very interesting effect on P₁ cells, where we saw bimodal distribution in ingression kinetics. Some cells (P₁-X) had a severely elongated ring assembly phase followed by rapid furrow initiation and constriction. The other cells (P₁-Y) had a shorter ring assembly phase followed by a very linear ingression until furrow closure, which resembles control AB cells. Since this project relies on partial knockdown of proteins (vs. null), we believe that we may have uncovered different threshold requirements for LET-502 in the P₁ cells. The P₁-X cells struggle to assemble a contractile ring, while the P₁-Y cells may have polarity reversal. This could explain why heterochronicity between AB and P₁ cell division is partially lost in some of the embryos (Guo and Kemphues, 1996; Osorio et al., 2018). Co-depletion of *ran-3* and *let-502* caused ingression kinetics that were more similar to control (P₀) or slower and more linear vs. control (AB and P₁) (**Figure 17**). Importantly, the different phases of ingression were extended and/or slower in rate compared to *ran-3*. Therefore, LET-502 is in the Ran pathway in P₀, AB and P₁ cells, but since LET-502 does not contain an NLS, we hypothesize that this is indirect, through regulation of contractility.

We were also interested to know how altering cell fate would influence ingression kinetics. As described in the introduction, P₀ embryos have anterior-posterior asymmetry with a

more contractile cortex in the anterior. Ingression occurs asymmetrically to produce the anterior AB and posterior P₁ cell, which is dependent on the PAR proteins. Since PAR-1 and PAR-2 are required for determining the posterior cortex, depletion of *par-1* is expected to cause expansion of the anterior cortex, with more global cortical contractility. Depletion of *par-3* or *par-6*, which encode components of the anterior PAR complex should cause expansion of the posterior cortex and overall lower global contractility. Not surprisingly, P₀ daughter cells in embryos depleted of *par-1*, *par-3* or *par-6* lost their fate and had similar ingression kinetics (data not shown). However, we were surprised to observe that all of the ingression kinetics resembled each other regardless of whether the posterior or anterior PAR was depleted, and resembled control AB cells (**Figure 18**). Therefore, our results suggest that changing cell fate does indeed change ingression kinetics. We plan to image actin and myosin in these cells to determine how their localization compares in *par-1* vs. *par-3* or *par-6* embryos. Our data supports that there is an increase in cortical contractility in AB cells (vs. P₀ or P₁ cells), and this increase may still occur when cell fate is lost, suggesting it may be part of a ‘default’ pathway/mechanism.

Our data also revealed that there is a strong correlation between overall rates of ingression and cell size that is ‘hidden’ in the presence of wild-type levels of RAN-3 (RCC-1) (**Figure 19**). While control embryos showed weak correlation with the rate of closure and cell size, *ran-3*-depleted embryos showed stronger correlation with size, such that larger cells had faster rates of ingression. A previous study hypothesized that rates of ingression increase proportionally with cell size. This is because the contractile ring in larger cells would have more units of active actomyosin filaments vs. smaller rings (Carvalho et al., 2009). However, their study was done by imaging at 20 second intervals (vs. 5 in this study), and they did not separate AB vs. P₁ cells in their analysis, which are different sizes. Due to these issues, they only

considered constriction (the last phase of ingression) to observe a strong R value. Our data shows that by manipulating kinetics to ‘equalize’ the phases as in the *ran-3* embryos, this correlation can be better revealed.

It is worth mentioning that one of the major caveats of this study is the use of partial RNAi, which may complicate the ordering, or placement of genes in pathways. In addition, there could also be different thresholds for gene requirements in cytokinesis and our conditions only permit us to observe one or two (*e.g.* as in the case of *let-502* RNAi in P₁ cells), but we could be missing others. Using separation-of-function mutations or null alleles where possible could provide a more accurate placement of these proteins in the Ran pathway. However, all of the genes tested in this study are required in the germline, and maternally required in the early embryo making the use of null alleles impossible. However, we could take advantage of temperature-sensitive alleles, which exist for *let-502* and *ect-2*, and generate CRISPR mutant alleles containing NLS mutations in *ect-2* and *ani-1*. Another experiment that is currently being done is to determine if importin- β phenocopies importin- α RNAi, and we will determine if *ran-2* (RanGAP) RNAi causes the opposite phenotype to *ran-3* and slows furrow ingression. In addition, we are examining the localization of contractile proteins (actin, myosin) and regulators such as ECT-2 and ANI-1 in the different RNAi conditions, which could help us to understand how Ran modulates their function for cytokinesis.

Our model is that Ran-GTP regulates cytokinesis through its inverse relationship with importins. Near the chromatin, importins are bound to active Ran, while they are free to bind to cargo near the cortex. We hypothesize that importin-alpha or beta binding to the NLS region of a contractile protein could influence its conformation and/or affinity for other binding partners, This is supported by data in mammalian cells showing that importin binding to anillin helps

increase its affinity for the cortex. Thus, in our system, reducing Ran-GTP via *ran-3* RNAi may free more importins for cargo binding, causing hypercontractility. Our data suggests that importin-alpha and -beta (although some of this hasn't been tested) are both able to bind and/or positively regulate NLS-containing contractile proteins, but the heterodimer may be less able to do so (**Figure 20**). Therefore, reducing one importin (i.e. importin-alpha, as described in this thesis) could reduce the ratio of heterodimer complex found in the cell, and favor a cortically enriched pool through binding to the other importin. Importin-beta has been shown to bind human anillin, and *Drosophila* anillin has been shown to bind to importin-alpha and beta (Beaudet et al., 2017; Silberman-Gavrila et al., 2008). Mammalian Ect2 also has been shown to bind to importin-alpha and beta through its NLS, and it is exciting to speculate that ECT-2 could similarly be regulated by importins for enhanced activation and/or cortical recruitment.

This thesis elucidates a role for Ran in cytokinesis and has uncovered interesting cell-specific differences in the regulation of contractile proteins. Studying mechanisms regulating division *in vivo* is crucial to uncover their biological importance. The varying requirements of Ran, and different regulation of contractile proteins in cells of different fates is crucial for development, where the timing of divisions ensures that correct cell-cell contacts are established at the right time (Rose and Gönczy, 2014). In addition, cancer cells with higher ploidy have been shown to have steeper Ran-GTP gradients, which may mean that the Ran pathway promotes division in aneuploid cells, making further investigation of this pathway an interesting research avenue (Hasegawa et al., 2013).

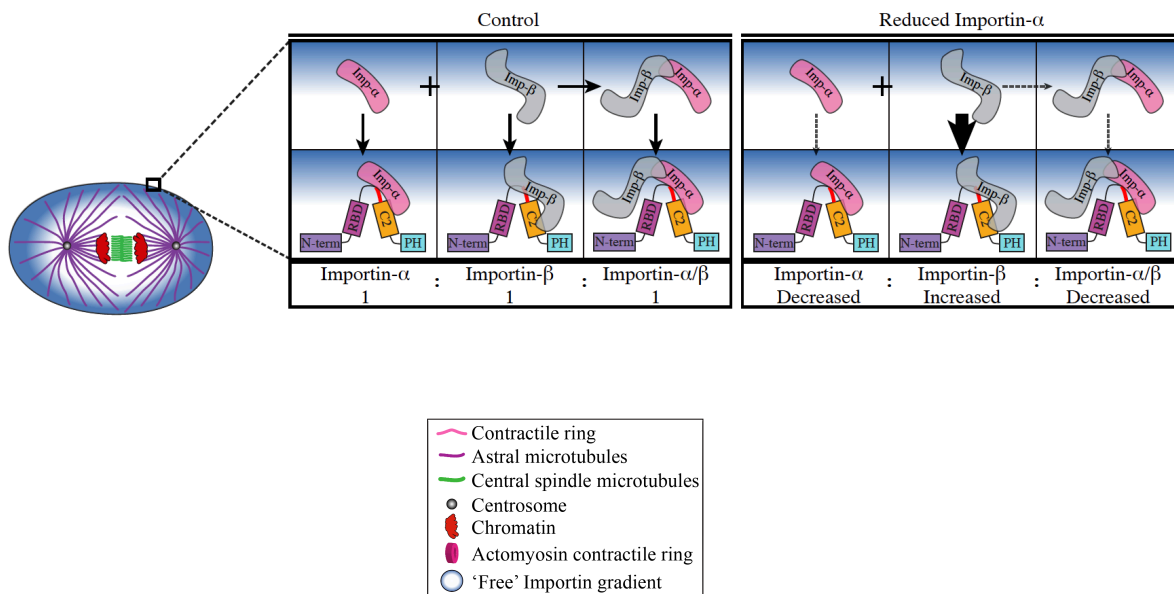


Figure 20. Model for the Ran regulation of cytokinesis. Schematic overview of the inverse gradient between Ran-GTP and importins, such that 'free' importins are in highest concentration (darkblue shading) by the cortex and lowest by chromatin (no shading). We propose that importin-alpha or beta-binding could potentiate the cortical recruitment of contractile proteins, but the heterodimer may not. Thus, reducing either importin-alpha or beta, while reducing binding through the heterodimer (dashed arrow), could favor a favor a cortically enriched pool via binding to the other importin (bold arrow). Similarly, reducing Ran-GTP levels would increase the overall availability of 'free' importins, also leading to cortically enriched contractile protein localization and faster ingression. Figure provided by Daniel Beaudet.

Chapter 5: References

- Askjaer, P., Galy, V., Hannak, E., & Mattaj, I. W. (2002). Ran GTPase Cycle and Importins α and β are essential for spindle formation and nuclear envelope assembly in Living *Caenorhabditis elegans* embryos. *Molecular Biology of the Cell*, 13(12), 4355–4370. <https://doi.org/10.1091/mbc.E02>
- Bamba, C., Bobinnec, Y., Fukuda, M., & Nishida, E. (2002). The GTPase Ran regulates chromosome positioning and nuclear envelope assembly in vivo. *Current Biology*, 12(6), 503–507. [https://doi.org/10.1016/S0960-9822\(02\)00741-8](https://doi.org/10.1016/S0960-9822(02)00741-8)
- Basant, A., Lekomtsev, S., Tse, Y. C., Zhang, D., Longhini, K. M., Petronczki, M., & Glotzer, M. (2015). Aurora B Kinase promotes cytokinesis by inducing centralspindlin oligomers that associate with the plasma membrane. *Developmental Cell*, 33(2), 204–215. <https://doi.org/10.1016/j.devcel.2015.03.015>
- Beaudet, D., Akhshi, T., Phillipp, J., Law, C., & Piekny, A. (2017). Active Ran regulates anillin function during cytokinesis. *Molecular Biology of the Cell*, 28(24), 3517–3531. <https://doi.org/10.1091/mbc.E17-04-0253>
- Bement, W. M., Benink, H. A., & von Dassow, G. (2005). A microtubule-dependent zone of active RhoA during cleavage plane specification. *Journal of Cell Biology*, 170(1), 91–101. <https://doi.org/10.1083/jcb.200501131>
- Benkemoun, L., Descoteaux, C., Chartier, N. T., Pintard, L., & Labbé, J. C. (2014). PAR-4/LKB1 regulates DNA replication during asynchronous division of the early *C. elegans* embryo. *Journal of Cell Biology*, 205(4), 447–455. <https://doi.org/10.1083/jcb.201312029>
- Brauchle, M., Baumer, K., & Gonczy, P. (2003). Differential Activation of the DNA Replication checkpoint contributes to asynchrony of cell division in *C. elegans* Embryos. *Current Biology*, 13(10), 819–827. <https://doi.org/10.1016/S>

- Brenner, S. (1974). The genetics of *Caenorhabditis elegans*. *Genetics*, 77(1), 71–94. <https://doi.org/10.1002/cbic.200300625>
- Bringmann, H., Cowan, C. R., Kong, J., & Hyman, A. A. (2007). LET-99, GOA-1/GPA-16, and GPR-1/2 are required for aster-positioned cytokinesis. *Current Biology*, 17(2), 185–191. <https://doi.org/10.1016/j.cub.2006.11.070>
- Budirahardja, Y., & Gonczy, P. (2008). PLK-1 asymmetry contributes to asynchronous cell division of *C. elegans* embryos. *Development*, 135(7), 1303–1313. <https://doi.org/10.1242/dev.019075>
- Cabernard, C., Prehoda, K. E., & Doe, C. Q. (2010). A mitotic spindle-independent cleavage furrow positioning pathway. *Nature*, 467(7311), 91–94. <https://doi.org/10.1038/nature09334>
- Canman, J. C., Lewellyn, L., Laband, K., Smerdon, S. J., Desai, A., & Oegema, K. (2008). Inhibition of Rac by the GAP activity of centralspindlin is essential for cytokinesis. *Science*, 322(5907), 1543–1546. <https://doi.org/10.1126/science.1163086>
- Carvalho, A., Desai, A., & Oegema, K. (2009). Structural memory in the contractile ring makes the duration of cytokinesis independent of cell size. *Cell*, 137(5), 926–937. <https://doi.org/10.1016/j.cell.2009.03.021>
- Clarke, P. R., & Zhang, C. (2008). Spatial and temporal coordination of mitosis by Ran GTPase, 9(6), 464–477. <https://doi.org/10.1038/nrm2410>
- Corsi, A. K., Wightman, B., & Chalfie, M. (2015). A transparent window into biology: A primer on *Caenorhabditis elegans*. *Genetics*, 200(2), 387–407. <https://doi.org/10.1534/genetics.115.176099>
- Cowan, C. R., & Hyman, A. A. (2007). Acto-myosin reorganization and PAR polarity in *C. elegans*. *Development*, 1043, 1035–1043. <https://doi.org/10.1242/dev.000513>

- Cuenca, A. A., Schetter, A., Aceto, D., Kempfues, K., & Seydoux, G. (2003). Polarization of the *C. elegans* zygote proceeds via distinct establishment and maintenance phases. *Development*, *130*(7), 1255–1265. <https://doi.org/10.1242/dev.00284>
- D'Avino, P. P., Giansanti, M. G., & Petronczki, M. (2015). Cytokinesis in animal cells. *Cold Spring Harbor Perspectives in Biology*, *7*(4), 1–18. <https://doi.org/10.1101/cshperspect.a015834>
- Dechant, R., & Glotzer, M. (2003). Centrosome separation and central spindle assembly act in redundant pathways that regulate microtubule density and trigger cleavage furrow formation. *Developmental Cell*, *4*(3), 333–344. [https://doi.org/10.1016/S1534-5807\(03\)00057-1](https://doi.org/10.1016/S1534-5807(03)00057-1)
- Deng, M., Suraneni, P., Schultz, R. M., & Li, R. (2007). The Ran GTPase mediates chromatin signaling to control cortical polarity during polar body extrusion in mouse oocytes. *Developmental Cell*, *12*(2), 301–308. <https://doi.org/10.1016/j.devcel.2006.11.008>
- Descovich, C. P., Cortes, D. B., Ryan, S., Nash, J., Zhang, L., Maddox, P. S., et al., Maddox, A. S. (2017). Crosslinkers both drive and brake cytoskeletal remodeling and furrowing in cytokinesis. *Molecular Biology of the Cell*, *29*(5), 622–631. <https://doi.org/10.1002/jcp.25016>
- Douglas, M. E., Davies, T., Joseph, N., & Mishima, M. (2010). Aurora B and 14-3-3 coordinately regulate clustering of centralspindlin during cytokinesis. *Current Biology*, *20*(10), 927–933. <https://doi.org/10.1016/j.cub.2010.03.055>
- Fededa, J. P., & Gerlich, D. W. (2012). Molecular control of animal cell cytokinesis. *Nature Cell Biology*, *14*(5), 440–447. <https://doi.org/10.1038/ncb2483>
- Gilbert, S.F. (2000). Early Development of the Nematode *Caenorhabditis elegans*. In *Developmental Biology* (6th edition). Sunderland, MA: Sinauer Associates. Retrieved from <https://www.ncbi.nlm.nih.gov/books/NBK10011/>
- Glotzer, M. (2005). The Molecular Requirements for Cytokinesis. *Science*, *307*(5716), 1735–1739. <https://doi.org/10.1126/science.1096896>

- Glotzer, M. (2017). Cytokinesis in metazoa and fungi. *Cold Spring Harbor Perspectives in Biology*, 9(10), 1–18. <https://doi.org/10.1101/cshperspect.a022343>
- Goldstein, B., & Macara, I. G. (2007). The PAR Proteins: Fundamental Players in Animal Cell Polarization. *Developmental Cell*, 13(5), 609–622. <https://doi.org/10.1016/j.devcel.2007.10.007>
- Goldstein, B. (1993). Establishment of gut fate in the E lineage of *C. elegans*: the roles of lineage-dependent mechanisms and cell interactions. *Development (Cambridge, England)*, 118, 1267–1277.
- Görlich, D., Pante, N., Kutay, U., Aebi, U., & Bischoff, F. (1996). Identification of different roles for RanGDP and RanGTP in nuclear protein import. *EMBO Journal*, 15(20), 5584–5594.
- Green, R. A., Paluch, E., & Oegema, K. (2012). Cytokinesis in Animal Cells. *Annual Review of Cell and Developmental Biology*, 28(1), 29–58. <https://doi.org/10.1146/annurev-cellbio-101011-155718>
- Grill, S. W., Gönczy, P., Stelzer, E. H. K., & Hyman, A. A. (2001). Polarity controls forces governing asymmetric spindle positioning in the *Caenorhabditis elegans* embryo. *Nature*, 409(6820), 630–633. <https://doi.org/10.1038/35054572>
- Guo, S., & Kemphues, K. J. (1996). A non-muscle myosin required for embryonic polarity in *Caenorhabditis elegans*. *Nature*, 382, 455. Retrieved from <https://doi.org/10.1038/382455a0>
- Hara, T., Abe, M., Inoue, H., Yu, L., Veenstra, T. D., Kang, Y. H., et al., Miki, T. (2006). Cytokinesis regulator ECT2 changes its conformation through phosphorylation at Thr-341 in G2 / M phase. *Oncogene*, 25(4), 566–578. <https://doi.org/10.1038/sj.onc.1209078>
- Hawkins, N., & Garriga, G. (1998). Asymmetric cell division: from A to Z. *Genes & Development*, 12(23), 3625–3638. <https://doi.org/10.1101/gad.12.23.3625>

- Heer, N. C., & Martin, A. C. (2017). Tension, contraction and tissue morphogenesis. *Development*, *144*(23), 4249–4260. <https://doi.org/10.1242/dev.151282>
- Jenkins, N., Saam, J. R., & Mango, S. E. (2006). CYK-4/GAP provides a localized cue to initiate anteroposterior polarity. *Science*, *313*(5791), 1298–1302.
- Kalab, P., Weis, K., & Heald, R. (2002). Visualization of a Ran-GTP gradient in interphase and mitotic *Xenopus* egg extracts. *Science*, *295*(5564), 2452–2456. <https://doi.org/10.1126/science.1068798>
- Kalab, P., Pralle, A., Isacoff, E. Y., Heald, R., & Weis, K. (2006). Analysis of a RanGTP-regulated gradient in mitotic somatic cells. *Nature*, *440*(7084), 697–701. <https://doi.org/10.1038/nature04589>
- Kalab, P., & Heald, R. (2008). The RanGTP gradient - a GPS for the mitotic spindle. *Journal of Cell Science*, *121*(10), 1577–1586. <https://doi.org/10.1242/jcs.005959>
- Kaletta, T., & Hengartner, M. O. (2006). Finding function in novel targets: *C. elegans* as a model organism. *Nature Reviews Drug Discovery*, *5*(April), 387–398. <https://doi.org/10.1038/nrd2031>
- Kemphues, K. J., Priess, J. R., Morton, D. G., & Cheng, N. S. (1988). Identification of genes required for cytoplasmic localization in early *C. elegans* embryos. *Cell*, *52*(3), 311–320. [https://doi.org/10.1016/S0092-8674\(88\)80024-2](https://doi.org/10.1016/S0092-8674(88)80024-2)
- Kiyomitsu, T., & Cheeseman, I. M. (2013). Cortical dynein and asymmetric membrane elongation coordinately position the spindle in anaphase. *Cell*, *154*(6), 391–402. <https://doi.org/10.1016/j.cell.2013.08.036>
- Kotynkova, K., Su, K., West, S. C., & Petronczki, M. (2016). Plasma Membrane Association but Not Midzone Recruitment of RhoGEF ECT2 Is Essential for Cytokinesis. *Cell Reports*, *17*(10), 2672–2686. <https://doi.org/10.1016/j.celrep.2016.11.029>

- Labbé, J. C., McCarthy, E. K., & Goldstein, B. (2004). The forces that position a mitotic spindle asymmetrically are tethered until after the time of spindle assembly. *Journal of Cell Biology*, *167*(2), 245–256. <https://doi.org/10.1083/jcb.200406008>
- Lekomtsev, S., Su, K.-C., Pye, V. E., Blight, K., Sundaramoorthy, S., Takaki, T., et al., Petronczki, M. (2012). Centralspindlin links the mitotic spindle to the plasma membrane during cytokinesis. *Nature*, *492*, 276. <https://doi.org/10.1038/nature11773>
- Lewellyn, L., Dumont, J., Desai, A., & Oegema, K. (2010). Analyzing the effects of delaying aster separation on furrow formation during cytokinesis in the *Caenorhabditis elegans* embryo. *Molecular Biology of the Cell*, *21*(22), 50–62. <https://doi.org/10.1091/mbc.E09>
- Lundquist, E. A. (2006). Small GTPases. *WormBook*. <https://doi.org/10.1895/wormbook.1.67.1>
- Maddox, A. S., Habermann, B., Desai, A., & Oegema, K. (2005). Distinct roles for two *C. elegans* anillins in the gonad and early embryo. *Development*, *132*(12), 2837–2848. <https://doi.org/10.1242/dev.01828>
- Maddox, A. S., Lewellyn, L., Desai, A., & Oegema, K. (2007). Anillin and the septins promote asymmetric ingression of the cytokinetic furrow. *Developmental Cell*, *12*(5), 827–835. <https://doi.org/10.1016/j.devcel.2007.02.018>
- Mangal, S., Sacher, J., Kim, T., Osório, D. S., Motegi, F., Carvalho, A. X., et al., Zanin, E. (2018). TPXL-1 activates Aurora A to clear contractile ring components from the polar cortex during cytokinesis. *Journal of Cell Biology*, *217*(3), 837–848. <https://doi.org/10.1083/jcb.201706021>
- Mendes Pinto, I., Rubinstein, B., & Li, R. (2013). Force to divide: Structural and mechanical requirements for actomyosin ring contraction. *Biophysical Journal*, *105*(3), 547–554. <https://doi.org/10.1016/j.bpj.2013.06.033>
- Moore, M. S., & Blobel, G. (1993). The GTP-binding protein Ran/TC4 is required for protein import into the nucleus. *Nature*, *365*, 661–663.

- Morton, D. G., Shakes, D. C., Nugent, S., Dichoso, D., Wang, W., Golden, A., & Kemphues, K. J. (2002). The *Caenorhabditis elegans* par-5 Gene encodes a 14-3-3 protein required for cellular asymmetry in the early embryo. *Developmental Biology*, 241(1), 47–58. <https://doi.org/10.1006/dbio.2001.0489>
- Motegi, F., Velarde, N. V, Piano, F., & Sugimoto, A. (2006). Two Phases of Astral Microtubule Activity during Cytokinesis in *C. elegans* Embryos. *Developmental Cell*, 10, 509–520. <https://doi.org/10.1016/j.devcel.2006.03.001>
- Murthy, K., & Wadsworth, P. (2008). Dual role for microtubules in regulating cortical contractility during cytokinesis. *Journal of Cell Science*, 121(14), 2350–2359. <https://doi.org/10.1242/jcs.027052>
- Niiya, F., Tatsumoto, T., Lee, K. S., & Miki, T. (2006). Phosphorylation of the cytokinesis regulator ECT2 at G2 / M phase stimulates association of the mitotic kinase Plk1 and accumulation of GTP-bound RhoA. *Oncogene*, 25(6), 827–837. <https://doi.org/10.1038/sj.onc.1209124>
- Oliferenko, S., Chew, T. G., & Balasubramanian, M. K. (2009). Positioning cytokinesis. *Genes and Development*, 23(6), 660–674. <https://doi.org/10.1101/gad.1772009>
- Osorio, D., Chan, F., Saramago, J., Leite, J., Silva, A., Sobral, A., et al., Carvalho, A. (2018). Flow-independent accumulation of motor-competent non-muscle myosin II in the contractile ring is essential for cytokinesis. bioRxiv <https://doi.org/https://doi.org/10.1101/333286>
- Petronczki, M., Glotzer, M., Kraut, N., & Peters, J. M. (2007). Polo-like Kinase 1 triggers the initiation of cytokinesis in human cells by promoting recruitment of the RhoGEF Ect2 to the central spindle. *Developmental Cell*, 12(5), 713–725. <https://doi.org/10.1016/j.devcel.2007.03.013>
- Petry, S. (2016). Mechanisms of mitotic spindle assembly. *Annual Review of Biochemistry*, 85(1), 659–683. <https://doi.org/10.1146/annurev-biochem-060815-014528>

- Piekny, A. J., & Glotzer, M. (2008). Anillin is a scaffold protein that links RhoA, Actin, and Myosin during cytokinesis. *Current Biology*, *18*(1), 30–36. <https://doi.org/10.1016/j.cub.2007.11.068>
- Piekny, A. J., & Maddox, A. S. (2010). The myriad roles of Anillin during cytokinesis. *Seminars in Cell and Developmental Biology*, *21*(9), 881–891. <https://doi.org/10.1016/j.semcdb.2010.08.002>
- Piekny, A. J., & Mains, P. E. (2002). Rho-binding kinase (LET-502) and myosin phosphatase (MEL-11) regulate cytokinesis in the early *Caenorhabditis elegans* embryo. *Journal of Cell Science*, *115*(11), 2271–2282.
- Piekny, A., Werner, M., & Glotzer, M. (2005). Cytokinesis: Welcome to the Rho zone. *Trends in Cell Biology*, *15*(12), 651–658. <https://doi.org/10.1016/j.tcb.2005.10.006>
- Price, K. L., & Rose, L. S. (2017). LET-99 functions in the astral furrowing pathway, where it is required for myosin enrichment in the contractile ring. *Molecular Biology of the Cell*, *28*(18), 2360–2373. <https://doi.org/10.1091/mbc.E16-12-0874>
- Riddle, D. L., Blumenthal, T., Meyer, B. J., & Priess, J. R. (1997). Introduction to *C. elegans*. In *C. elegans II*. (pp. 1-6). Plainview, NY: Cold Spring Harbor Laboratory Press.
- Rivers, D. M., Moreno, S., Abraham, M., & Ahringer, J. (2008). PAR proteins direct asymmetry of the cell cycle regulators Polo-like kinase and Cdc25. *Journal of Cell Biology*, *180*(5), 877–885. <https://doi.org/10.1083/jcb.200710018>
- Rodrigues, N. T. L., Lekomtsev, S., Jananji, S., Kriston-Vizi, J., Hickson, G. R. X., & Baum, B. (2015). Kinetochores-localized PP1–Sds22 couples chromosome segregation to polar relaxation. *Nature*, *524*(7566), 489–492. <https://doi.org/10.1038/nature14496>
- Rose, L. S., & Gönczy, P. (2014). Polarity establishment, asymmetric division and segregation of fate determinants in early *C. elegans* embryos. *WormBook*, 1–30. <https://doi.org/10.1895/wormbook.1>

- Roubinet, C., Decelle, B., Chicanne, G., Dorn, J. F., Payrastré, B., Payre, F., & Carreno, S. (2011). Molecular networks linked by Moesin drive remodeling of the cell cortex during mitosis. *Journal of Cell Biology*, *195*(1), 99–112. <https://doi.org/10.1083/jcb.201106048>
- Sáenz-Narciso, B., Gómez-Orte, E., Zheleva, A., Gastaca, I., & Cabello, J. (2016). Control of developmental networks by Rac/Rho small GTPases: How cytoskeletal changes during embryogenesis are orchestrated. *BioEssays*, *38*(12), 1246–1254. <https://doi.org/10.1002/bies.201600165>
- Schmutz, C., Stevens, J., & Spang, A. (2007). Functions of the novel RhoGAP proteins RGA-3 and RGA-4 in the germ line and in the early embryo of *C. elegans*. *Development*, *134*(19), 3495–3505. <https://doi.org/10.1242/dev.000802>
- Schubert, C. M., Lin, R., De Vries, C. J., Plasterk, R. H. A., & Priess, J. R. (2000). MEX-5 and MEX-6 function to establish soma/germline asymmetry in early *C. elegans* embryos. *Molecular Cell*, *5*(4), 671–682. [https://doi.org/10.1016/S1097-2765\(00\)80246-4](https://doi.org/10.1016/S1097-2765(00)80246-4)
- Sedzinski, J., Biro, M., Oswald, A., Tinevez, J. Y., Salbreux, G., & Paluch, E. (2011). Polar actomyosin contractility destabilizes the position of the cytokinetic furrow. *Nature*, *476*(7361), 462–468. <https://doi.org/10.1038/nature10286>
- Severson, A. F., Baillie, D. L., & Bowerman, B. (2002). A Formin Homology protein and a profilin are required for cytokinesis and Arp2/3-independent assembly of cortical microfilaments in *C. elegans*. *Current Biology*, *12*(24), 2066–2075. [https://doi.org/10.1016/S0960-9822\(02\)01355-6](https://doi.org/10.1016/S0960-9822(02)01355-6)
- Silverman-Gavrila, R. V., Hales, K. G., & Wilde, A. (2008). Anillin-mediated targeting of Peanut to pseudocleavage furrows is regulated by the GTPase Ran. *Molecular Biology of the Cell*, *19*(9), 3735–3744. <https://doi.org/10.1091/mbc.E08>
- Straight, A. F., Field, C. M., & Mitchison, T. J. (2005). Anillin Binds Nonmuscle Myosin II and Regulates the Contractile Ring. *Molecular Biology of the Cell*, *16*(1), 193–201. <https://doi.org/10.1091/mbc.E04>

- Tatsumoto, T., Xie, X., Blumenthal, R., Okamoto, I., & Miki, T. (1999). Human ECT2 Is an Exchange Factor for Rho GTPases, Phosphorylated in G2/M Phases, and Involved in Cytokinesis. *Journal of Cell Biology*, *147*(5), 921–927.
- Tse, Y. C., Piekny, A., & Glotzer, M. (2011). Anillin promotes astral microtubule-directed cortical myosin polarization. *Molecular Biology of the Cell*, *22*(17), 3165–3175. <https://doi.org/10.1091/mbc.E11-05-0399>
- Tse, Y. C., Werner, M., Longhini, K. M., Labbe, J. C., Goldstein, B., & Glotzer, M. (2012). RhoA activation during polarization and cytokinesis of the early *Caenorhabditis elegans* embryo is differentially dependent on NOP-1 and CYK-4. *Molecular Biology of the Cell*, *23*(20), 4020–4031. <https://doi.org/10.1091/mbc.E12-04-0268>
- van Oostende Triplet, C., Jaramillo Garcia, M., Haji Bik, H., Beaudet, D., & Piekny, A. (2014). Anillin interacts with microtubules and is part of the astral pathway that defines cortical domains. *Journal of Cell Science*, *127*(17), 3699–3710. <https://doi.org/10.1242/jcs.147504>
- von Dassow, G., Verbrugghe, K. J. C., Miller, A. L., Sider, J. R., & Bement, W. M. (2009). Action at a distance during cytokinesis. *Journal of Cell Biology*, *187*(6), 831–845. <https://doi.org/10.1083/jcb.200907090>
- Wallenfang, M. R., & Seydoux, G. (2000). Polarization of the anterior-posterior axis of *C. elegans* is a microtubule-directed process. *Nature*, *408*(6808), 89–92. <https://doi.org/10.1038/35040562>
- Watts, J. L., Etemad-Moghadam, B., Guo, S., Boyd, L., Draper, B. W., Mello, C. C., et al., Kemphues, K. J. (1996). Par-6, a gene involved in the establishment of asymmetry in early *C. elegans* embryos, mediates the asymmetric localization of PAR-3. *Development (Cambridge, England)*, *122*(10), 3133–3140.
- Wernike, D., van Oostende, C., & Piekny, A. (2014). Visualizing Neuroblast Cytokinesis During *C. elegans* Embryogenesis, *J. Vis. Exp.* *85*(1), 1–13. <https://doi.org/10.3791/51188>

- Wolfe, B. A., Takaki, T., Petronczki, M., & Glotzer, M. (2009). Polo-Like Kinase 1 Directs Assembly of the HsCyk-4 RhoGAP / Ect2 RhoGEF Complex to Initiate Cleavage Furrow Formation. *PLoS Biology*, 7(5), e1000110. <https://doi.org/10.1371/journal.pbio.1000110>
- Xu, L., & Massagué, J. (2004). Nucleoplasmic Shuttling of Signal Transducers. *Nature Reviews Molecular Cell Biology*, 5(March), 209–219. <https://doi.org/10.1038/nrm1331>
- Yüce, Ö., Piekny, A., & Glotzer, M. (2005). An ECT2-centralspindlin complex regulates the localization and function of RhoA. *Journal of Cell Biology*, 170(4), 571–582. <https://doi.org/10.1083/jcb.200501097>
- Zanin, E., Desai, A., Poser, I., Toyoda, Y., Andree, C., Moebius, C., et al., Oegema, K. (2013). A conserved RhoGAP limits M phase contractility and coordinates with microtubule asters to confine RhoA during Cytokinesis. *Developmental Cell*, 26(5), 496–510. <https://doi.org/10.1016/j.devcel.2013.08.005>
- Zonies, S., Motegi, F., Hao, Y., & Seydoux, G. (2010). Symmetry breaking and polarization of the *C. elegans* zygote by the polarity protein PAR-2. *Development*, 137(10), 1669–1677. <https://doi.org/10.1242/dev.045823>